THE LASER STATIONS FOR THE SIRIO-2 LASSO EXPERIMENT

Dr. B.E.H. SERENE
LASSO Payload & Mission Manager

EUROPEAN SPACE AGENCY
Centre Spatial de Toulouse
18, avenue Edouard Belin
31055 TOULOUSE CEDEX
France

Summary

1. Introduction

The SIRIO-2 satellite will be launched in the spring of 1982. One of the satellite payloads is called LASSO (LAser Synchronisation from Stationary Orbit). It will enable time synchronisation between distant atomic clocks on the ground to the nanosecond level (1 nsec = 10^{-9} sec). LASSO will employ the services of existing laser stations in Europe, Asia and the Americas. As described in detail below, the stations will fire laser pulses towards the satellite at predetermined times according to their local time standard. The arrival times of these laser pulses at the satellite, and of their reflected "echos" at the originating stations, provide a measure of the asynchronism between the participating local time standards, or "clocks".

2. The LASSO Experiment

Principle:

The LASSO experiment is based on the use of laser stations emitting monochromatic light impulses at pre-determined times and directed towards a geosynchronous spacecraft (Fig.1). An array of retro-reflectors on board the spacecraft sends back a fraction of the received signal to the originating laser station. An on board electronic device detects and time-tags the arrival of the laser pulses. Each station measures the two-way travel times of the laser pulses and computes the one-way travel time between station and spacecraft, taking into account the station's geographical coordinates, the spacecraft position, and the Earth's rotation.

./.

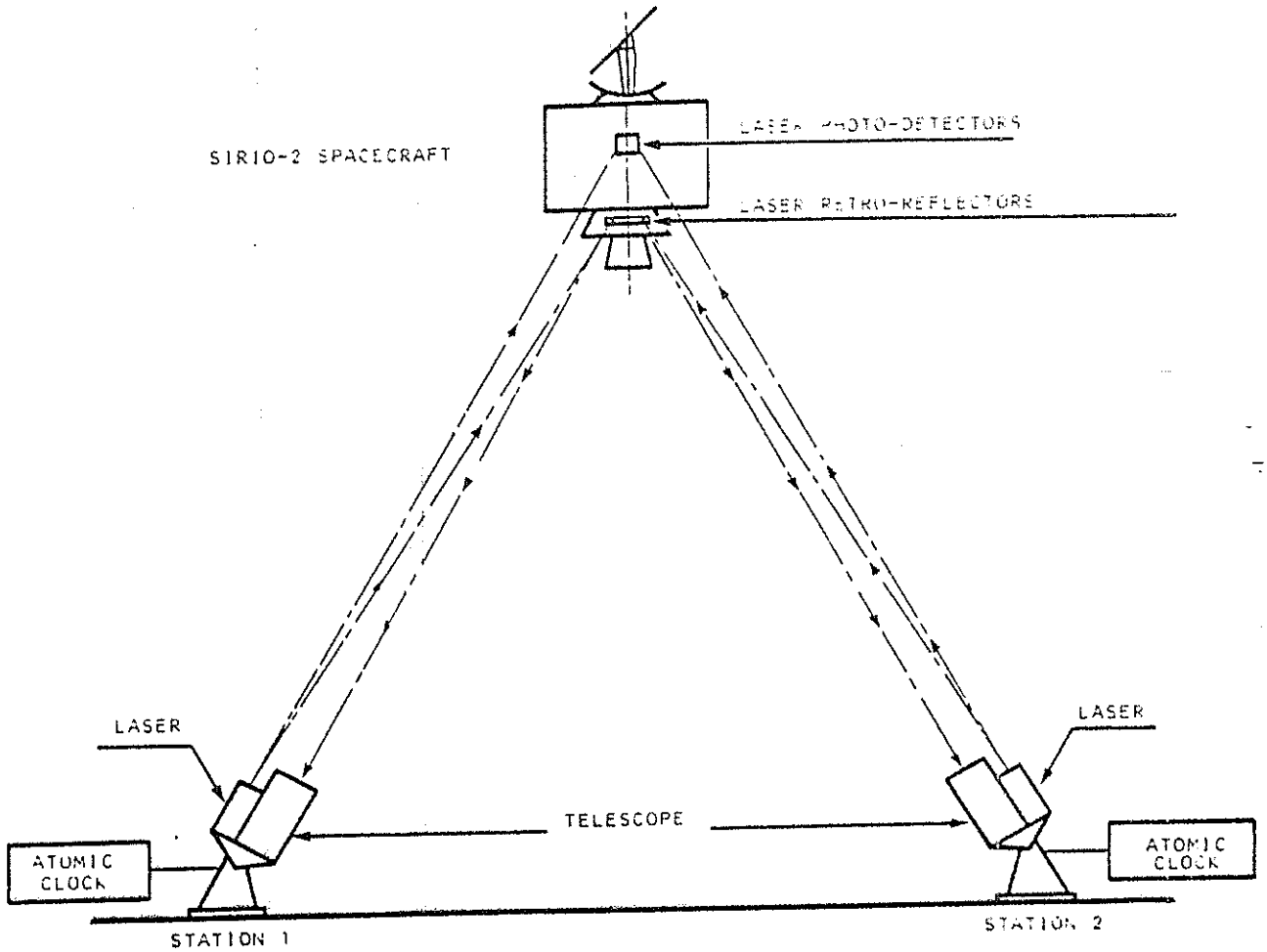

Figure 1

The differences between the clocks that provide the time reference for each of the laser stations can be deduced from the data emanating from the spacecraft and the ground stations (Fig.2).

For two stations, we have :

$$D_{21} = (H_D^2 - H_D^1) + (T_2 - T_1) - (H_S^2 - H_S^1), \qquad (1)$$

where :

D_{21} = time difference between the clocks at stations 2 and 1

H_D^1, H_D^2 = departure times of laser pulses from stations 1 and 2

./.

T_1, T_2 = travel times between stations and spacecraft, with $T = [(H_R - H_D)/2] + \varepsilon$

H_S^1, H_S^2 = arrival times on board the spacecraft of the laser pulses from stations 1 and 2

H_R^1, H_R^2 = return times of laser pulses from stations 1 and 2

ε = corrective factor depending on the station and satellite positions.

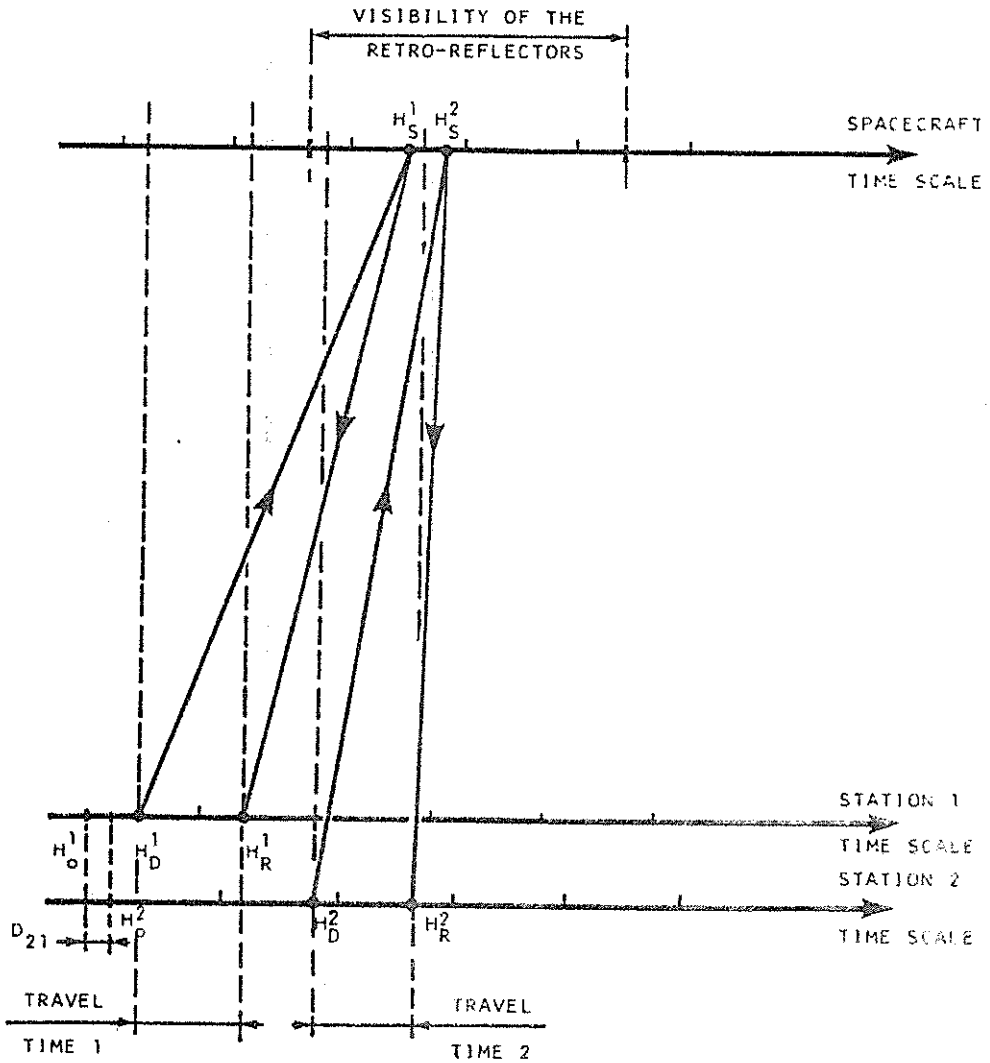

Figure 2

./.

Thus :

$$D_{21} = \left(\frac{H_D^2 - H_D^1}{2}\right) + \left(\frac{H_R^2 - H_R^1}{2}\right) + (\varepsilon_2 - \varepsilon_1) - (H_S^2 - H_S^1) \qquad (2)$$

Performance:

Error Analysis

Using the above information, the global error is:

$$\Delta D = \Delta H_D + \Delta H_R + 2\Delta\varepsilon + 2\Delta H_S \qquad (*)$$

where ΔH_D = error in departure time
ΔH_R = error in return time
$\Delta\varepsilon$ = in correction factor
ΔH_S = error in arrival time on board the spacecraft.

Link Budget

Bearing in mind the two planned orbital positions for the SIRIO-2 spacecraft (25°W and 20°E), the parameters of the on board equipment, and the assumed characteristics for a number of laser stations, different algorithms have been used to compute :

- P_r the power density received by the spacecraft :

$$P_r = K \frac{J}{T} \cdot \frac{T_A}{\frac{4}{\pi}\theta^2 D^2}$$

where :

J = emitted energy (joules)
T = pulse width (ns)
θ = beam divergence (arc.s)
D = station - spacecraft separation (km)
$T_A = (0.7)^{1/\cos z}$: atmospheric transmission coefficient (z= zenithal distance)
K = 0.7 coefficient of energy distribution.

./.

(*) B. Serène & P. Albertinoli, 1980

For LASSO,

$$P_r \ (mW/cm^2) = 3.79 \times 10^{12} \cdot \frac{J}{\tau} \frac{1}{\epsilon^-} \frac{1}{D^2} T_A$$

- $\bar{N}_d$, the mean number of photons received by the photo-detector:

$$N_d = \frac{N_d}{T} = P_r \ A_{op} \ s \ \frac{\lambda}{hc} \ \text{(photons/ns)}$$

where: A_{op} = 4.25 gain of optical detection
s = 0.2 mm^2 photodiode sensitive surface
λ_R = 694.3 nm (ruby)
λ_N = 532.0 nm (neodyme)
h = 6.6256×10^{-34} joules.s
c = 2.9979×10^{8} m/s

Consequently :

$$\bar{N}_d = kP_r \begin{cases} k_R = 29710 \\ k_N = 22760 \end{cases}$$

- N_e, the number of photo-electrons collected at the laser station, from the Fournet formula :

$$N_e = E \cdot TR_1 \cdot R \cdot TR_2 \cdot D$$

where :

$E = KJ \frac{\lambda}{hc}$ — photons emitted by the laser station

$TR_1 = \frac{T_A}{\frac{\pi}{4} \left(\frac{\pi}{180} \cdot \frac{\theta}{3600} 10^5 D\right)^2}$ — travel effect station-spacecraft

$R = R_{cc} \Sigma f(G_i)$ — retro-reflector effect

R_{cc} = 0.84 (coefficient of reflection)

$\Sigma f(G_i)$ = 23.8 for ruby (mean value)
= 22 for neodyme

$TR_2 = 0.328 \ T_A / D^2$ — travel effect station-spacecraft

$D = AT_r\rho$ — station detection effect ./.

where A (cm^2) is the receiving surface of the telescope, T_r the transmission coefficient of the telescope optics, and ρ the quantum efficiency of the photo-multiplier.

3. The Ground Segment Requirements

The LASSO mission is planned to last a total of two years. The experiment 'working sessions' will occupy an average of one hour per day. There will be no constraints at the satellite level on the time of day at which one or more 'sessions' can be performed, but the constraints will rather be of a procedural nature.

After a 2-month period of satellite commissioning, each daily working session will consist in synchronisation of the pulse transmissions from each participating station with respect to the rotation of the spacecraft and associated time measurements.

Because of the design of the satellite's on-board equipment, the laser pulses from the various ground stations must be timed to arrived at the spacecraft with the temporal distribution shown in Figure 3.

Each sequence of measurements lasts approximately 4 to 6 s (bound to the minimum pulse rate of the laser stations), and in each sequence a time slot of 5×10^{-3} s is reserved for the arrival of the pulse from a particular station (this figure is bound by the accuracy of the time of departure of the pulse from the station and by the accuracy of the computation of the travel time of light from the station to the spacecraft).

Consequently each subsession lasts about 3 min and is separated from the next subsession by a time interval of 10 min, to allow laser stations to reset the firing time based on the spin rate drift of the spacecraft.

Successive sequences differ from one another since not all of the laser stations send pulses in each sequence. The use of pattern recognition techniques in the ground processing ensures that any false pulses detected by the on-board equipment is discarded.

./.

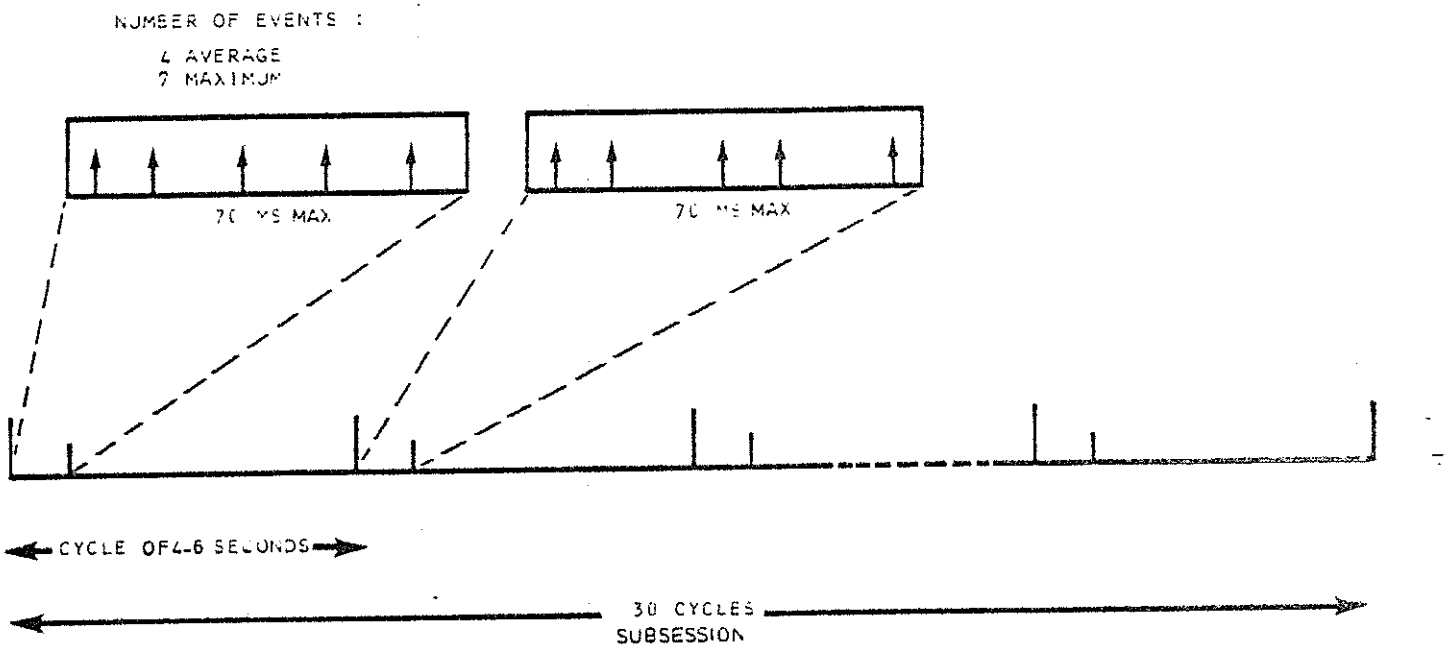

Figure 3

An alternative spin-asynchronous mode of experiment operation is currently being investigated. Several data processing modes are also under study in consultation with the various principal investigators.

Station location and performance

Because of the need to correct the transit time of light from the laser station to the spacecraft, the laser station should be located in a common Earth reference frame with a minimum specific accuracy :

- latitude : ± 10" (or ± 300 m)
- longitude : ± 10" (or ± 300 m)
- altitude : ± 10 m

Two sets of conditions are imposed on laser-station characteristics : one by the satellite-detector and retro-reflector characteristics, the other by the laser station detector system.

./.

In order to ensure laser detection on-board the spacecraft, the laser station must deliver sufficient energy in a sufficiently narrow beam for a finite time. If J is the total energy (in joules) of the light in the beam during one pulse from the laser station, T the equivalent pulse duration in nanoseconds, and θ the laser station beam divergence in arc seconds, bearing in mind the link budget and the two sensitivities (nominal and high) of the on-board detectors, the laser station should satisfy the performance relationship :

$$\theta \leqslant \alpha \left(\frac{J}{T}\right)^{1/2}$$

where α is a coefficient given in figure 4.

In order to detect the return pulse from the retro-reflectors on board SIRIO-2 (544 cm^2 of surface, reflection coefficient = 0.84, efficiency > 20), the laser station should also satisfy the relationship giving the number of photons received by the station :

$$N = \beta \left(\frac{J}{\theta^2}\right) T_R A$$

where β is a coefficient given in figure 5.

A = effective area of the telescope used to collect the light (cm^2)

T_R = transmission factor of the telescope

J = energy of the laser flash (joules)

θ = beam divergence (arc.s)

N = number of photons collected by the telescope equipment

A minimum of 10 photons must be detected by the laser station from the retro-reflected signal.

The number of photo-electrons detected is :

$Ne = N.\rho$ where ρ = quantum efficiency of the photon-multiplier.

./.

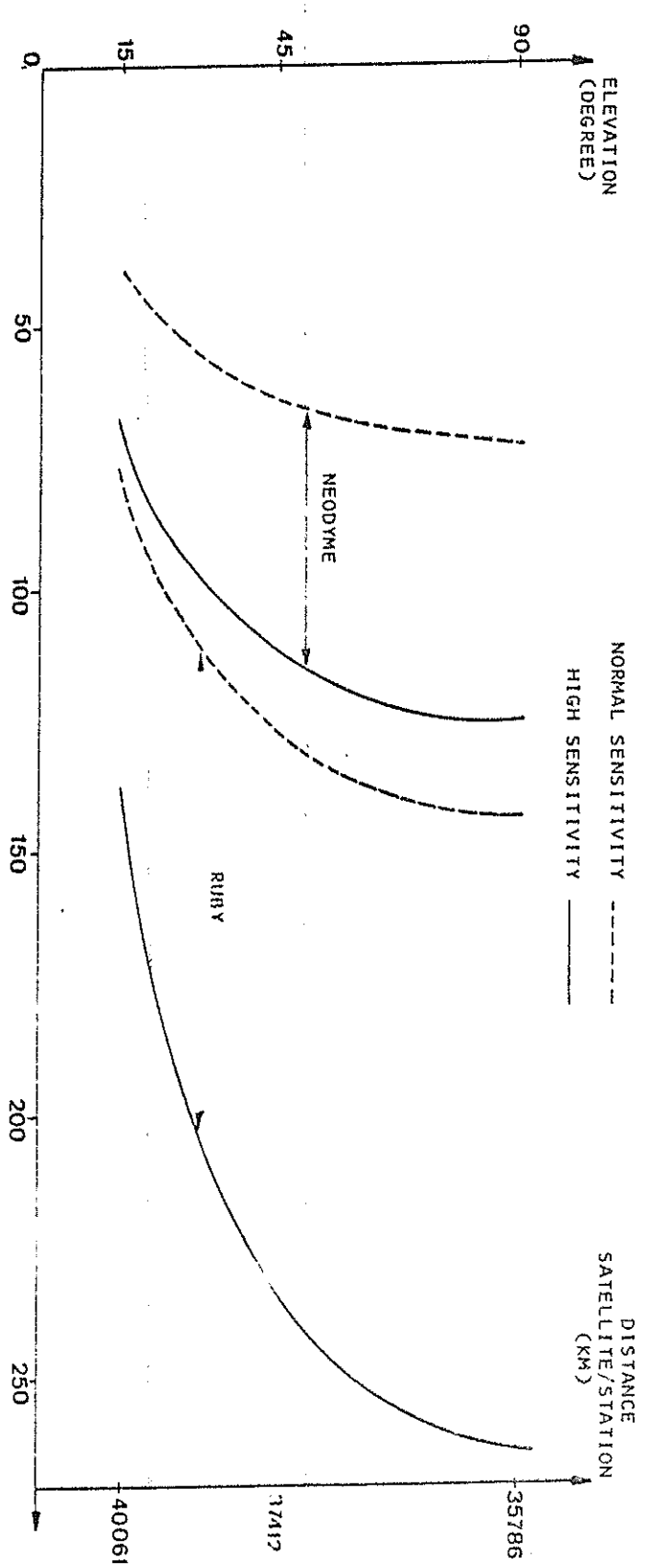
ELEVATION (DEGREE)
0
15
45
90
COEFFICIENT α
50
100
150
200
250
NEODYME
RUBY
NORMAL SENSITIVITY
HIGH SENSITIVITY
DISTANCE SATELLITE/STATION (KM)
35786
40061

Figure 4

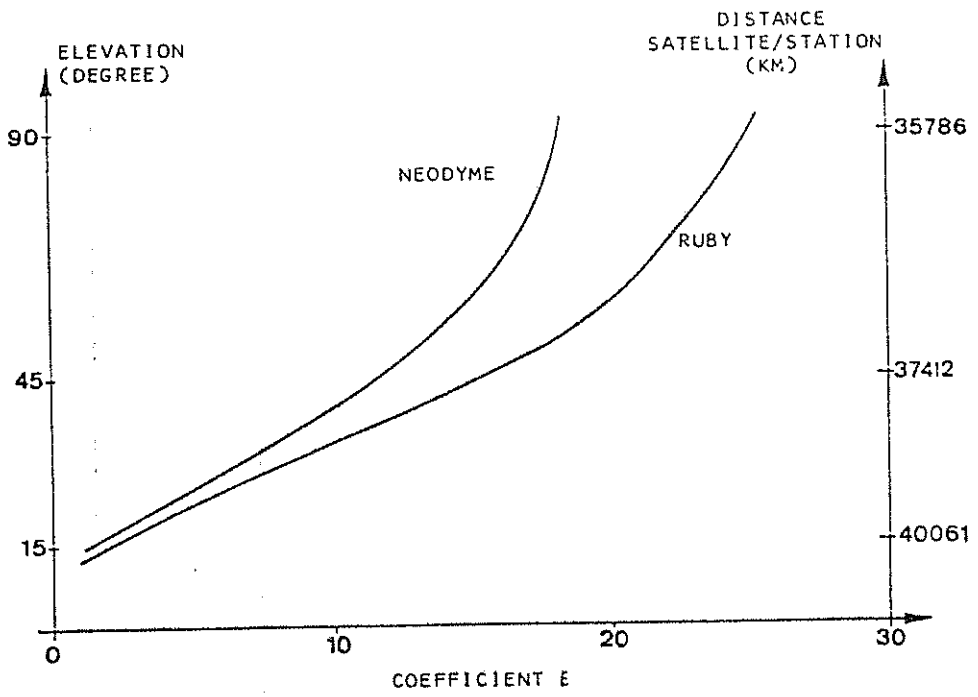

Figure 5

Sufficient beam divergence is necessary at each laser station to ensure that the pulse does in fact arrive at the satellite, taking into account small errors in satellite position (known 'à priori' within ± 1 km). The laser stations must therefore have a beam divergence of :

$\theta \geq 10'' + 2 \times$ (angular error of tracking).

The time-measurement devices at the participating laser stations must also satisfy a number of criteria. They should permit synchronisation with a standardised time source in their zone (e.g. IAT) by terrestrial means on a daily basis, with a precision of a few microseconds. ./.

The maximum error in synchronisation between two stations participating in the experiment should be less than 1 ms before LASSO measurements commence.

Each pulse transmitted by the laser station should be pre-programmed at T_0. If T_1 is the real time at which the laser pulse was transmitted, one should have :

$(T_0 - T_1) < 1$ ms.

T_1 should be measured with an accuracy of $\pm$ 0.1 ns 'à posteriori'

T_2 the time of arrival of the pulse returning from the satellite, should be measured with an accuracy of $\pm$ 1 ns, and the maximum elapsed time from transmission to return of a given pulse should be conditioned by :

270 ms $< T_2 - T_1$.

4. Status of Laser Stations

Using the technical specifications provided by the laser stations, a computer programme has been run. The results are used as the basis for laser station classification :

- two-way laser stations

  power density received by the satellite detection unit above the threshold; number of photons detected by telescope;

- one-way laser stations (type N)

  power density received by the satellite detection unit above the threshold for normal sensitivity;

- one-way laser stations (type H)

  power density received by the satellite detection unit above the threshold for high sensitivity;

- laser stations unable to participate without modifications.

./.

The classification is made purely as a mathematical exercise to estimate the probability of successful participation. It does not, in any way, prejudge the interest of accommodating a particular user in the LASSO mission as a whole.

4.1 Two-way laser stations

France	Grasse 'Satellite' Grasse 'Lune'
Spain	San Fernando
F.R.G.	Wettzell
Netherlands	Kootwijk (marginal)
Austria	Lustbuhel
U.S.A.	NASA/GSFC 1 NASA/GSFC 2

4.2 One-way laser stations, type N

Netherlands	Kootwijk (possibly two-way)

4.3 One-way laser stations, type H

G.D.R.	Potsdam	$50 < \theta < 90$ arc.s
Italy	Cagliari	(marginal)
Brasil	SAO Natal	(marginal)

4.4 Laser stations apparently unable to participate without modifications

India	Kavalur

./.

5. Laser Station Calibration

A problem of calibration arises at the laser stations due to the fact that they have been designed for laser ranging rather than for clock synchronisation. The need for calibration is caused by a small but inevitable discrepancy between the measured and actual emission times of laser pulses. The magnitude of the discrepancy varies from station to station and can be translated directly into a laser travel time uncertainty which, in turn, degrades the potential time synchronisation accuracy between the clocks.

5.1 Necessity

The basic equation (1) masks in fact a rather sophisticated technological application. The calibration consists theoretically in three types of measures :

i/ Measure of the travel time 2Γ

Such a calibration is classical in laser ranging. It could be done either by firing on a target at a very well known distance or by double round trip using an additional retro-reflector (E. Silverberg method). One thus obtains the time delay difference between emitting and receiving channels. The delays are due to the time elapsed between the moment when the laser pulse passes through the reference point and the internal triggering of the event timer.

ii/ Satellite time-tagging

LASSO relies only upon the short term stability of the on board oscillator; stability drift calibration is therefore not necessary.

iii/ Definition of the emission time

The moment when the emitted laser pulse is passing through the reference point must be time tagged with an accuracy better than 1 nsec if the LASSO objectives are to be met. This implies that the delay τ between this moment and the memorised time H in the event-timer must be

./.

calibrated with an uncertainty of less than 1 nsec. It is this third type of calibration which will be solved by the mobile calibration device.

5.2 Concept

We will consider here only the aspect relevant to the definition of the emission time.

We have : $H_D = H - \tau$

$$D_{21} = (H^2 - H^1) - (\tau^2 - \tau^1) + (T_2 - T_1) - (H_S^2 - H_S^1) \qquad (4)$$

This new relation shows that keeping the accuracy of the time synchronisation does not involve the knowledge of the absolute values of τ, but only their differences. A method of solving the problem is to use a second laser ranging equipment, in parallel with the laser station to be calibrated, bearing in mind that potential drift will be monitored by an internal return path.

5.3 Equipment

The European Space Agency is in the process of procuring a calibration device in order to establish a relative measure of this discrepancy between stations, thus allowing the necessary time corrections to be made in the calculation of atomic clock asynchronisms. The intention is to obtain a facility which is sufficiently small, light, rugged, and stable that it can be transported in a jeep-type vehicle and by air to participating laser stations all over the world without suffering any degradation on performance.

6. CONCLUSION

It appears that the most critical parameters for a successful participation of the laser stations are :

- a small divergence of the laser beam,
- a good pointing accuracy,
- at least a medium size telescope (60 cm)
- a photo-multiplier with high quantum efficiency.

./.

Laser stations with marginal link performance will often be able to raise the probability of success by improving only one or two of these parameters, the choice of modifications being subject e.g. to the planning and cost considerations at the laser station.

- o0o -

References:

Serène B. & Albertinoli P., 1980, The LASSO Experiment on the SIRIO-2 Spacecraft, ESA Journal 4, 1, pp 59-72

Serène B., 1980, The Progress of the LASSO Experiment, Proc 12th Annual Precise Time & Time Interval (PTTI) Conference, NASA-GSFC, Greenbelt, Maryland, 2/3/4 Dec. 1980.

Serène B., February 1981, The LASSO Experiment and its operational organisation, International Symposium on Time and Frequency, New Delhi.

COMPARISON OF MEASURED AND THEORETICAL PERFORMANCE OF A MAXIMUM LIKELIHOOD LASER RANGING RECEIVER

CONTACT: J.B. ABSHIRE
CODE 723
NASA/GODDARD SPACE FLIGHT CENTER
GREENBELT, MARYLAND 20771 USA

Abstract and Summary

A maximum-likelihood laser ranging receiver recently has been built and tested. Its configuration includes a high quantum efficiency (30% at 532 nm) detector, a single start-stop channel, and a matched filter followed by a peak detector to implement the maximum-likelihood signal processing algorithm in real time. The receiver was designed to operate with signals from 5 to 5000 photoelectrons per 7 nsec laser pulse, with a 50:1 dynamic range on a shot-to-shot basis. It can operate with background rates of up to 375 pulses/μsec, which are the rates expected when the receiver and its 20 cm telescope are pointed at sunlit clouds. Measured receiver detection probabilities were in excellent agreement with theory for signals in the 3 to 62 photoelectron level. Measured false alarm rates also agreed with theory for low receiver thresholds, but exceeded theory for high threshold values due to photomultiplier feedback events. Range jitter values were 0.8 db from theoretical at the 10 cm level, and increased to 2.7 db from theoretical at the 2 cm ranging level.

System Description

A block diagram of the laser receiver is shown in Figure 1. The fire signal from the minicomputer triggers the laser and the generation of a start gate signal. The optical pulse from the laser is divided by a beam splitter and approximately 0.1% is reflected into a variable optical attentuator used to control the the start pulse amplitude. The pulse from the attenuator is directed to the single photomultiplier, and the amplitude of its electrical signal output is controlled by a variable attenuator. The attenuator output signal is amplified, matched-filtered, reamplified, and split into four paths. One output triggers the peak detector, which is enabled by the start gate signal. The gate generator triggers only the start charge-digitizer, after

it is triggered by the discriminator output. The input to the charge digitizer is delayed by a coaxial cable, to compensate for the peak detector and the gate generator propagation delays. The event timer also registers the peak detector output, and records it as the start occurence time.

The remainder of the laser output energy is transmitted through the beam splitter, and is directed through a pointing system to the target corner cube. The return signal is collected by the telescope, and is spatially and spectrally filtered. The return signal then is recollimated, and focused onto the photomultiplier. This signal passes through the same electrical path as the start signal, and triggers the same peak detector as the start pulse. The peak detector is only enabled for the return pulse during the range gate generated by the event timer. This gating signal also enables the stop charge-digitzer, which measures the received pulse energy. The event timer is triggered by the peak detector output and registers the occurence time of the return pulse.

Both the start and return pulse energy readings from the charge digitizers are used in a feedback loop to control the signal levels in the single channel receiver. The electrical attenuator is controlled by the return pulse amplitude through an averaging algorithm in the minicomputer. This technique allows the average return signal level to be kept within the center of the dynamic range of the common signal channel. The start optical attenuator is then controlled to compensate the optical level of the start pulse, also to keep it centered in the receiver's dynamic range. This is feasible since the 2000:1 dynamic range of the photomultiplier is much larger than the 50:1 range of the electronic channel.

A summary of the specifications of the receiver is given in Figure 2. Both the telescope and the filter are standard commercial products. The photomultiplier is a Varian 152 model, with a high quantum efficiency "S"-type photocathode. The value of photomultiplier gain was selected to be sufficiently high that thermal noise from the preamplifiers would not dominate the system's ranging performance, but low enough to prevent saturation of the last few photomultiplier dynodes

SGRS LASER RANGING RECEIVER

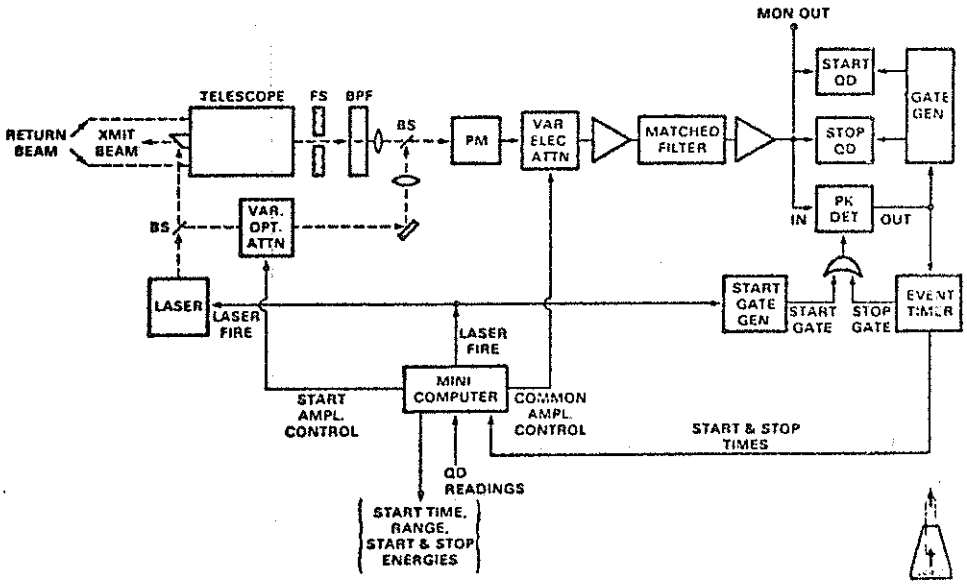

Fig. 1 - Block diagram of SGRS receiver

RECEIVER SPECIFICATIONS

TELESCOPE	: 20 cm DIA, f10 CASSEGRAIN, FOV = 1.4 mrad
BANDPASS FILTER	: 10 Å FWHM
DETECTOR	: 10^5 GAIN, 30% QE @ 532 nm, 2000:1 DYNAMIC RANGE
AMPLIFIERS	: 25 & 35 dB GAIN, 400 MHz BW
MATCHED FILTER	: TAPPED DELAY LINE CORRELATOR, 8 TAPS AT 2nsec/TAP
TIMING DISCRIMINATOR	: GATABLE PEAK DETECTOR,
TIME WALK	: { UNCORRECTED = ± 500 psec; CORRECTED = ± 75 psec
LEVEL DETECTOR	: CAMAC COMPATIBLE CHARGE DIGITIZER, 10 BIT RESOLUTION
EVENT TIMER	: RMS ACCURACY = 17 psec, DEAD TIME = 5.3 μsec, TIME LIMIT = 131 DAYS
MINICOMPUTER	: DEC PDP 11/40
PACKAGING	: SINGLE CAMAC CRATE & NIM BIN

Fig. 2 - Summary of receiver specifications

during reception of large amplitude signals. The amplifiers in the system compensate for the signal loss in the matched-filter and the various power splitters in the channel, and give the low photoelectron signals sufficient gain to trigger the peak-timing discriminator. The matched filter was constructed in a tapped delay line configuration, to allow adjustment of its impulse response. This is accomplished by adjusting variable attenuators in each of the 8 taps.

The peak timing discriminator was a custom unit built by Lawrence-Berkeley Laboratories. It triggers on the peak of the matched filter output, and includes a gating capability. The time-walk for the unit was measured to be ±500 psec. However, by measuring and storing the time walk curve before ranging, the charge-digitizer readings can be used to correct for the time-walk on a shot-by-shot basis. By using this technique, the residual time walk was reduced to ±75 psec. The charge digitizers in this system are commercially available 10-bit units, and are read through the CAMAC dataway. The event-timer was also custom built by Lawrence-Berkeley Labs, and has a timing resolution of 17 psec. Since it also has a single input channel, the minimum dead-time between start-stop events is 5.3 μsec. It can unambigiously record the occurence times of start-stop event pairs for a period of 131 days. A PDP 11/40 minicomputer was used as the controller of for the development of this receiver, although almost any mini- or micro-computer which can control a CAMAC crate would have been adequate. The ranging receiver is packaged in a single CAMAC crate and NIM bin.

Receiver Testing

The LED pulse shape used to test the performance of the receiver is shown in Figure 3. This 7.6 nsec full-width at half-maximum (FWHM) pulse was generated by driving the LED from a fast-risetime pulse generator through a pulse shaping network. The impulse response of the matched-filter is shown in Figure 4. It had a 7.3 nsec FWHM for these tests, and the shape was adjusted to give a close match to that of the laser transmitter of the SGRS system.

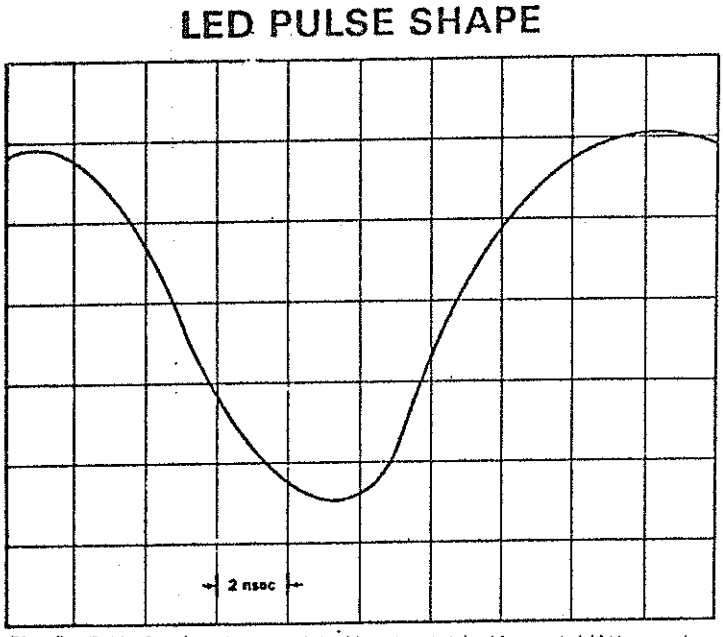

Fig. 3 - Optical pulse shape used in timing and detection probability tests

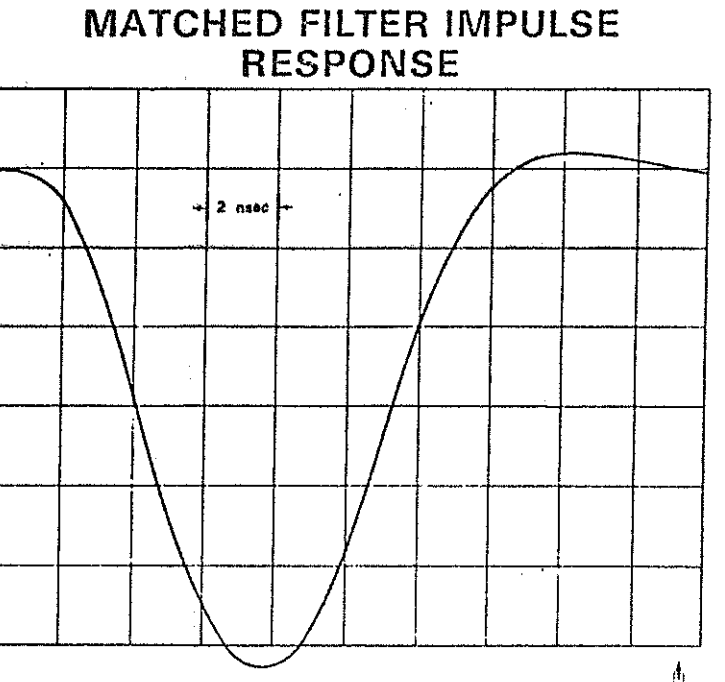

Fig. 4 - Impulse response of receiver matched filter

The receiver photoelectron calibration was performed by measuring the single photoelectron voltage from the photomultiplier, and then measuring the receiver channel amplitude response to the same level signal. A plot of the results is shown in Figure 5, where Monitor Point 2 is labeled as MON in Figure 1. This calibration data was used to determine the received photoelectron level on all subsequent tests.

The test configuration for measuring the receiver performance is shown in Figure 6. The pulse generator output was used to drive the LED, which emits a shaped optical pulse. This pulse was used to simulate the laser pulse incident to the photomultiplier. The output trigger from the generator was used to start the time interval unit when measuring the system timing performance. The LED output was attenuated by a variable ND stack, and focused onto the photomultiplier photocathode. A small flashlight bulb controlled by a variable DC supply was used to provide optical background for timing and false alarm measurements. The photomultiplier output was connected to either a meter to measure the average photomultiplier anode current, or to the SGRS receiver. The threshold of the receiver was adjusted by varying the electrical attenuator preceding the peak detectors. The average photoelectron level in the detected pulses was measured by a waveform digitizer connected to the MON port of the receiver. The discriminator output was connected to the time interval unit for timing tests, and to the frequency counter for detection probability and false alarm tests.

For the timing measurements, the optical pulse energy was varied by using the ND filters, and the RMS timing jitter was measured using the time interval unit. The detection probability tests were performed by varying both the optical pulse strength and the receiver threshold, and by measuring the percentage of the optical pulses which exceeded the receiver threshold with the frequency counter. False alarm measurements used only the DC background illumination, and the rate of receiver triggering was measured as a function of average illumination level and threshold setting.

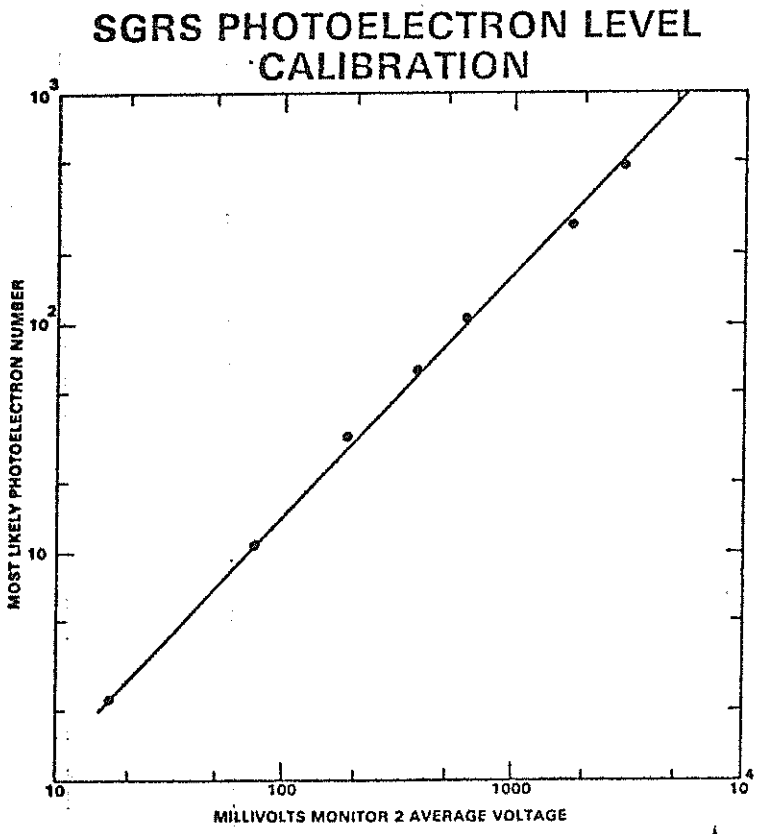

Fig. 5 - Photoelectron calibration of receiver

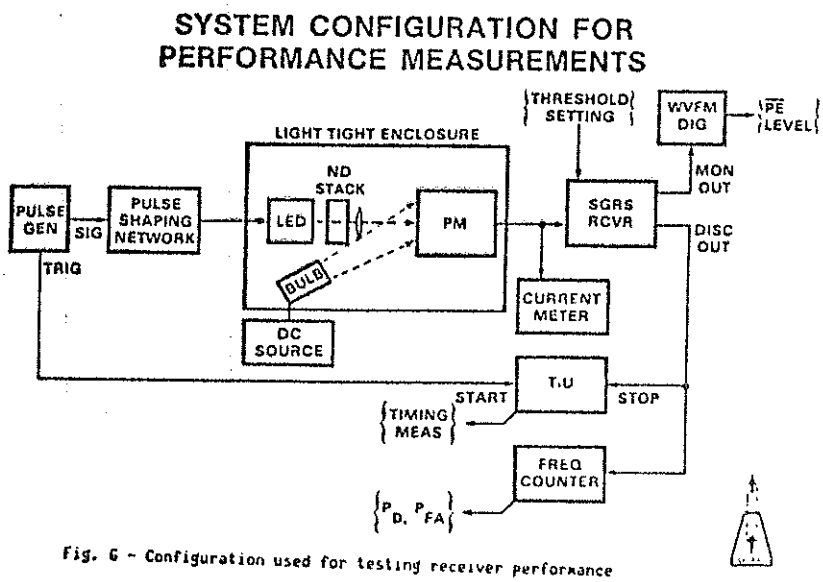

Fig. 6 - Configuration used for testing receiver performance

Theoretical and Measured Results

The theoretical calculations shown in Figure 7 are based on the assumption that the receiver is a sliding window photon counter. Further assumptions were made that the receiver observation window was much longer than its integration time, and during its integration time the receiver simply counts the input photoelectrons. For this analysis the integration time was taken to be equal to the FWHM of the receiver impulse response. For the false alarm calculations, the noise count rate was assumed to be constant over the observation time. Finally, the occurence of false alarms and optical pulse detections were assumed to be independent events, so that their probabilities could be calculated independently. This assumption is not strictly true for actual single channel receivers, since a false alarm will trigger the channel, and preclude detection of a laser pulse following it in the observation window. However, it is a very good approximation for such systems operating under low false alarm probabilities.

Measured detection probabilities and point theoretical calculations are shown in Figure 8. The plot shows excellent agreement between the theory and the measured detection rates, for average optical pulse levels from 10 to 62 photoelectrons. Agreement was not as good for the 3 photoelectron level. The spread in the single photoelectron voltage from the photomultiplier is thought to be responsible for this discrepency.

The measured and calculated false alarm probabilties are shown in Figure 9. There is good agreement between the theory and measurements for low threshold values and low photomultiplier anode currents, but substantial differences at higher thresholds and currents. These are due to receiver dead-time effects at low threshold levels and high background rates. For high threshold settings, the measured false alarm rates considerably exceed those predicted by theory. This is caused by the ion-feedback mechanism in the photomultiplier, which causes a small fixed percentage of photoelectrons to generate large amplitude bursts of photoelectrons. This mechanism is more evident in photmultipliers with more open dynode structures, such as static-crossed field types.

SIMPLIFIED THEORY

DETECTION AND FALSE ALARM PROBABILITIES:

- **ASSUME:**
  - RECEIVER IS SLIDING WINDOW INTEGRATOR, WIDTH τ
  - OBSERVATION WINDOW OF TSEC, $T \gg \tau$
  - RECEIVER COUNTS PE OVER LAST τ SEC
  - NOISE COUNT RATE n_b IS CONSTANT OVER T
  - DETECTION & FALSE ALARMS ARE INDEPENDENT
- $P_D = P_r\{N_{s_\tau} \geq \text{THRESH (L)}\} = 1 - e^{-Q} \sum_{k=0}^{L-1} \frac{Q^k}{k!}$
- $P_{FA} = P_r\{N_{n_\tau} \geq L, \text{ SOMETIME DURING } T\} = 1 - \exp\left\{\frac{-n_b T (n_b \tau)^{L-1}/(L-1)!}{\sum_{k=0}^{L-1} (n_b \tau)^k/k!}\right\}$
- REF: LEE & SCHROEDER, IEEE TRANS. INF. THY, IT-22, 114 (1976).

Fig. 7 - Theoretical basis for detection and false alarm calculations

PROBABILITY OF DETECTION VERSUS THRESHOLD LEVEL

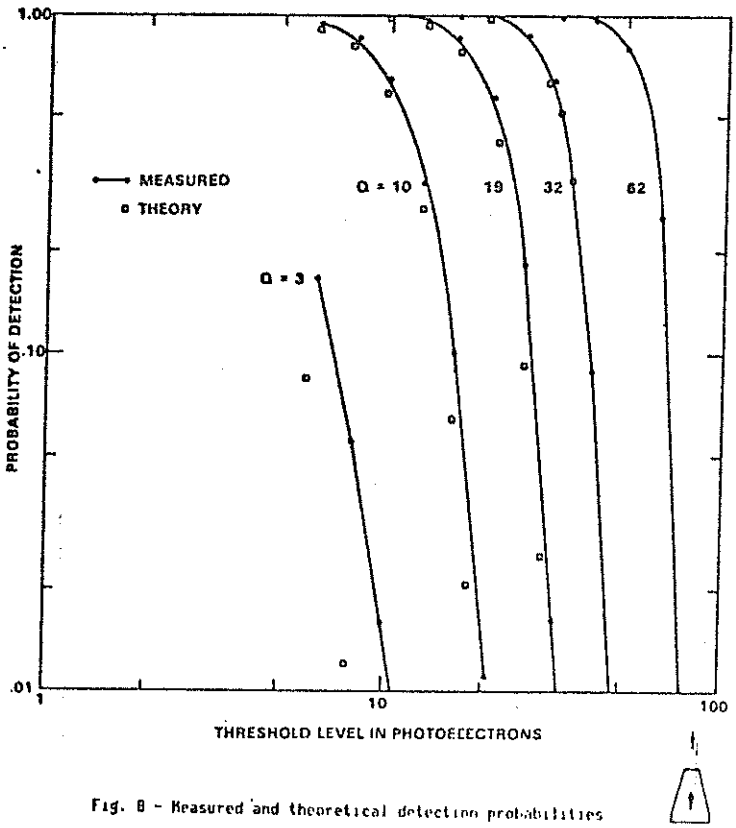

Fig. 8 - Measured and theoretical detection probabilities

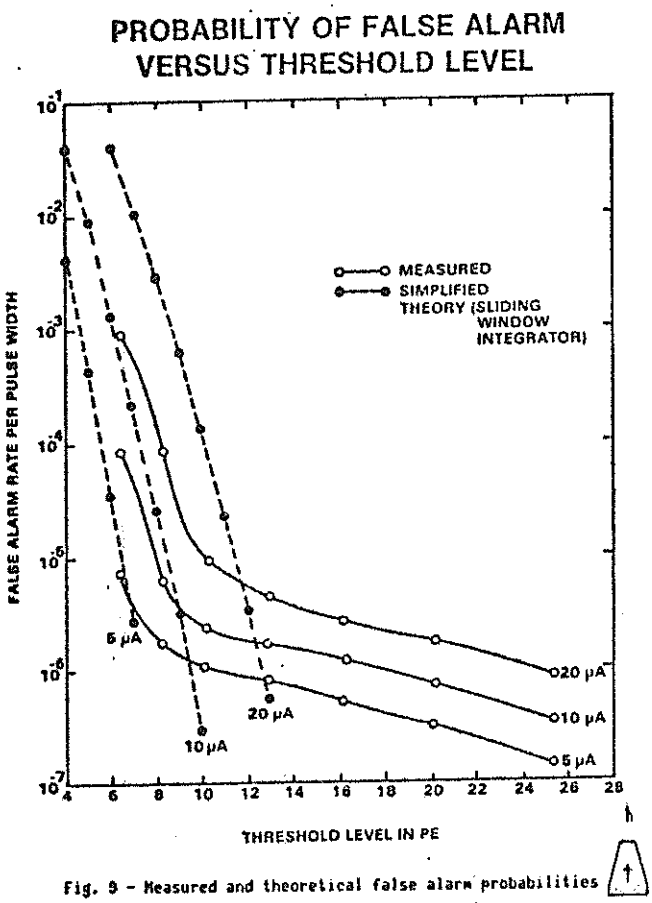

Fig. 9 - Measured and theoretical false alarm probabilities

SIMPLIFIED THEORY

TIMING PERFORMANCE:

- ASSUME:
  - ML RECEIVER WITH RAISED COSINE
  - OPTICAL PULSE
  - $\lambda n = 0$

- $\sigma_R = \frac{\tau}{2\pi\sqrt{Q}}$, τ = TRANSMITTED PULSE FULL WIDTH AT BASE,

  $Q = \int_{T/2}^{T/2} \lambda_s(t)dt$ = EXPECTED SIGNAL COUNT

- REF: BAR-DAVID, IEEE TRANS. INF. THY, IT-15, 31 (1969)

Fig. 10 - Theoretical basis for receiver timing performance

The theoretical timing performance for a maximum-likelihood receiver operating with a raised-cosine optical pulse is shown in Figure 10. For background rates which are less than 10% of the expected signal count within the optical pulse width, the simple formula in the figure is adequate. This was always the case for the SGRS receiver, since the false alarm probability would have been excessive for higher background rates.

A comparison of theoretical and measured timing performance is shown in Figure 11. The receiver performance was only 0.8 db from theory at the 10 cm ranging level, and 2.7 dB from theory at the 2 cm level. The growth in the difference between the curves is due to the fixed jitters of the amplifiers and the time interval unit in the measurement system. These effects are small compared to the timing jitter caused by the photon-limited signal at low photoelectron levels, but are a relatively larger source at higher photoelectron levels.

A summary of the receiver description and calibration results is shown in Figure 12. The single channel design of the receiver was used to minimize drifts between start and stop channels, while amplitude measurements of both the start and return pulses were used to correct for discriminator time walk. These measurements also were used in a feedback arrangement with variable optical and electrical attenuators to control the gain of the receiver. The timing and detection probabilities were in good agreement with simple theoretical models. The false alarm probabilities were considerably higher than those predicted by theory, due to photomultiplier feedback events. The rate of these events depends upon both the illumination level and the design of the photomultiplier, and must be taken into account when designing multiphotoelectron ranging receivers for daylight operation.

SGRS TIMING PERFORMANCE WITH 7.3 NS LED PULSE

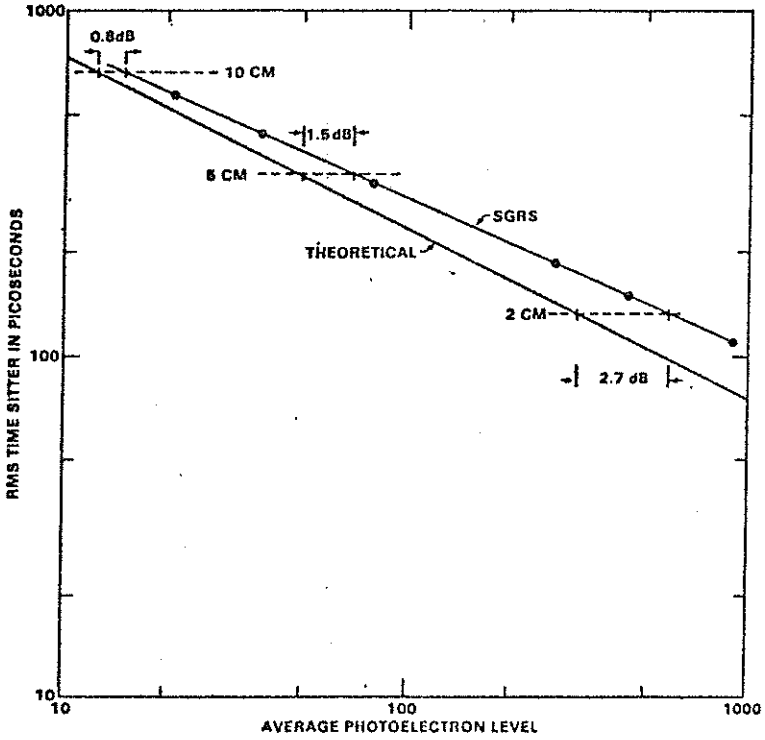

Fig. 11 - Measured and theoretical timing performance

SUMMARY

- SINGLE CHANNEL ML LASER RANGING RECEIVER HAS BEEN DESIGNED BUILT & TESTED
- SINGLE CHANNEL MINIMIZES DRIFTS
- START & STOP AMPL. MEAS. MINIMIZE DISC TIME WALK
- SYSTEM TESTED WITH 7.6 NSEC LED PULSE & CW BACK-GROUND
- TIMING PERFORMANCE { 0.8dB FROM THEORY AT 10 cm / 2.7dB FROM THEORY AT 2 cm
- USED SLIDING WINDOW INTEGRATOR AS THEORETICAL BASIS FOR P_D & P_{FA}
- MEASURED P_D AGREED WITH THEORY FOR SIGNALS IN 10-32 PE RANGE
- MEASURED P_{FA} AGREED WITH THEORY FOR LOW RATES & THRESHOLDS
- FOR HIGH RATES & THRESHOLDS P_{FA} DEPARTS FROM THEORY DUE TO DISC DEAD-TIMES AND PM FEEDBACK EVENTS

Fig. 12 - Summary of receiver description and performance

ATMOSPHERIC TURBULENCE EFFECTS ON LASER RANGING EXPERIMENTS

by P. ASSUS
CERGA, Grasse, France

Abstract. In the recent years, the speckling phenomena have arrested the special attention of many investigators (1,2,3,4) from their fundamental properties and applications in scientific and industrial fields. We study here the effect of this phenomenon on laser ranging (Moon and satellites).

I. INTRODUCTION

The theoretical models and experimental studies on atmospheric turbulence allow us to know light intensity distribution of a star image given by a telescope.

First, let us assume that we have a diffraction limited telescope (D.L.T.).The image of a star through atmospheric turbulence given by a D.L.T. is shown in fig. 1 (very narrow bandwidth):

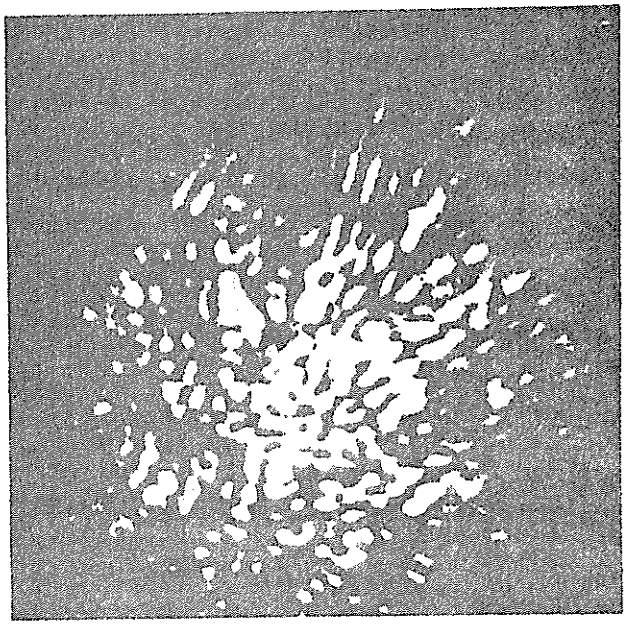

Fig. 1. Speckled image of a stellar point source at the Palomar 200" telescope (by courtesy to Labeyrie)

The diameter of the speckle pattern is given by atmospheric turbulence but the mean diameter of speckles is only given by telescope resolution.

Any variation on the turbulence changes only the number of speckles and the diameter of the speckle pattern.

Example : Lunar laser ranging at CERGA (telescope looking at an unresolved star filtered with a narrow bandwidth) :

$$\text{Speckle diameter} \qquad \alpha = \frac{1.22\lambda}{D} = 0.1 \text{ arc sec.}$$

taking $\lambda = 6943$ Å and telescope diameter $D = 1{,}5$ meter.

II. LASER EMISSION TOWARDS SPACE THROUGH ATMOSPHERE

We have the same phenomenon when the light is a point source in the focal plane of a D.L.T. and the observer is outside Earth atmosphere (light inverse return principle).

The very short duration of laser shooting allows us to consider atmospheric turbulences as frozen during the impulse. Between two following impulses, the position of speckles is completely decorrelated (more than 2 seconds).

III. NATURAL DIVERGENCE OF LASER, OPTICAL POLISHING IMPERFECTIONS, ABERRATIONS.

The natural divergence of lasers is mainly due to inhomogeneities in the amplifying medium. The spatial coherence of laser implies that the laser beam is the result of a diffraction limited beam through an inhomogeneous medium.

This effect is the same for polishing imperfections of "coudé" mirrors or aberrations of the telescope.

The spot diameter grows up with this effect while speckle diameters stay the same. So, the number of speckles grows up with the spot diameter.

We must note that without turbulence, this effect lets conservative positions of speckles in the speckle-pattern during the tracking. For an Alt.Az. mount for instance without "coudé" or telescope mirror imperfections, the position of speckles only turns with the field rotation.

IV. APPLICATION

A/ Lunar laser ranging of CERGA

Ruby pulsed laser natural divergence is about $\beta = 2.5.10^{-4}$ radian for an output diameter, $d = 19$ mm.

At the output of the 1.5 m telescope, the natural divergence will be :

$$\beta' = \beta \frac{19.10^{-3}}{1.5} = 3.2 \cdot 10^{-6} \text{ rad} \qquad \sim 0{,}6 \text{ arc sec.}$$

Atmosphere turbulence is very often situated between 1 and 3 arc sec. which is morely higher.

Taking an average atmospheric turbulence of 2 arc sec., we have about 600 speckles of 1/10 arc sec. diameter each (near 200 m on the Moon) in a spot of 2.6 arc sec. diameter (5 km). Between speckles, there are dark zones where light intensity can decrease down to total extinction. So there is a great difference of light efficiency between bright zones and darker zones.

So, statistic repartition of return power is very influenced by speckled aspect of laser spot. The signal possessing must take it into account(5).

B/ Satellite laser ranging of CERGA

Emission : D = 20 cm
speckle diameter : α = 0.8 arc sec. (about 4 m at 1000 km)

For a pointing problem of the mount, the beam is defocalised and the spot diameter is about 20 arc sec. (100 m at 1000 km). The speckle diameter does not stay the same in a defocalised beam but we can assume that there are a few hundred speckles in the spot. Thus, we have also a great power difference between the returns on account of this phenomenon.

Discussion : is it possible to change these effects of atmospheric turbulence ?

By modifying the emission diameter, the speckle dimension changes. For example, taking an emission diameter of 5 cm * , speckle dimension is about 3.5 arc sec. Turbulence agitation is lower.

Without natural divergence of the laser beam, this hypothesis would nearly neutralize the speckle effect by having only one speckle. But the minimal speckle number is given by laser natural divergence. With the same pulsed ruby laser, we have here :

$$\beta' = \beta \frac{19.10^{-3}}{5.10^{-2}} = 9.5 \cdot 10^{-5} \qquad \sim 19 \text{ arc sec.}$$

---

* Fried defines a correlation length of wavefront perturbation r_0. Usually, 5 cm < r_0 < 10 cm according to turbulence.

The speckle pattern diameter is corresponding to the size of r_0 and speckle diameter to the size of telescope (6)

So we could have therefore about 30 speckles in a spot with diameter of 19 arc sec.

The speckle position in the spot would be conservative. It would be better to have lasers with less natural divergence. In that case, it would be necessary to have :

- good optical surfaces in emission afocal optics,
- good "coudé" mirror adjustments,
- a good relative pointing quality of the mount.

REFERENCES

(1) RODDIER C & F, 1975, J. Opt. Soc. Am. 65, p. 664.

(2) LABEYRIE, A., 1978, "Stellar Interferometry Methods", Ann. Rev. Astron. Astrophys., 16, p. 77.

(3) DAINTY, J.C., "Laser speckle and related phenomena".

(4) ERF, R.K., 1978, "Speckle metrology", Academic Press, New York.

(5) COLLATO, M., 1981, "Possibilités d'utilisation des photodiodes à avalanche pour la détection du laser-Lune du CERGA. Influence de l'existence des speckles sur le nombre de photons de retour", rapport de stage de DEA, Nice University.

(6) FRIED, D.L., 1965, J. Opt. Soc. Am., 55, p. 1427.

A Receiver Package for the U.K. Satellite Laser Ranging System

P.S. Cain, D.R. Hall, R.L. Hyde, D.G. Whitehead

Applied Physics Department
Hull University, Hull, England.

The U.K. Satellite Ranging Facility is to be sited at the Royal Greenwich observatory at Herstmonceux. It will utilise a Contraves Goertz tracking telescope, in common with the Observatory Lustbühel, Graz.

The receiver package is to be mounted in the Cassegrain focus region, and has been designed and is being constructed at the University of Hull.

The object of this receiver is to:

(a) Image the system entrance pupil onto the detector photocathode.

(b) Accommodate a narrow band filter to reduce background signals.

(c) Provide an area for density filtering and a protection shutter.

This has all to be contained in a volume situated within the telescope yoke.

To satisfy all these requirements it is necessary to produce an overall demagnification of x 15 in two stages.

(a) A beam reducing telescope reduces the collimated telescope output by a factor 3 to enable the narrow band filter étendue to be accommodated The density filter and a backscatter shutter is also sited in this part of the beam.

(b) A lens, situated within the detector housing demagnifies by 5 to finally image the telescope mirror onto the photo cathode (0.5m to 2mm). The detector is a Varian photo-multiplier (152S) and the sub system is designed to detect single photo-electron events using the four stop Event Timer designed and built by the University of Maryland.

Fig. 1 shows the receiver package and Fig. 2 the overall scheme.

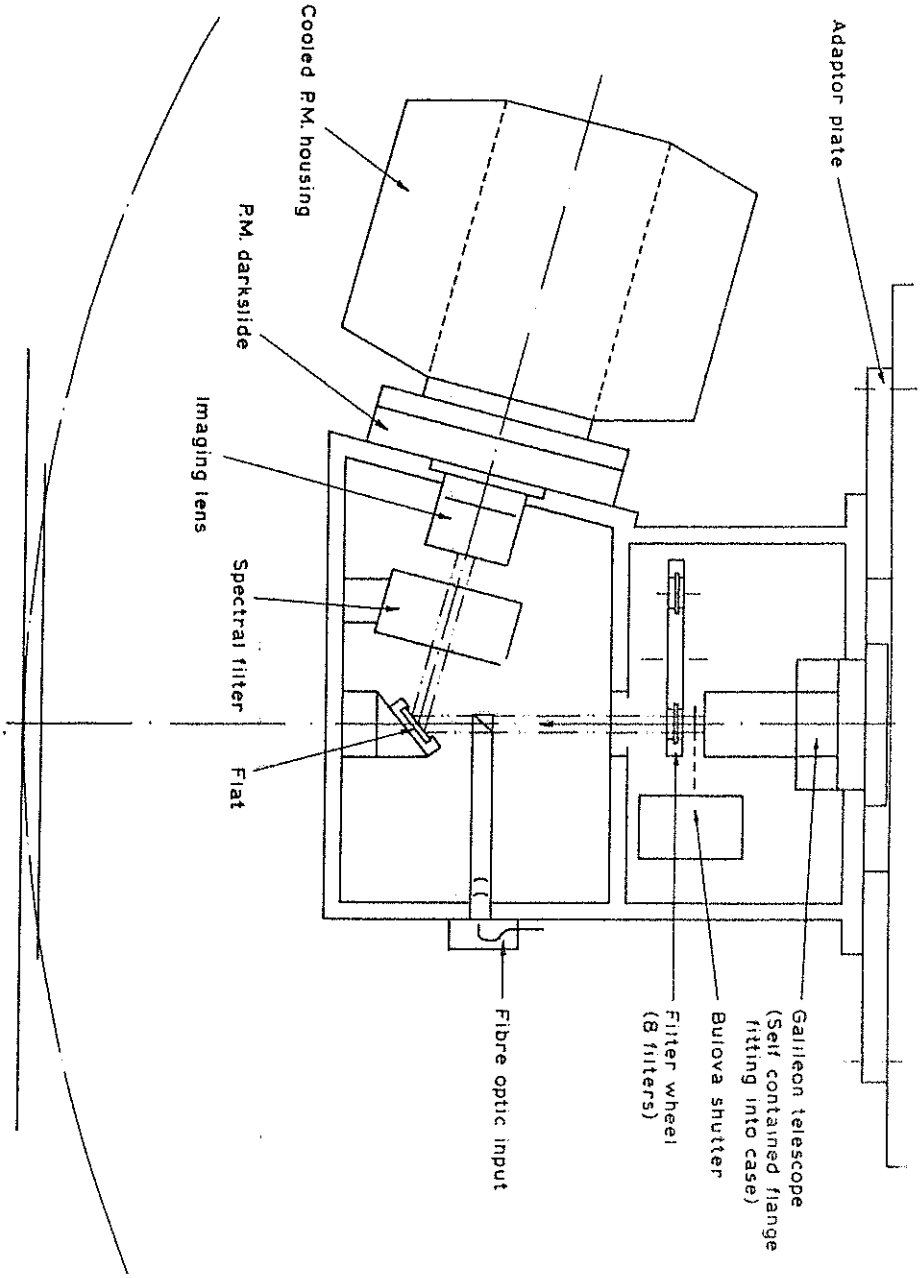

Fig. 1 Receiver: Optical Package.

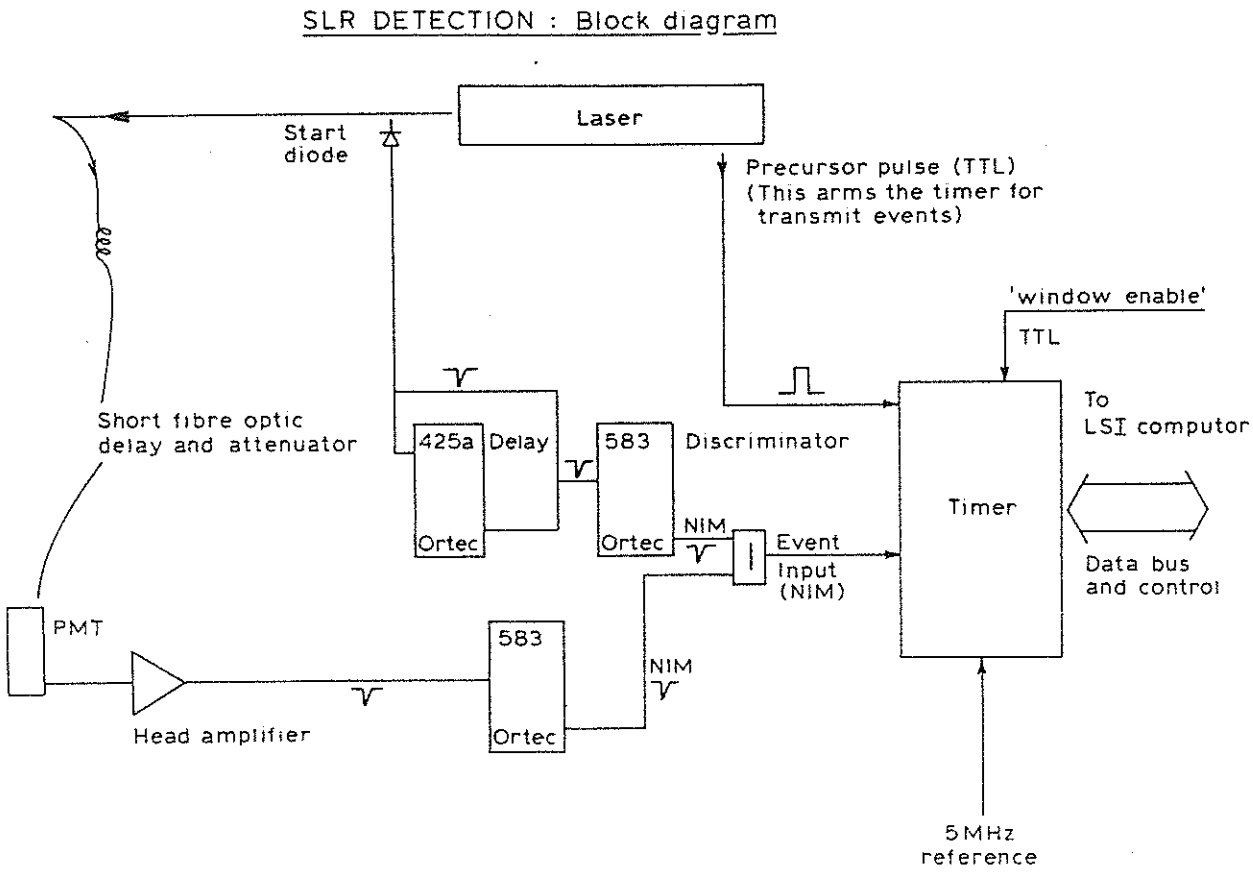

Fig. 2 Receiver: Overall Scheme.

DIGITAL VS ANALOG RECEIVED SIGNAL PROCESSING RESULTS IN 4 NS PULSE LASER RADAR

W.KIEŁEK, A.JASTRZĘBSKI

Technical University of Warsaw, Poland

and

K.HAMAL

Technical University of Prague, Czechoslovakia

INTERKOSMOS group

I ABSTRACT

The results of experimental comparison between some analog and digital estimates of delay at Interkosmos Laser Radar at Helwan for 4 ns laser pulse are described. Results indicate that the digital, software implementations are much better than analog ones for the mean value of result change with signal level. For digital case, there are also results of the influence of number of digitized points on the accuracy.

II INTRODUCTION

We tried to compare the quality of some analog and software digital implementations of the delay estimates using the 4 ns laser station calibration link in Helwan. Comparisons were done for the following estimation methods: analog fixed threshold and half area /median/, and digital software half area /HA/, center of gravity /CG/, half max /HM/, and filtering matched to the signal shape with subsequent finding of the maximum /NML/.

III METHOD OF MEASUREMENTS

The received signal strength control was done via the iris change at the photoelectric receiver. The connections of the electronic instruments used are shown at Fig.1. To make comparisons for the same trials of the signal, we used parallel connection of 2 systems. The analog system of half-area estimate implementation [1] consists of analog integrating circuit, followed by analog constant 0.5 fraction discriminator [2], and PS 500 time interval meter. Constant threshold system consists of constant threshold discriminator built according to [3], followed by minimum range gating circuit and Hewlett-Packard 5360 time interval meter. The digital system consists of the previous one, equipped additionally with Tektronix type 7912AD Programmable Digitizer and Hewlett-Packard 9830 desk-top calculator. The shape of the received signal, at the output of photomultiplier tube PMT, f/t/, /Fig.2./. was digitized and stored in HP 9830. The time interval from the start pulse to the t_R moment of time at Fig.2. was registered in time interval meter. This t_R moment of time occurs when the input signal level crosses, for the first time, the discrimination level of the constant threshold discriminator /set at approx. 120 mV/. The t_R moment of time should be always at the same place at the digitizer screen independent of the input voltage level. But due to some instability of the threshold, and also due to inadequate model of the threshold, there is some instability of this time value.

IV ESTIMATION METHODS

Reiffen and Sherman [4] have showed that the maximum likelihood estimate of delay, for Poisson statistics, can be implemented by the filtration of the incoming pulse signal with the filter matched to the logarithm of the signal shape /quantum limited case/, or matched to the signal shape /high level of additive noise case/ followed by locating the maximum in time. In our case, characteristics of the matched filter must be

composed of the response of the photomultiplier tube, and additional filter. Registering of signal shape of PMT, we need to filter this signal by addi onse only. This additional filter can be obta 1PE pulse time shape and transmitted pulse d of troubles with de-convolution in ti screte fast Fourier transforms of transmi nals, matched and additional filters, he width of matched filter time response r than the width of f_{SER}. From this pe of additional filter time response f such filter in time domain are, may ency domain such filter is fully re mputations of Fourier coefficient

The tim s stable. To compensate for tr ability, there exists the possib btain the additional filter ch ed pulse. Having 1 digitizer tics of additional filter usin the transmitted pulse from uares method.

Othe xed threshold, analog and etector, and digital imp tector. This last one 5], maximum likeli- error/ estimate

that the maximum l t for the ones tatistics, can be ng pulse signal wi nd the digitization e signal shape /qu g using only al shape /high lev e receiving sig- ting the maximum in error, we inter- matched filter must s interpola- hts and 3-d

degree polynomial to approximate the signal between each pair of digitized points.

V RESULTS

Examples of laser pulse used are given at Fig.1 together with mean shape of this pulse obtained using least squares method. Some deterioration of shape when using semiconductor photodiode is visible. Table 1 gives the correlation coefficients between some characteristic time moments in this pulse, and also the standard deviations of them from position of the same moment in mean pulse. Some statistics of signals received from ground target as obtained on 18.07.79., are given in Table 2.

We obtained in some cases non - Poisson results for the number of photoelectrons distribution in the signal reflected from the target. We obtained the variance smaller than expected, the coefficients of this decrease are given in Table 2. It is somewhat strange, when having in mind, that besides of Poisson fluctuations, there are here also transmitted energy fluctuations /± 15%/, atmospheric turbulence and eventually target fluctuations from coherent effects. Probably the last effect does not exist due to, may be, greater than 120 kcps bandwidth of our laser or due to reflecting properties of our wooden, painted, flat target.

The results of comparison of the estimation methods quality, can be seen at Figs 3 and 4 for the material obtained on 18.07.79. In tables and 6 there are the comparisons of results for matched to the signal shape filtering and half-max, when using time steps 98 ps and 686 ps.

The material obtained on 17.07.79. is similar; then, statistical error is of no great influence for the results. The results can be summarized as follows:

a/ time interval bias change with signal level is substantially greater for analog systems than for digital ones

b/ the improvement in standard deviation of results for near maximum likelihood estimate is also substantial

c/ unexpectedly, we obtained better results of both parameters for digital half area, than for digital center of gravity estimate. Also unexpectedly, the results for digital halfmax are better in standard deviation than for both above mentioned. The best are results for near ML estimate /filtration matched to the signal shape/.

We are not succesful up to this time in developing good digital ML estimate. Our filter matched to the logarithm of the signal is not in order - there are fluctuations at the signal after filtering. Due to this effect, the results for such filter are better in standard deviation than for other processing methods for smallest number of photoelectrons only /Fig.3/. We plan to improve this filter, but we have no idea about the fault yet.

The interpolation method used for the signal digitized with the big time step of 686ps was fully succesful. The results of processing for such signal are nearly the same as, for original signal digitized with the 98 ps time step. The differences obtained for such signal in relation to the results of Figs 3 and 4 are summarized in Table 3.

Due to slowness of the measurements /hours/, the long-term stability of measuring system is of value for the results. Also the statistical error can be big for used sample size. But the results obtained on 18.07. are similar to the ones obtained on 17.07., so the influence of the statistical error can be much smaller than bounds.

The analog components of digital circuit, such as constant threshold discriminator, or digitizer and time interval meter trigger circuits can be the sources of errors, especially for long passes. Using adequate model of work of threshold discriminator is of some value for the results too.

The tables of correlation coefficients /Tables 4, obta-

ined for original received signals/ reveal above 90% correlation between half-max and near maximum likelihood estimates. The difference in results between them is small for standard deviation and, unexpectedly, for bias too /Figs 3 and 4/.

VI REFERENCES

1. Hamal, K.et al. Observations of Artificial Satellites of the Earth, No 19 /Interkosmos publication/
2. Polish patent No 102469
3. Basiładze, S.G., 1972; International Institute of Nuclear Research, USSR,Dubna, Report No 13-6331
4. Reiffen, B., Sherman, H., 1963; IEEE, p.1316
5. Bar-David I., 1969. IEEE Trans. IT-15, p.31
6. Bar-David I., 1975. IEEE Trans. IT-21, p.326

Table 1. Laser signal data

Moment of interest	Stand. dev. ns	Cross-correlation coefficients					
		CG	HA	MX	HMX	FR	MR
CG	.12						
HA	.10	.70					
MX	.14	-.34	-.48				
HMX	.11	-.08	-.34	.02			
FR	.11	-.10	-.36	.12	.87		
MR	.20	.04	-.38	.15	.39	.28	
FT	.18	.44	.27	-.34	.55	.49	.24

where:
CG-center of gravity
HA-half area
MA-maximum
HMX-half max. at front
FR-half /in voltage/ of the fast rise region at front of the pulse
MR-Point in time, at which the derivative of voltage is first time half of its max. value at front of the pulse
FT-fixed treshold

Table 2. Signal from target data.

Iris No	7	8	9	9
Mean value of the amplitude /mV/	848	413	209	205
No of trials of the signal	29	26	24	27
RMS value of deviations of the amplitude /mV/	202	103	77	57
Mean value of the area /mV.ns/	8130	4128	1723	1820
RMS value of deviations of the area /mV.ns/	1645	1038	592,5	535
Variance of area decrease coefficient in relation to Poisson distribution	1	1,25	1,6	2,1

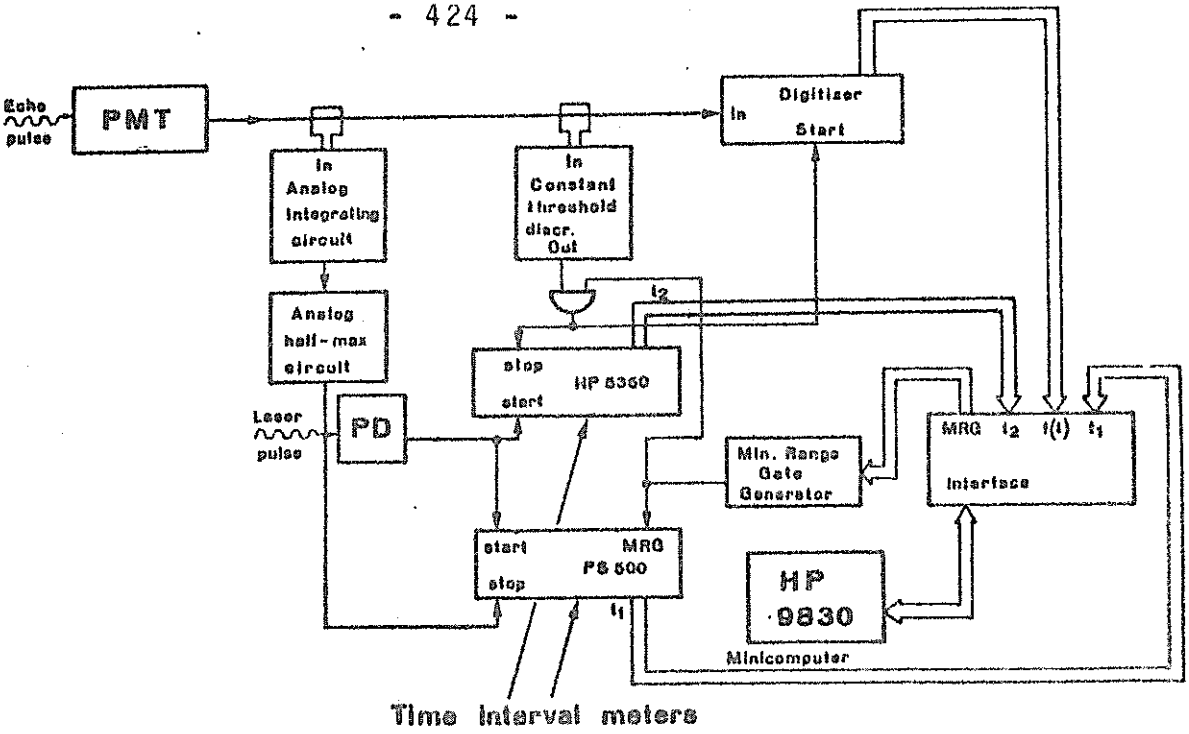

Fig.1. Scheme for the analog and digital time delay estimates comparisons.

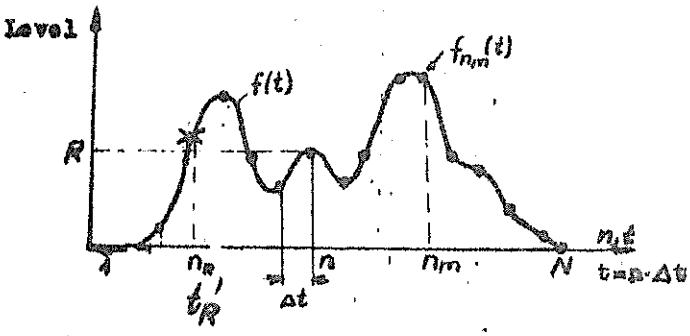

Fig.2. f(t) example at the digitiser

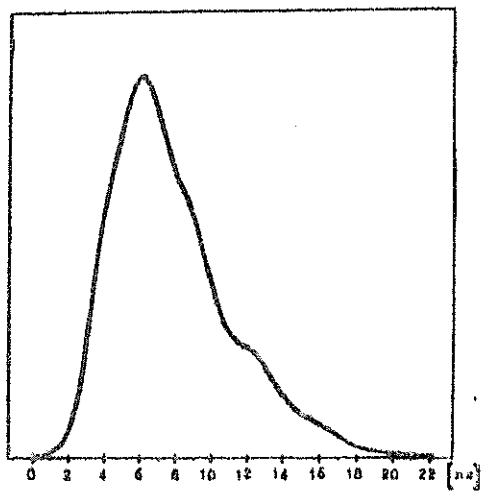

Fig.5. Averaged shape of transmitted pulse from the sample on 21.07.

Influence of digitization time step - differences in cm

for mean value - Table 5 for standard dev - Table 6

PE	CG	HA	HM	ML	NML	CG	HA	HM	ML	NML
5,37	0	0	-1,5	-4,5	-1,5	-0,15	-0,3	-0,15	+0,07	-0,3
6,25	-0,7	+0,4	-0,6	-3	0	+0,15	+0,15	-0,15	+1,9	+2,1
14,6	0	0	0	0	0	+0,3	+0,15	0	+0,3	-0,15
28	0	0	0	-1,5	-1,5	0	-0,15	0	-0,15	-0,15

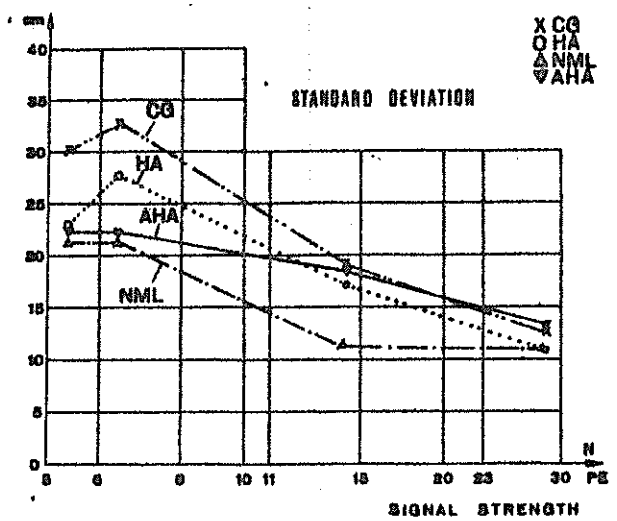

Fig. 3a

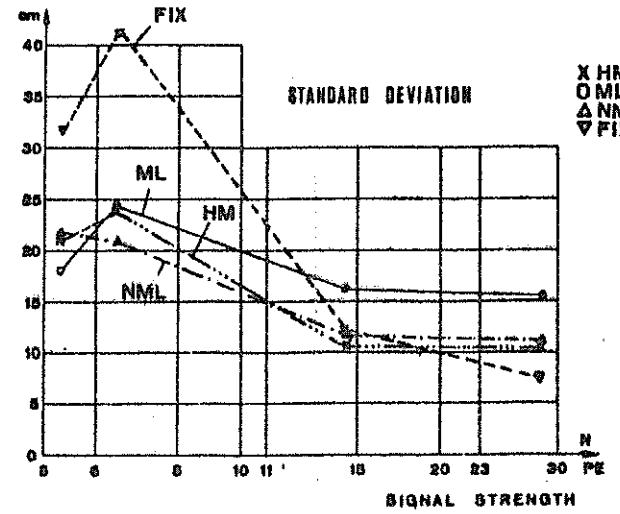

Fig. 3b

CG center of gravity

HA digital half area

HM half max

NML filter matched to the signal shape

AHA analog half area

FIX fixed threshold

Tables 4. Correlation coefficients in %

6 photoelectrons

	CG	HA	HM	NML	AHA
HA	93				
HM	68	74			
NML	63	74	96		
AHA	80	92	75	77	
FIX	77	83	95	93	76

11 photoelectrons

	CG	HA	HM	NML	AHA
HA	90				
HM	38	46			
NML	57	66	91		
AHA	66	69	34	47	
FIX	57	58	63	66	83

23 photoelectrons

	CG	HA	HM	NML	AHA
HA	87				
HM	61	62			
NML	71	75	97		
AHA	50	67	47	37	
FIX	52	54	45	50	67

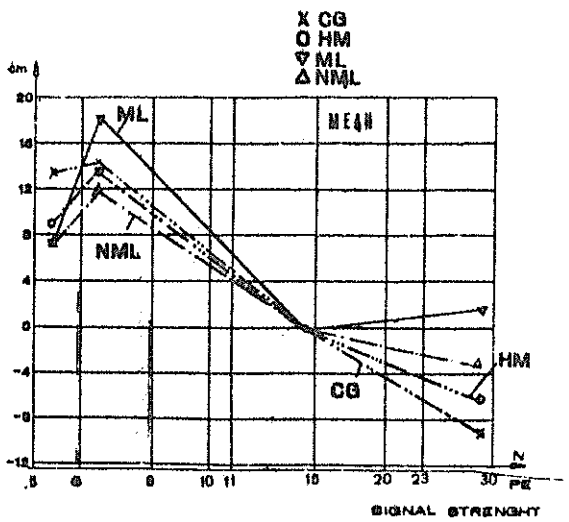

Fig. 4a

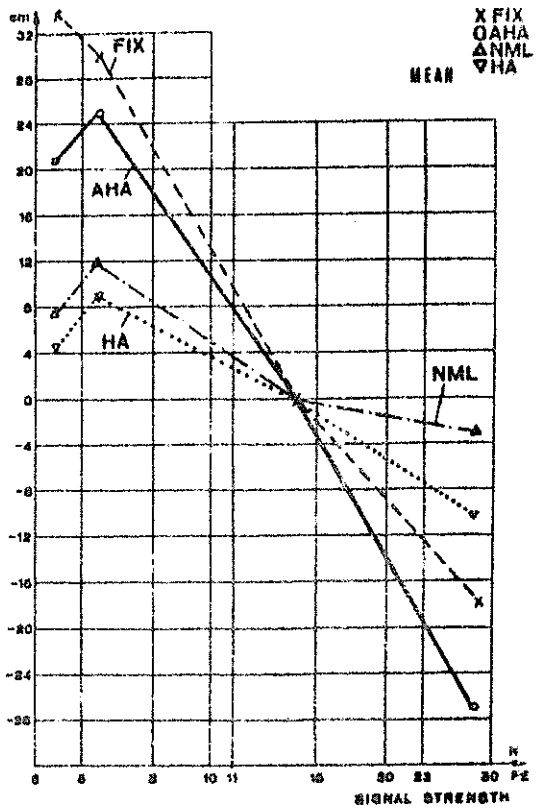

Fig. 4b

COMMENTS ABOUT RECEIVED ENERGY FLUCTUATIONS

W.KIEŁEK

Technical University of Warsaw, Poland

K.HAMAL

Technical University of Prague, Czechoslovakia

S.SCHILLAK

Borowiec observatory, Poland

INTERKOSMOS group

There exists the opinion, that laser reflections from goedetic satellites, in multielectron case, fluctuate nearly exponentially in energy due to coherence effects at retroreflector([1], [2], [3], [4]). Some experimental results are in agreement with this opinion (see Fig.1 drawn from [5]). But some our results from Borowiec 1-st generation station in Poland are only of little fluctuations (Fig.2).
Coherence effects are independent on energy, and are of the type, that when do not exist once, do not exist at all.
Our opinion is, that this effect does not exist, at least in the case of our multimode 20 ns laser. One possible explanation of this phenomenon can be as follows: Suppose, that the laser is not of single frequency, but the spectrum occupies some bandwidth, and is continuous or discrete but uniformly filled with energy. The retroreflector array normally has got some depth, or is tilted. When the difference in number of wavelengths at the target depth is near one or greater for extreme frequencies of laser frequency band, all possible phases instead of one phase from each individual corner cube are present at the receiver aperture. This is the situation as in the case of incoherent light, and amplitude fluctuations are absent.

This realizes typically for about 700 MHz bandwidth, which means spectral line width of 0.05 A^{o}. The bandwidth of laser

can be smaller than this value or as great as 10 GHz for some multimode YAG, and both possibilities exist, to have or not to have coherency effects in the case of satellite retroreflections.

After inventing of this explanation, we found the similar opinion in [7].

The difference in wavelength number for extreme frequencies of laser frequency band at the distance between the plane at the satellite, parallell to the receiver aperture, and this receiver aperture, can not give similar averaging effect. But the explanation given in [7] at page 112 is unconvincing for us. Due to lack of space, our own explanation is available at request.

For the calibration link and flat, wooden, painted target we obtained, in our opinion, Poisson and PMT gain fluctuations only, in case of 4 ns laser at Helwan, summer of 1979 - see Table 1 and Fig.3.

For the sample of 60 calibrations of 20 ns laser at Borowiec, for approx. 200 PE signals, the fluctuations are greater than Poissonian, but can be explained by PMT gain, atmospheric turbulence and transmitted power fluctuations, being typically 17 % for standard deviation in relation to mean value.

Then, in our opinion, the "rough target" concept, developed for radio and microwave region targets [6] is inapplicable for our case.

Literature

1. J.I.Bufton, R.S.Iyer, L.S.Taylor. Applied optics vol.16 No 9, p.2408-2413
2. J.L.Bufton. Applied optics, vol.16 No 10, 1977, p.2654--2660
3. D.A.Arnold. SAO Special Report No 382, p.117-149
4. D.A.Arnold. Optical and IR transfer function of the Lageos retroreflector array. SAO Report for NASA, May 1978, p.159-178
5. M.Pearlman et al. Lageos orbital acquisition and initial assessment. S.A.O. report, 1976
6. R.L.Mitchell. Radar signal simulation. Artech House, 1976 pp.17,22,23,32
7. R.H.Kingston. Detection of optical and IR radiation. Springer, 1978, pp.110-113

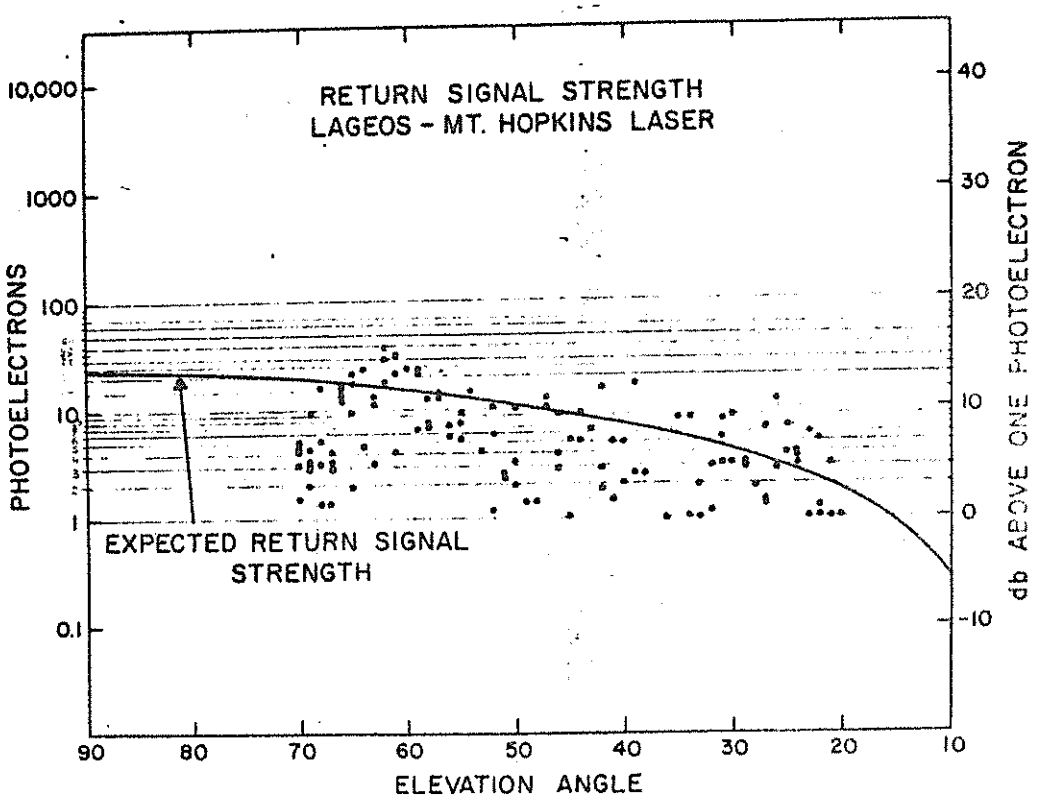

Fig. 1 Example of satellite signal strength data, Mt Hopkins USA

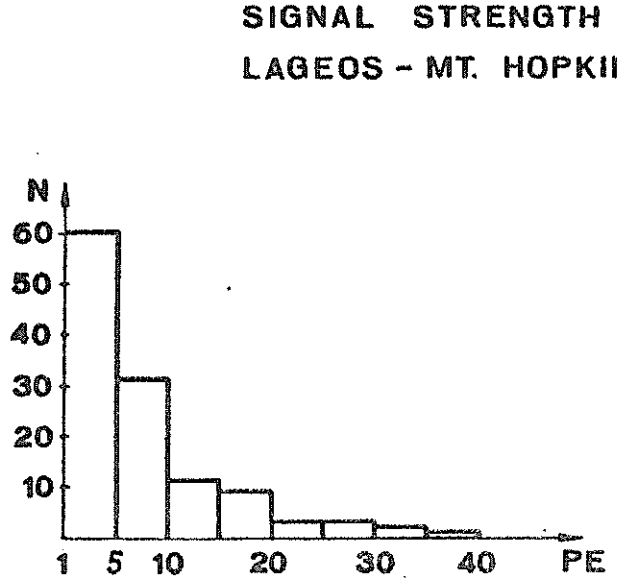

Table 1. Characteristics of target calibration signals, Helwan

Mean signal strength in PE	5,3	6,3	14,6	26,5
Standard deviation in PE	2,36	2,44	2,36	5,36
Variance decrease coefficient in relation to Poisson density	1,5	1,95	1,2	0,92

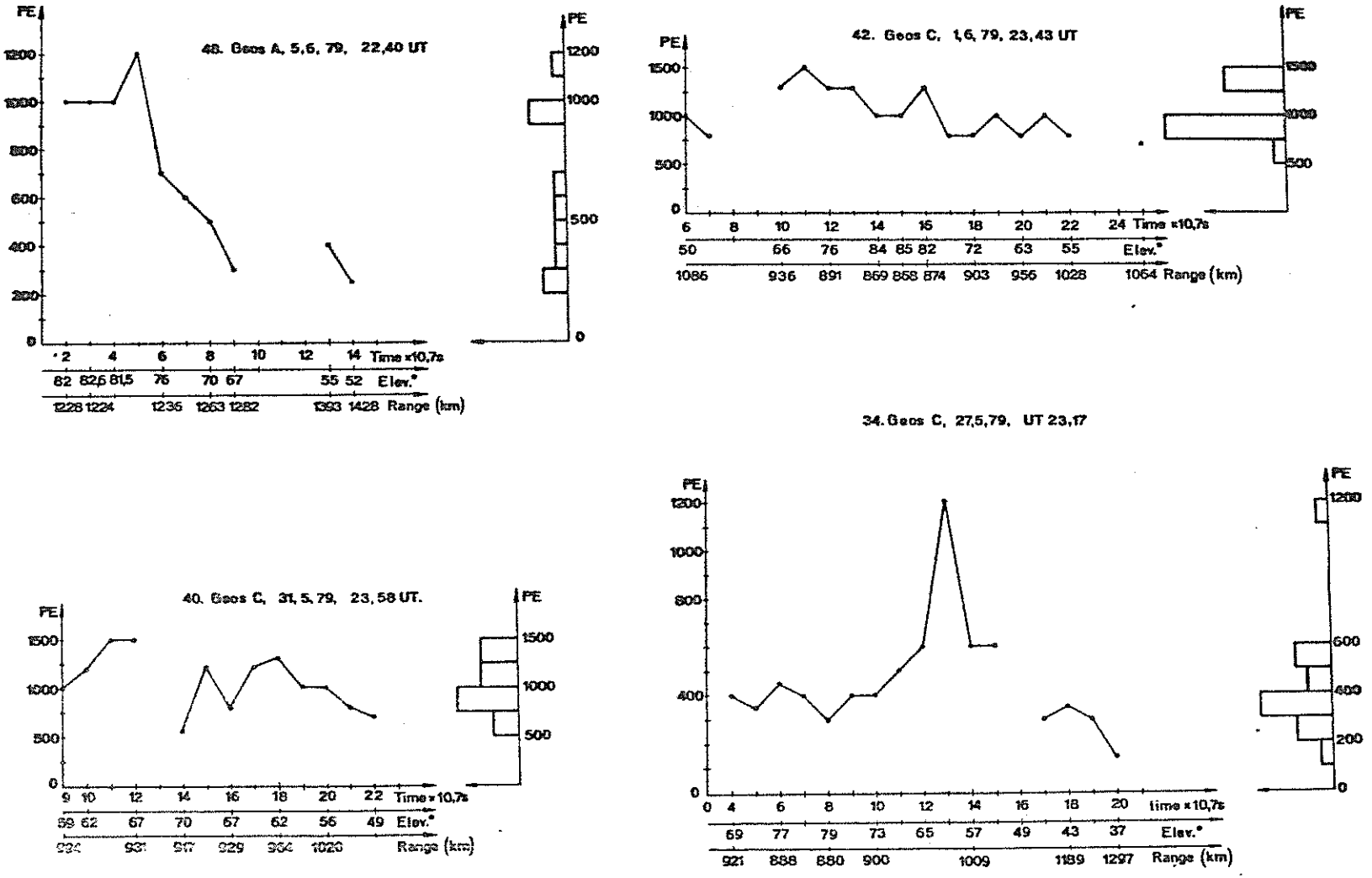

Fig.2. Examples of satellite signal strength data, Borowiec, Poland

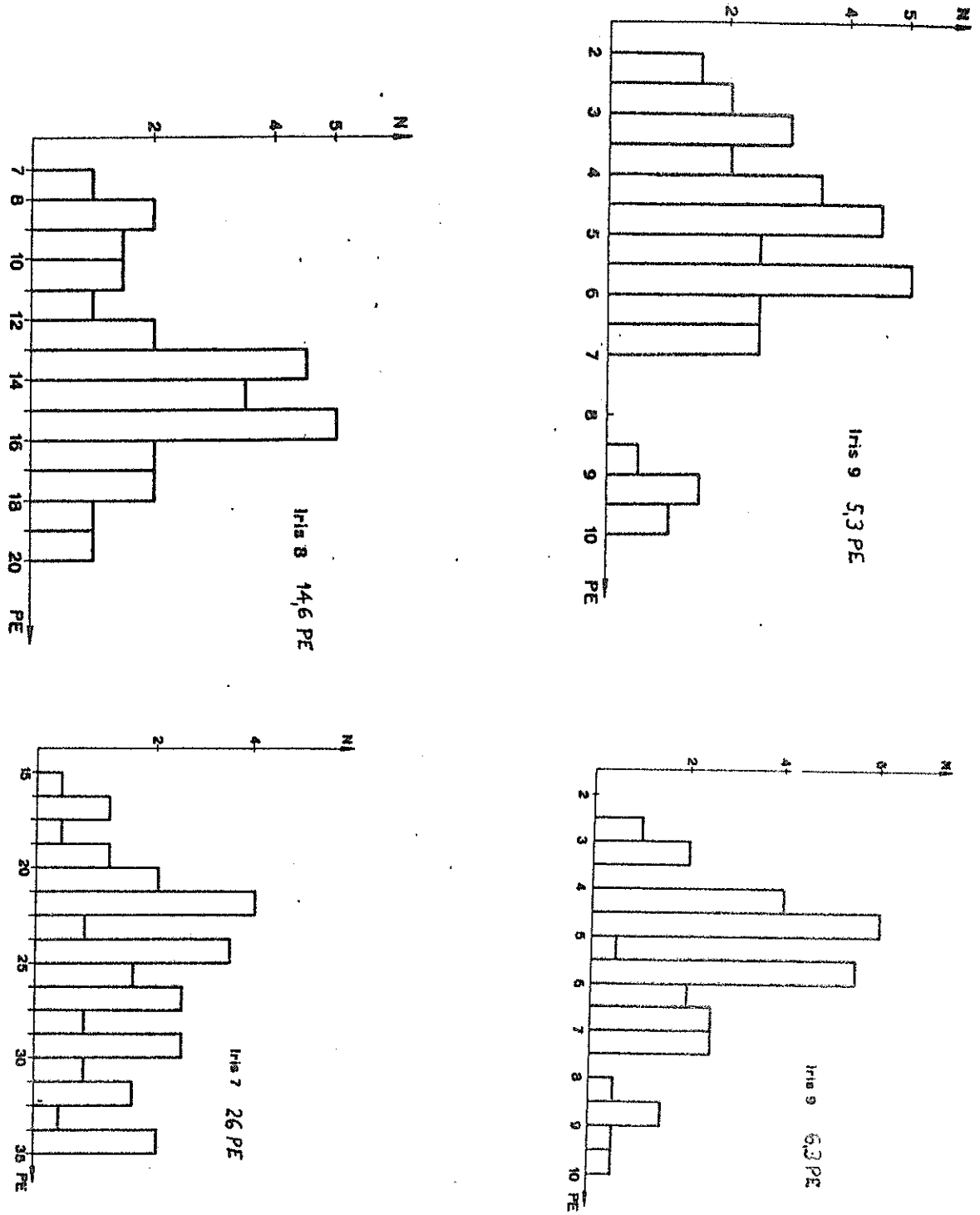

Fig.3. Calibration target signal strength densities, Helwan, Egypt.

USE OF APPROXIMATED MATCHED FILTERING AND PHOTON COUNTING IN SATELLITE LASER RANGING

Matti V. Paunonen*

Finnish Geodetic Institute
Ilmalankatu 1 A
SF- 00240 Helsinki 24, Finland

1. INTRODUCTION

The application of matched filtering in estimating the arrival time of a light pulse is well known /1-3/. The photoelectron impulses are applied to a filter with an impulse response of $\ln [1 + S(T_d-t)/n_B]$, where $S(T_d-t)$ is the delayed, time-inverted shape of the signal intensity, and n_B is the background noise rate. The peaking time is then the best estimate of the arrival time (the maximum likelihood estimation). The filter shape $S(T_d-t)$ has also been shown to give good results with Q-switched laser pulses, especially under high background noise/4/.The implementation of these filters can be somewhat tedious, and so approximate forms are also worth studying /5,6/.

The return signal from the distant LAGEOS satellite (height 6000 km) is about 1000 times weaker than the signal from the close Earth satellites and may contain only single photoelectrons. A technique called photon counting can then be used.

This report describes the detection equipment and some results of the use of approximated matched filtering both during night and daylight operation and photon counting

---

*Also with the Communications Laboratory, Helsinki University of Technology, SF- 02150 Espoo 15, Finland

in satellite laser ranging at the Metsähovi laser station.

2. EQUIPMENT

The ranging apparatus is described elsewhere /6/. In the receiver the photoelectron impulses from the photomultiplier (RCA 8852 and C 31034 are used) are filtered using an amplifier-filter with an impulse response shape best described by

$$h(t) = t \cdot \exp(-t/\tau), \quad t \geq 0 \qquad (1)$$

which is a low-order approximation (two low pass stages) of the Q-switched laser pulse shape, adequately given by $\exp(-t^2/2\sigma^2)$, with proper τ and σ to give equal half-widths. The time interval counter (Nanofast 536B, M/2 half-maximum timing unit, resolution 0.15 ns) detects the 50% point of the incoming pulse. The duration of the laser pulse and the impulse response of the detector system are about 25 ns. The start pulse is filtered in the same way, to lessen the effects due to laser mode interference. Theoretical degradation in the resolution with respect to the optimal scheme is by a factor of 1.47 /8/, if no background noise is present. Because the average timing point depends on the photoelectron content of the received pulse /9,10/, it is necessary to calibrate the system using the signal levels expected in the ranging. The trigger levels used are 1, 6 and 15 photoelectrons for LAGEOS, STARLETTE and GEOS-3, respectively. The level of amplification is adjusted by the feed voltage to the photomultiplier.

3. RESULTS

3.1. Calibration measurements

Calibration measurements are performed using a flat target at a distance of 333 m. The resolutions of an analog median detector /11/(integration with long RC-time constant and 50% detection) and the approximated matched detector under discussion were found to be very similar when the return energy was high (more than 200 photoelectrons). The r.m.s. resolutions of a single shot were in the range 0.5 to 0.8 ns using about 600 photoelectrons. When the average return was 10 times smaller, the performance of the approximated matched detector appeared to be somewhat better. The return signal at the signal levels was highly fluctuating. The timing shift was less than 1 ns.

In order to test the instrumental resolution the ranging operation was performed to a diffusely reflecting plate at a distance of 4 m from the photomultiplier. The standarddeviation of a single measurement was 0.23 ns after removing a slight timing drift and observations deviating by more than three times the standard deviation(5 out of 116 observations).

3.2. Ranging to satellites

Range observations to satellites have been performed since 1978. Two examples of range residuals after short arc orbit fitting are shown in Fig. 1. The standard deviations are 0.27 m and 0.22 m. No deletions were made. Generally the precision has been in the range of 0.3 m to 1 m in night work.

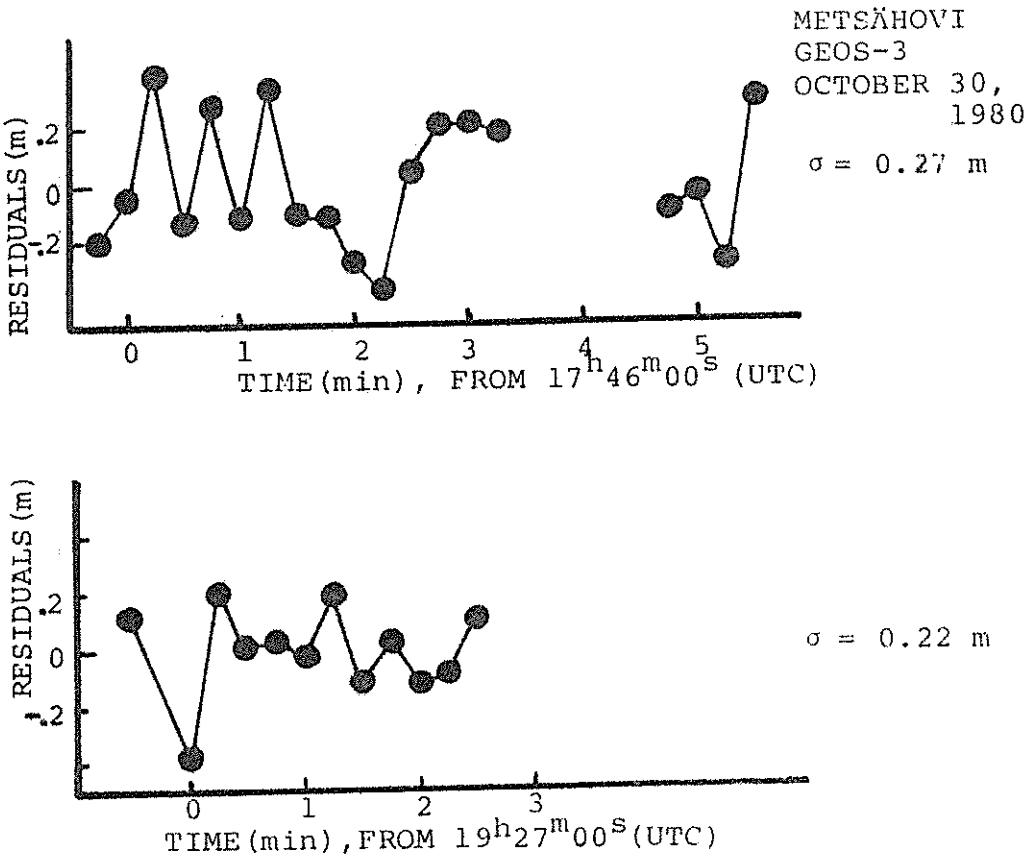

Fig.1. Two examples of range residuals after short arc fitting.

Some improvement in performance could be obtained, at least theoretically, by preintegration before the filter (i.e. moving towards median detection). The error performance of this method, both in resolution and bias, has been found to closely approach the ideal /10/ if the pulse and filter shapes are equal Gaussian. The method could also be called filtered median detection. This principle, using the filter given by Eq. 1, is at present being tested in ranging to satellites.

3.3. Daylight ranging

Daylight operation was recently found feasible with the equipment in use. The field of view of the receiver was reduced to 1.2 mrad and the voltage of the photomultiplier RCA 8852 to -1650 V, which produced an anode current of 0.3 mA. The appropriate PMT voltage was obtained by adjusting the voltage until the counter was stopped by the background noise not more than once per 10 dummy trials. The time offset of GEOS-3 and its time derivative were determinated from the preceding night's observations. On November 5, 1980, six concecutive passes of GEOS-3 were observed. The first two of these were under a bright sky, the next just after the sunset and three passes were observed in darkness. The data from short arc orbit fits are shown in Table 1. The quality of the measurements of the daylight passes differs little from that obtained in darkness. This demonstrates the advantage of the approximated matched filtering under high background noise conditions.

Table 1. Short arc orbit fits of GEOS-3, Nov. 5, 1980

Time (UTC)	Pass duration	Observations	Obs.	Fit (m)	Light conditions
$11^h20^m31^s.4$	3^m45^s	13	13	0.57	Daylight
12 59 31.4	5 45	19	17	0.52	"
14 38 16.4	6 00	14	13	0.53	Sunset 14^h17^m
16 17 01.35	5 15	15	15	0.51	Dark
17 54 31.4	7 15	18	18	0.83	"
19 34 01.55	5 15	17	17	0.91	"

3.4. Photon counting and ranging to LAGEOS

The range equation for LAGEOS predicts a signal about 1000 times weaker than that from GEOS-3. For this reason its ranging is generally considered difficult for systems designed mainly for close orbiting satellites. Because signal prediction left some hope to acquire LAGEOS, attempts at ranging have been made at the Metsähovi station from the very beginning. The gain of the photomultiplier (RCA 8852) was increased (voltage -2500 V, gain about 10^8) until single photoelectrons triggered the timing discriminator. Hence the first photoelectron within the range window, whether signal or noise, stops the counter. This method is called single photoelectron detection, or photon counting. It is well known in nuclear electronics and is also regularly used in ranging to the Moon /12 / and now also in satellite laser ranging/13,14/.

The propability of occurrence of the first photoelectron is /15/

$$R_1(t) = NS(t)\exp[-N\int_0^t S(t')dt'] , \qquad (2)$$

where N is the average photoelectron content of the pulse and S(t) its normalised shape. When the signal is very weak, say less than 0.1 photoelectrons on average, $R_1(t)$ can be approximated as /15/

$$R_1(t) \propto S(t) . \qquad (3)$$

The probability also follows the illumination curve. The variance of the occurrence time is the same as the variance of the pulse shape. For Gaussian light pulses the timing standard deviation is

$$\sigma_t = 0.425\ T,$$

where T is the pulse duration (FWHM). The effect of single electron time jitter of the RCA 8852 photomultiplier is insignificant with 25 ns long laser pulses.

Use of a higher threshold quickly invalidates the photon counting method. If the average return rate is 30% , use of the threshold of two photoelectrons would give six times fewer signal counts.

The photon counting method can effectively be used only under low noise conditions, i.e. dark sky and a cool detector, without multistop counters. The range gate used, 10 - 20 μs, has been sufficient to give a satisfactory signal-to-noise ratio. Noise counts have sometimes amounted to 10-

20 %,but this does not yet represent any significant loss in signal counts or difficulties in signal recognition.

The summary of the LAGEOS observations for the period of March-April 1980 are shown in Table 2. The average precision is 0.9 m after slight statistical screening of the observations.

Table 2. LAGEOS observations in March-April 1980

Date	Time (UT)	Pass duration	Obs.	Sterne orbit fit Deleted	σ/m	Polynomial O-C fit Deleted	σ/m	Degree
10 III	$18^h22^m15^s$	20^m30^s	16	0	1.52	o	1.46	4
13	17 50 15	26 00	39	4	0.84	4	0.87	6
13	21 28 30	18 15	27	2	0.69	2	0.63	4
14	19 58 45	28 30	60	-	-	3	0.51	6
15	18 36 15	28 15	42	3	0.80	2	0.53	6
16	17 12 00	27 15	15	2	1.28	2	1.09	4
19	20 11 45	29 45	27	1	0.97	1	0.76	6
20	18 46 45	34 15	50	-	-	4	0.93	6
22	19 46 15	21 45	18	3	0.82	2	1.17	4
23	18 12 45	33 30	48	-	-	3	0.78	6
23	22 05 00	9 15	8	0	0.60	0	0.93	2
24	20 28 30	22 30	21	1	0.96	1	0.86	4
25	19 02 00	33 15	29	4	1.20	3	1.34	6
22 IV	19 45 30	25 00	20	0	0.83	0	0.88	4

Median 0.88 m
Arithmetic mean 0.91 m
Deletion level 6.5 %
Quadratic mean 0.95 m
Weighted mean (pooling) 0.88 m

An example of range residuals in a short arc fit are shown in Fig. 2. Three observations with deviations of 4.1 m, 1.9 m and 1.8 m were deleted. It is probable that not all events are single photoelectron ones. This does not adversely affect the ranging precision because of the smoothing property of the approximated matched filtering. In a monitored pass (April 22) there were 20 signal events from 102 trials and 5 noise events. Most events were seen to contain a single photoelectron and only two larger pulses containing two photoelectrons were noticed (RCA 8852 tube with high gain first dynode is suitable for estimating the photoelectron content at this level). The fit obtained, 0.83 m, conforms well with the data obtained in March.

In ranging to LAGEOS averaging can be used over three

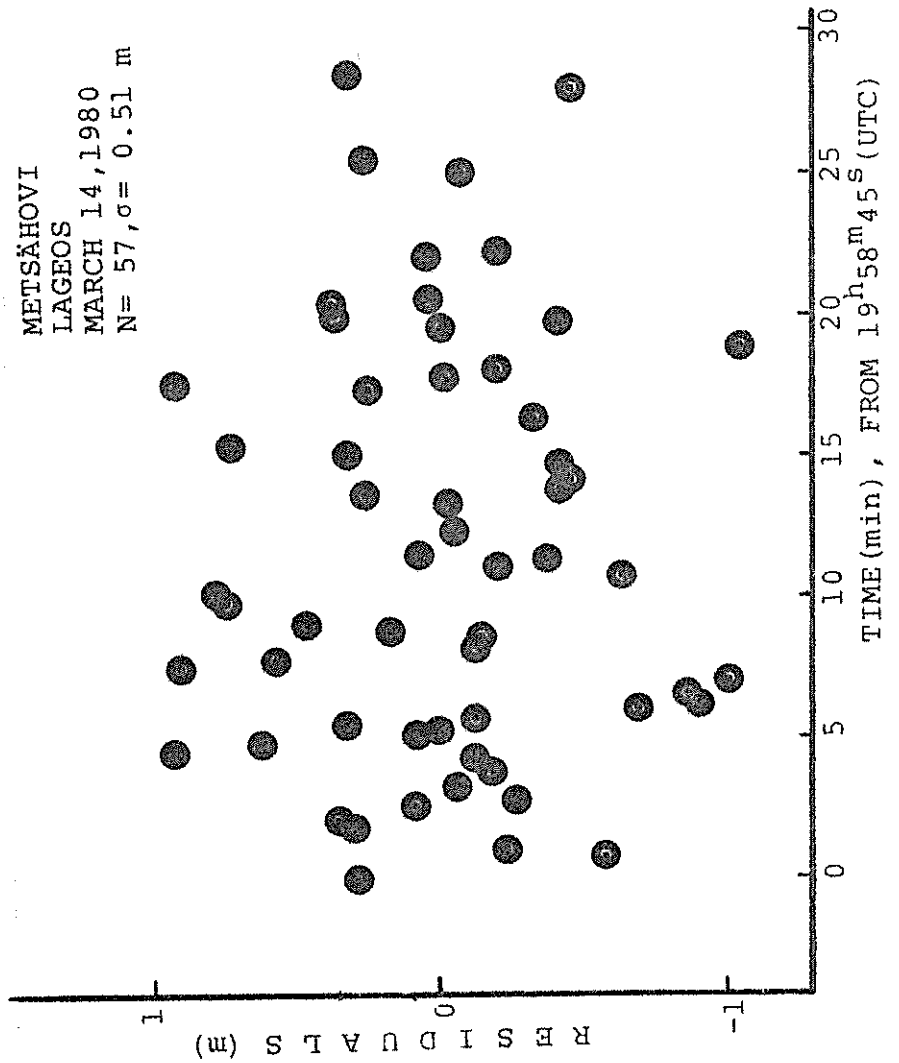

Fig. 2. Range residuals in a LAGEOS pass

minutes, the so-called normal point method /16,17/. Hence the 60 % return rate achieved allows an improvement in precision by a factor of 2.8 (time interval between shots is 15 s). Because the single shot precision has been 0.9 m, the normal point precision could be 0.3 m. This figure corresponds to a relative precision of about $4 \cdot 10^{-8}$. Some passes have shown an even better precision. In the light of these figures, ranging to LAGEOS and the close-Earth satellites gives equal range precision, which is perhaps an unexpected result. The precision achieved is also close to the theoretical value.

4. CONCLUSION

The use of approximated matched filtering in receiving Q-switched laser pulses has been found experimentally to be advantageous, especially in a low-signal regime. Performance in daylight operation was also found to be satisfactory. The same equipment can be effectively used in photon counting, simply by increasing the gain of the photomultiplier.

5. REFERENCES

/1/ B.Reiffen and H.Sherman, An optimum demodulator for Poisson processes: Photon source detectors. Proc. IEEE 51,10(1963)1316-1320.

/2/ I.Bar-David, Communication under the Poisson regime. IEEE Trans. Information Theory IT-15,1(1969)31-37.

/3/ J.B.Abshire, Comparison of measured and theoretical performance of a maximum likelihood laser ranging receiver. J. Opt. Soc. Am. 70,12(1980)1595.

/4/ E.Gatti and S.Donati, Optimum signal processing for distance measurement with lasers. Appl. Opt. 10,10 (1971)2446-2451.

/5/ V.A.Ovsyannikov and A.M.Romanov, Accuracy of timing photoelectron pulses. Sov. J. Opt. Tech. 40,10(1973) 651-652.

/6/ M.Paunonen, Estimation of the arrival time of light pulse using approximated matched filtering. Paper presented at the Third International Workshop on Laser Ranging Instrumentation, Lagonissi, Greece,May 23-27, 1978.

/7/ M.Paunonen, Metsähovi satellite laser ranging station. This conference.

/8/ O.Ojanen, unpublished (1977)

/9/ W.A.Kiełek, Influence of detecting system on the accuracy of laser pulse range meters. Proc. European Conf. on Precise Electrical Measurement (Euromeas.-77), IEE Conf. Publ. 152, 1977, 44-46.

/10/ O.Ojanen, On the analysis of the return pulse of the satellite laser. Reports of the Finnish Geodetic Institute, 79:1, Helsinki 1979, 38 pp.

/11/ A.B.Sharma and S.J.Halme, Receiver design for laser ranging to satellites. IEEE Trans. Instrum. Meas. IM-30, 1(1981)3-7.

/12/ S.K.Poultney, Single photon detection and timing in the lunar laser ranging experiment. IEEE Trans. Nucl. Sci. NS-19,3(1972)12-17.

/13/ C.O.Alley, J.D.Rayner, R.F.Chang, R.A.Reisse, J.Degnan, C.L.Steggerda, L.Small, and J.Mullendore, Experimental range measurements at the single photo-electron level to the GEOS-A and BE-C satellites. Paper presented at the Third International Workshop on Laser Ranging Instrumentation, Lagonissi, May 23-27, 1978.

/14/ E.C.Silverberg, Early laser ranging data with the TLRS. CSTG Bulletin, No 2, Nov. 1, 1980, 70-73.

/15/ S.K.Poultney, Single photon detection and timing: experiments and techniques. Advances in Electronics and Electron Physics (Ed. L.Marton),vol. 31, 1972, pp. 39-117.

/16/ R.I.Abbott, P.J.Shelus, J.D.Mulholland, and E.C.Silverberg, Laser observations of the Moon: Identification and construction of normal points for 1969-1971. Astron. J. 78,8(1973)784-793.

/17/ P.L.Bender and C.C.Goad, Probable Lageos contributions to a worldwide geodynamics control. Proc. Int. Symp. on the Use of Artificial Satellites for Geodesy and Geodynamics (Ed. G.Veis and E.Livieratos), National Technical University of Athens,Athens 1979, pp. 145-161.

DETECTION PACKAGE FOR THE GERMAN/DUTCH MOBILE SYSTEM

H. Visser
Institute of Applied Physics, Delft, The Netherlands

F.W. Zeeman
Delft University of Technology, Delft, The Netherlands

1. Introduction

In a paper entitled "Mount and Telescope for the German/Dutch mobile system", that has been presented during this Workshop, the mechanical and optical configuration of the mobile ranging system has been described. The detection package was left out of the description and this will be presented here. Especially the optical configuration of the detection package has some details that are new in laser ranging. Although the optical/mechanical hardware of the detection system is considerably more complicated than in most laser ranging systems, the operation of the detection system will be simple. In many circumstances the detection system can provide the operator with immediate information on the position of the satellite in the field of view and in the window of the range gate generator. With this information it will be possible to optimize the adjustments of the ranging system so that once the satellite has been acquired it will not easily be lost again because of bad predictions and/or background noise problems.
Because the received light is also directed through the coudé optical train the detection package is mounted in a fixed position at the base of the telescope mount. Such a configuration has the advantages of a less stringent space and weight limitation for the detection package, the controls on the package are always accessible and the number of cables in the telescope mount is considerably reduced.

2. Description of the detection package

In figure 1 the optical configuration of the detection package is presented in a somewhat simplified form. For the ease of the explanation the optical system is drawn entirely in the plane of the paper although in reality this is not true.
As already described in the paper about the telescope mount the received light coming from the telescope is split up at a "dichroic beamsplitter". A wavelength band around the laser wavelength (539 nm or 532 nm, depending on the laser rods) is reflected to the detection optics while the rest of the visual spectrum is transmitted to an eyepiece. The reflected wavelength band is focussed on the "entrance diaphragm" of the detection system. This adjustable entrance diaphragm limits the field of view (FOV) of the detection system to values ranging from 0,05 mrad (10 arcsec) to 1,75 mrad (0,1 degree) in ten discrete steps.
Just in front of the adjustable entrance diaphragm a chopper rotates at a velocity of 10 r.p.s. This chopper is synchronized to the firing of the 10 p.p.s. repetition rate of the pulse laser. The phase of the chopper blade is adjusted so that the hole in the blade is in front of the entrance diaphragm (chopper open) when the return signal from the satellite is expected. The chopper will be closed then at the moment of firing of the pulse laser also for the low satellites. The chopper protects the detectors from stray light of the pulse laser coming from the common telescope system and coudé optics. It also limits the average detector current during day time measurements.

The light transmitted through the entrance diaphragm is directed to a "concave mirror" where it is collimated to a parallel beam of 50 mm diameter. This parallel beam is dispersed by a higher order diffraction grating ("echelle grating").
The theory of diffraction gratings will not be discussed here, it is described in many optical handbooks.

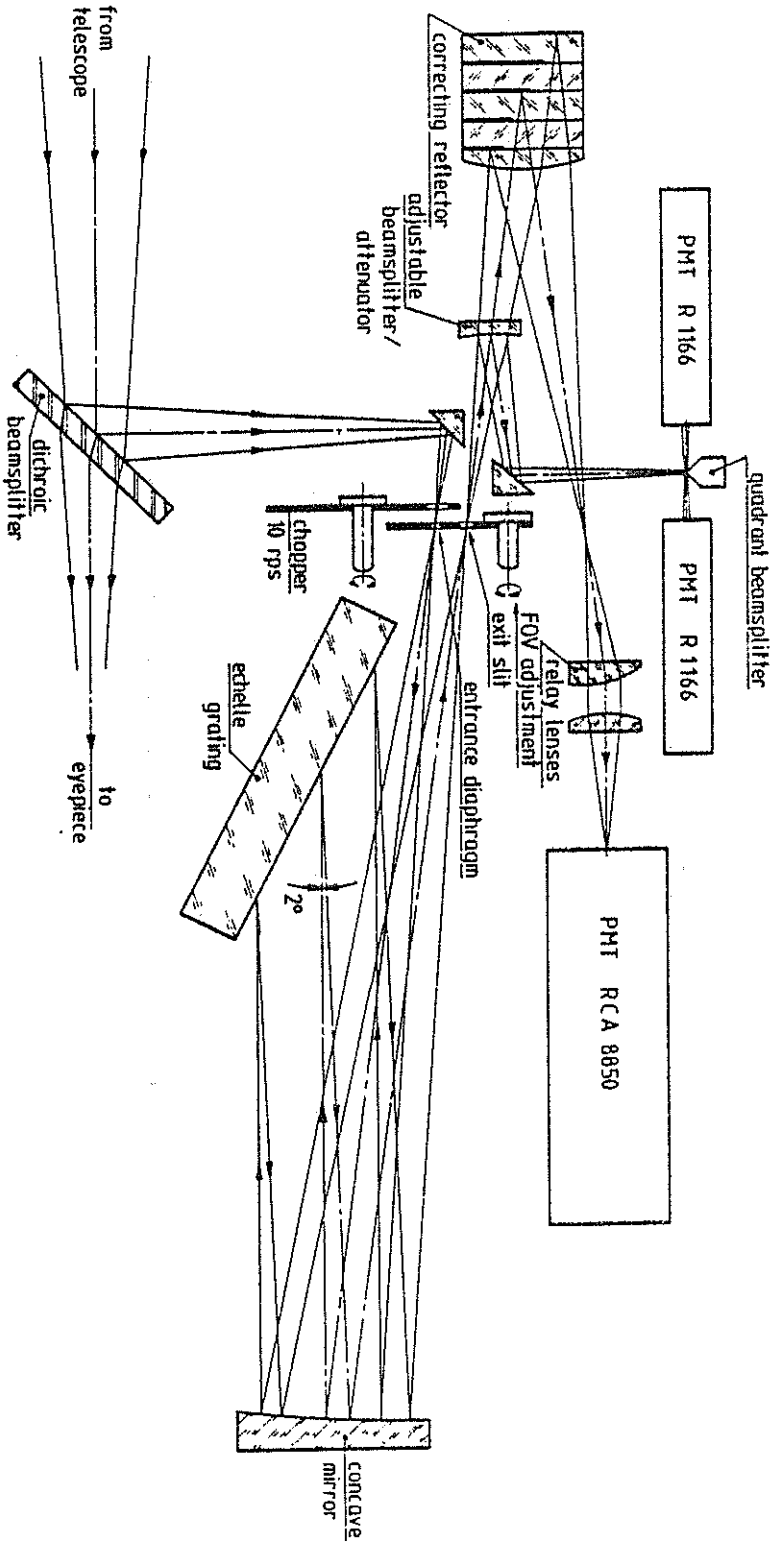

FIGURE 1 OPTICAL CONFIGURATION OF DETECTION PACKAGE

The echelle grating of figure 1 has 300 grooves per millimeter and a blaze angle of 63 degrees. The angle between the incident beam and the diffracted beam of the grating that will be transmitted through the "exit slit" is chosen at 2 degrees. For the laser wavelength the maximum efficiency of this echelle is reached in the 11th order. At the exit slit, that has the same width as the diameter of the entrance diaphragm, a narrow wavelength band around the laser wavelength will be transmitted. The dispersion of the monochromator of figure 1 is such that a one arc minute field of view (FOV) entrance diaphragm corresponds to a wavelength bandwidth of about 0,35 nm. The bandwidth of such a monochromator is proportional to the dimension of the entrance diaphragm in contrast with the fixed bandwidth of an interference filter. The presented monochromator has for instance a bandwidth of 1,2 nm for a 1 mrad FOV and 0,1 nm for a FOV of 17 arcsec; corresponding to 0,35 nm per arcmin FOV.

The use of an echelle grating instead of one or more interference filters has some advantages and some disadvantages. The main disadvantages are:

- A more complicated optical system that requires a good mechanical stability is necessary.
- It can be difficult to get a good high efficiency echelle. Although in theory an efficiency of almost 100% is possible, in practise values between 30% and 70% can be expected. A realistic grating efficiency is about 60% although it is not sure at this moment that grating manufacturers are able to deliver that efficiency at the laser wavelength from their present standard delivery programs. One grating has been delivered now and that one showed a disappointing efficiency of 40% although the manufacturer claimed 60% in his catalogue. We are still in contact with several suppliers about the possibility to get a high efficiency grating.

The main advantages are:

- No temperature control necessary. Grating blanks are made out of borosilicate glass or fused silica. The thermal expansion coefficient of borosilicate glass is about 4×10^{-6}, which results in a wavelength change of 0,1 nm over a temperature range of 50 ^{o}C. With fused silica even considerably better temperature stability is obtained.
- Easy and direct wavelength adjustment over a limited wavelength range. By rotating the grating about an axis normal to the plane of the paper of figure 1 the wavelength is scanned. An angular rotation of a few degrees results in a wavelength scan of about 10 nm without noticeable change in efficiency.
- One optical arrangement for day and night time ranging. Day time operation usually requires a smaller field of view and a narrower wavelength bandwidth due to the background signal of the bright sky. Because for the described grating monochromator the field of view and the wavelength bandwidth are proportional to each other this coupling is automatically obtained.

The exit slit transmits a narrow wavelength band around the laser wavelength to an "adjustable beamsplitter/attenuator".
For the high accuracy range measurements the transmitted light of this beamsplitter is used while the reflected light is focussed on a "quadrant beamsplitter" that will be described later. The transmitted light is reflected at the "correcting reflector". This reflector refocusses the beam and corrects for the not completely negligible range differences over the echelle surface (almost 100 mm top-top). In the correcting reflector the beam is split up by five mirrors with different optical path lengths so that the 100 mm top-top range difference over the grating surface is reduced to 20 mm top-top. Finally two "relay lenses" image the FOV on the cathode surface of a photomultiplier tube (PMT).

The preliminary PMT choice is the conventional RCA tube 8850. This tube will be used at the single photo-electron level. The amplified PMT signal will trigger a high accuracy counter (HP 5370) via a constant fraction discriminator. Although the rise time of the RCA tube is not extremely fast the stability of its single photo-electron response (transit time, pulse height, etc.) seems adequate in combination with a good constant fraction discriminator. Installation of any other PMT, amplifier, discriminator or HPIB interfaced counter will be a more or less plug-in operation.

Because the ranging system will be operated at the single photo-electron response level the received signal usually has to be attenuated to this level. This can be achieved by adjusting the transmitted energy, the divergence of the transmitted beam or by an attenuator in the detection optics. In the mobile ranging system all these three adjustments can be executed. The continuously adjustable attenuator in the detection system is the already mentioned "adjustable beamsplitter/attenuator". Two concave spherical mirrors can be turned into the beam from both sides perpendicular to the plane of the drawing of figure 1. The slit between the two mirrors transmits the central part of the beam to the "correcting reflector" while the two side parts of the beam are reflected to the "quadrant beamsplitter". By changing the slitwidth between the two mirrors the ratio of the number of transmitted and reflected photons can be adjusted from 100% transmission to almost 100% reflection. The photons that are not used for the accurate range measurement are not lost but they are reflected to the quadrant detection system. At the quadrant beamsplitter an image of the field of view, as transmitted through the "entrance diaphragm" and the "exit slit", is located. This image of the field of view is split up into four quadrants and the light in each quadrant is directed to its own small PMT of which two of the four are shown in figure 1. For these PMT's the less expensive Hamamatsu tube R 1166 has been selected.

These PMT's have sufficient gain to be operated at the single photo-electron level. If possible however they should be operated at a higher level (2 photo-electrons or more) so that the sky background noise of these detectors is considerably reduced. Information on where the satellite is located in the field of view is obtained from which of the four PMT's is triggered by the return signal of the satellite. With this information an immediate correction to the predictions will be possible. This correction can result in a better divergence of the transmitted beam which leads in turn to a higher signal level on the four quadrant PMT's, and therefore to better information on the position of the satellite in the field of view, etc. In practise each of the four PMT's will be connected via a discriminator to one channel of a four channel timer with moderate resolution and accuracy (50 ns).
This timer also gives information about where the satellite is within the window of the range gate generator so that the window, which is the same for the four quadrant PMT's and the RCA 8850 tube, can be adjusted to a very narrow band around the return signals.

AIRBORNE LASER RANGING SYSTEM FOR RAPID LARGE AREA GEODETIC SURVEYS

CONTACT: JOHN J. DEGNAN
CODE 723
NASA/GODDARD SPACE FLIGHT CENTER
GREENBELT, MARYLAND 20771 USA

1. Introduction

Geophysicists investigating phenomena such as fault motion, dilatancy, and strain buildup and relief have expressed a desire for an instrument capable of monitoring crustal deformation at hundreds of locations within an extended seismic region (e.g. 200Km X 200Km). In order to deduce the needed strain rates, the instrument must be able to measure 100 Km baseline distances with centimeter accuracies and in a time frame short compared to the scale of expected motions on the earth's surface.

During the past year, the Goddard Space Flight Center has been engaged in the design of a centimeter accuracy, multibeam, Airborne Laser Ranging System (ALRS)[1]. The basic philosophy is to invert the usual laser ranging configuration by placing the ranging and pointing hardware in a high altitude aircraft and replacing the expensive ground stations by low cost (<$1000) passive retroreflectors. The instrument would be constructed on a standard aircraft pallet so that it can be easily removed and reinstalled. This capability eliminates the need for a dedicated aircraft and allows special flights to be scheduled quickly in response to increased seismic activity.

The system is necessarily multibeam since the location of the aircraft is not known with cm precision at each point where a set of range measurements is made. Thus, a minimum of four simultaneous range measurements is required- three to resolve the new coordinates of the aircraft and one to acquire information on the relative locations of the ground targets. The ALRS system will be capable of ranging simultaneously to six retroreflectors. At a laser repetition rate of 100 pps, a potential 1.3 million individual range measurements can be made and an area as large as 60,000 square kilometers can be surveyed during one six hour flight. Computer simulations have demonstrated

that, with range biases and single-shot RMS standard deviations on the order of 1 cm, the ALRS will be capable of resolving baseline distances on the order of 100 Km to the subcentimeter level. Furthermore, the data reduction technique simultaneously resolves the aircraft position to the cm level at each point in the flight path where a laser pulse is transmitted. The system is expected to be a powerful new research tool for monitoring regional crustal deformation and tectonic plate motion because it will provide a "snapshot" of the target positions (all three axes) over an extended area with high spatial resolution (20 Km or less).

2. Ranging and Pointing Subsystems

A block diagram of the ALRS system is described in Figure 1. The current system concept is as follows. The on-board system computer generates a fire command to the short pulse laser transmitter at the rate of 10 pulses per second. The transmitter is a modelocked, PTM Q-switched Nd:YAG laser oscillator followed by a double-pass Nd:YAG laser amplifier and KD*P frequency doubler and generates a single, 150 picosecond (FWHM) pulse containing several millijoules of energy at the 5320 A green wavelength. The energy of the outgoing pulse is split six ways and directed toward six independently controlled pointing systems which are in turn directed at six different ground targets via pointing commands from the system computer.

The outgoing start pulse, as well as the incoming stop pulse, is recorded in each of the six receiver channels. In this way, most instrument-related systematic biases, which may vary slowly with time, are cancelled out automatically. In addition, biases related to the amplitude of the received signal will be compensated for by recording the integrated energy in the start and stop waveforms and applying a software-generated range correction which is based on extensive receiver testing and calibration. Provisions will also be made for on-board calibration of the instrument. The instrument-related random errors are expected to be on the order of six millimeters RMS based on projections of recent laboratory data.

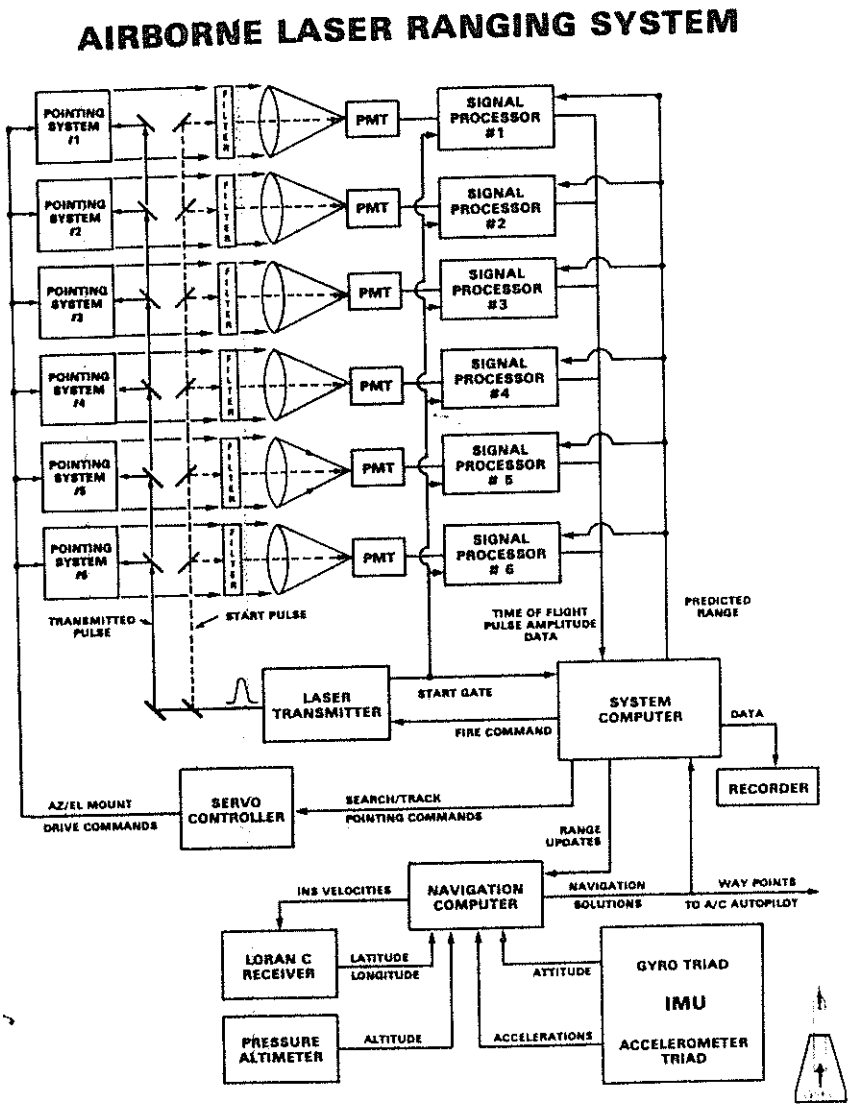

FIGURE 1: BLOCK DIAGRAM OF THE AIRBORNE LASER RANGING SYSTEM

The laser transmitter, beam splitting optics, receiver optics, and photomultiplier tubes are mounted on an optical baseplate which is isolated vibrationally from the aircraft fuselage. Six azimuth-elevation pointing mounts with 5 cm receive apertures are rigidly attached to the bottom of the optical bed. Each pointing system consists of a four mirror coelostat mounted on an azimuthally rotating stage. The laser beam enters the pointing system through a hole in the optical baseplate and the rotation stage. The final mirror rotates about an axis parallel to the optical bench to a given elevation angle. This particular configuration was chosen because it can be placed very close to the aircraft window to provide near hemispherical viewing capability.

Each pointing mount is equipped with two servo systems (azimuth and elevation). A single computer servocontroller drives all twelve stepper motors. Optical encoders attached to the motor shafts provide an independent measurement of angular position for error detection. Command angles and predicted range gates are generated by the system computer using aircraft navigation solutions provided by the navigation and attitude determination subsystem.

With laser beam divergences on the order of eight milliradians, absolute pointing accuracies at the mrad level are adequate. This performance is a factor 10 to 20 times less stringent than typically required for ground based satellite laser ranging systems.

3. Target Acquisition and Tracking

The approximate coordinates of the ground targets are stored in the system memory. The accelerations and angular rates of the optical bed are continuously monitored by a dedicated inertial measurement unit (IMU) mounted to the bed. The latter is isolation mounted to the aircraft pallet to eliminate high frequency vibrations. The navigation computer performs coordinate transformations and integrates the equations of motion to provide estimates of velocity, position and attitude relative to a set of initial conditions. In addition, independent latitude and longitude information from a LORAN C receiver is utilized to update and stabilize the corresponding INS solutions via a Kalman filter algorithm

in the NC. Similarly, barometric altimeter measurements of altitude are processed in the NC to stabilize the equations for vertical velocity and altitude. The Kalman filter also updates attitude information and provides best estimates of sensor errors such as misalignments, accelerometer biases and scale factors, gyro drift rates, etc. The INS velocity solution assists the LORAN C receiver in the acquisition of Doppler-shifted signals from the LORAN ground network. In the event of certain types of failure, the proposed navigational system can be restarted and calibrated in flight. Flight tests of a LORAN-aided INS performed for the U.S. Air Force have demonstrated a 60 meter absolute position accuracy (one sigma) and a 15 meter RMS random noise error (one sigma) and angular accuracies of a few tenths of a milliradian[2].

The navigation data is combined with the stored apriori target positions to compute the estimated range gates and the pointing mount command angles. As the targets come within range, the laser is activated and the presence or absence of range returns is noted. If no returns are detected, a search pattern is executed until range data is acquired. Selected range data is then passed to the navigation Kalman filter to update the estimate of aircraft position. The ALRS then shifts from the acquisition to the tracking mode.

In the tracking mode, triangulation on the highly accurate laser returns results in an aircraft position estimate which is virtually error free (better than a meter standard deviation) so that, except for aircraft attitude estimation errors contributed by the gyros, the computed command angles and range gates are essentially correct. The instrument remains in the tracking mode as long as sufficient range data is available to maintain an accurate estimate of aircraft position. In making the transition to a new set of six targets, the system triangulates on laser returns which are common to the new and the previous set. In this way, the aircraft position is known with better than meter accuracy during the transition.

4. Mission Scenario and Simulation Results

Simulations[3] have shown that range measurements must be taken at two widely separated altitudes in order to strengthen the geometry sufficiently to recover baselines at the centimeter level. Thus, in a typical mission, the aircraft approaches the target grid at an altitude of 40,000 feet (assuming the RB-57 A/C) as in Figure 2. After

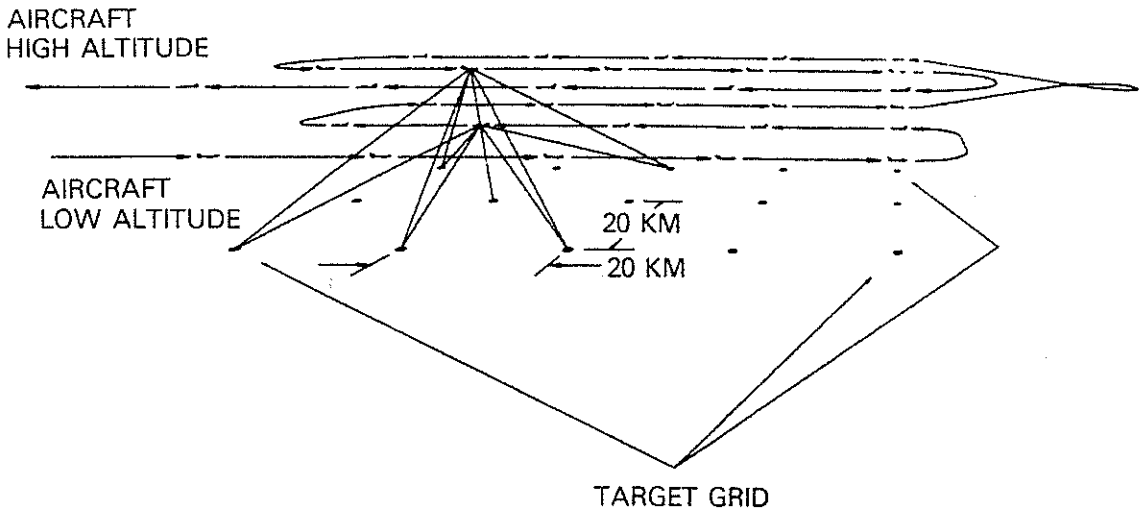

FIGURE 2: TYPICAL ALRS MISSION SCENARIO PERSPECTIVE SHOWING RANGING FROM TWO DIFFERENT ALTITUDES

acquiring the first few targets, the instrument shifts to the tracking mode for the remainder of the mission. After overflying the rows of targets at 40,000 ft, the aircraft climbs to its maximum cruise altitude (60,000 ft) for a second set of passes over the target grid.

The spacing between targets will depend on several factors including the scientific objectives of the mission, the maximum aircraft altitude, and terrain limitations. For the RB-57, the spacing is nominally 20 to 27 Km. The baseline errors grow linearly with the length at a rate of 60,000 feet. The maximum target spacing varies linearly with the maximum aircraft altitude while the baseline error growth rate varies inversely with the altitude. The simulations have also demonstrated that it is not necessary to provide meteorological instrumentation at all of the target sites in order to correct for atmospheric refraction errors. Instrumentation at one site at the center of the grid provides sufficient information to resolve the other site positions to the centimeter level even if one assumes that the site surface pressures are totally uncorrelated. This is a consequence of the simultaneous multibeam trilateration approach at two altitudes and the exponential dependence of pressure with altitude. In effect, the surface pressure at each site can be solved for along with the site coordinates.

5. Program Plans

A demonstration system is currently being constructed for use onboard the NASA NP3A Research aircraft. Initial tests will take place in the vicinity of Mary's Rock, VA in late 1983. The latter location is well surveyed and reasonably close to the aircraft's home base. The aircraft's maximum altitude of 20,000 feet will require target sites 7 km apart and increase the baseline error growth rate to about .036 cm/km.

REFERENCES

1. J.J. Degnan, "Airborne Laser Ranging System for Monitoring Regional Crustal Deformation," Proceedings of the 1981 International Geoscience and Remote Sensing Symposium, pp. 234-244, June 8-10, 1981, Washington, D.C.

2. R.D. Wierenga, Lear-Siegler, Inc., Grand Rapids, Michigan, 49508, private communication.

3. T.S. Englar, Jr., C.L. Hammond, and B.P. Gibbs, "Covariance Analysis of the Airborne Laser Ranging System," Business and Technological Systems, Inc., BTS-FR-81-143, February 1981.

SATELLITE LASER RANGING AT 10μm WAVELENGTH

D.R. Hall

Department of Applied Physics, Hull University,
Hull, England.

There has been increasing discussion in recent years concerning the possibility of developing systems operating at wavelengths around 10μm and based on carbon dioxide lasers which have the capability of ranging to satellites (1). For such systems to be of any significant interest, the resolution attained must be comparable with the centimetric performance of existing 'third generation' visible systems. Moreover, given the large investment in the technology of high resolution visible ranging systems over the last fifteen years, any potential competitive system should exhibit some decided advantage(s).

This paper considers three main aspects of this topic: First of all a summary is presented of the potential benefits which could accrue from operation in the mid infra-red 9-11μm spectral region. This is followed by a brief discussion of the techniques and hardware most likely to form the basis of such a system and finally a short assessment of the present state of the art in terms of available hardware, coupled with an indication of the technological development which would be necessary to allow a 10μm based system capable of ranging to the main satellites of interest (Lageos, Geos, Starlette) to be realised.

WHY CONSIDER 10μm SYSTEMS

There has been near continuous development of visible wavelength (based on ruby or Nd:YAG lasers) satellite laser ranging (SLR) systems during the past 15 years, and we have heard during this Workshop of the success of the most recently developed systems based on passively mode-locked, frequency doubled Neodymium YAG lasers, in achieving

night and day time ranging to Lageos with resolution at the level of a few centimetres, under ideal atmospheric conditions. Given this impressive level of performance, any potential new system, such as we are discussing here, must be shown to have clear advantages before any significant level of development is undertaken.

The evidence presently available suggests that with reasonable care and maintenance, the third generation systems presently operational can be made to achieve a level of range resolution which is adequate for modelling purposes and an acceptable level of reliability in terms of the 'down' time made necessary by equipment malfunction. The clear limitation, however, of present systems relates to their dependence on near perfect weather conditions with zero or minimal cloud and haze, and the impact this has on the frequency with which satellite ranging activities are possible. This problem obviously manifests itself to a greater or less extent, depending on geographical location, but it is apparently a significant limitation at all stations. One benefit which has been claimed for 10μm systems is that they can take advantage of the 8-14μm 'atmospheric window'. This topic has been the subject of considerable interest, particularly as it affects 'terrestrial' ranging and is one of the reasons for the recent upsurge in interest in the development of 10μm wavelength military surveillance systems, including rangefinding.

Unfortunately, despite considerable experimental and theoretical studies, the relative merits of visible and IR wavelengths as regards atmospheric extinction is not clear cut, and much depends on atmospheric conditions. Atmospheric extinction is due mainly to molecular absorption and scattering by aerosols, and whereas the latter is most effective in attenuating near and IR visible signals (i.e. Nd:YAG and frequency doubled Nd:YAG wavelengths) they have negligible effect on 10μm signals. Conversely, broad-band water vapour and CO_2 molecular absorption is effective in attenuating 10μm radiation but has very little effect on visible signals. Thus, while 10μm radiation has superior penetration through aerosols (such as water droplets in fog and light cloud), it is severely attenuated in conditions of high water vapour content (high humidity).

Consequently, although 10μm radiation can be claimed to have superior penetration in certain "artificial" atmospheres dominated by dust, smoke and hydrocarbons, the same cannot be universally claimed for 'natural' atmospheres under all conditions. Thus, it is by no means clear that 10μm systems will provide any significant improvement over the visible under a wide range of atmospheric conditions and geographic locations.

A second area of concern with regard to visible systems is the question of eye safety. It is desirable to operate SLR systems in an intrinsically eye-safe manner, so that one could dispense with the aircraft detection and laser lock-out systems currently causing headaches for some groups. Even with large transmitting apertures and using very sensitive (single photo-electron) receiving techniques, this does not appear to be feasible with visible systems because of the low value of maximum permissible exposure (MPE) in the green (2). The MPE in the infra-red allows a benefit of a factor of 10^5 in using a 10μm wavelength as compared with using the green, so that an intrinsically eye-safe IR system could in principle be built.

Existing visible wavelength SLR systems rely on direct detection, whereas any feasible 10μm based system will, for detection sensitivity reasons, be required to use a heterodyne receiver. With such a receiver it is possible to determine a single component of the satellite velocity from measurements of the Doppler shift on the return signal. Thus, a 10μm based system could, in principle, be designed to produce velocity and/or range information. From the standpoint of the data users, certainly in the context of crustal dynamics, any such 'range rate' data would need to achieve a resolution of about 10μm per second in order for the orbit model to produce useful results(3). This implies the need to measure Doppler shifts with a precision of a few hertz. Carbon dioxide lasers, operating in the continuous wave mode at 28.4 THz, have been stabilised to 1 part in 10^{12} under laboratory conditions, but this is not likely to be routinely achievable in the field. Moreover, atmospheric turbulence introduces a degree of frequency 'smear' and a resolution of 100 Hz - 1 kHz is likely to be the best achievable in practice. The conclusion, therefore is that the use of cw CO_2

lasers, heterodyne detection and Doppler tracking is unlikely to produce data on range rate with adequate resolution to be useful for geodesy.

One final reason which has been advanced for consideration of 10μm systems is the advanced level of technology available in this spectral region, based on carbon dioxide lasers and mercury cadmium telluride photon detectors. This question is examined later.

EXISTING 10μm RANGING SYSTEMS

There has been a rapid increase in interest during the past 5-7 years in the use of 10 micron systems for terrestrial rangefinding particularly in a military context. Such systems typically operate over ranges of less than a few tens of kilometers and with relatively coarse range resolution in the 1-5 meter bracket. They are however, typically used against "uncooperative" diffuse reflecting targets, i.e. no retroreflectors. Three types of system can be identified. The first to be employed, and probably still the most common, are the pulsed laser-direct detection systems (4). These employ a pulsed TEA (transverse, electric, atmospheric pressure) CO_2 laser which produces pulses of about 1 Mwatt peak, 50 nanoseconds duration at a repetition rate of 1-2 Hz. Transmit and receive optics (which may be common) are $\lesssim$ 15cm in diameter and a cryogenically cooled photon detector is employed in a direct detection mode.

A second general type of system uses a modulated cw transmitter and a heterodyne receiver. One such system (5) uses a cw waveguide CO_2 laser and an acousto-optic modulator to produce a linear frequency chirped output of less than 1 watt average power. The receiver uses part of the transmitter base signal as a local oscillator and a surface acoustic wave device as a good approximation to a matched filter. This type of system is modulator bandwidth limited to about 15 MHz/5 metre resolution and has a range $\lesssim$ 10km. The third type of system couples the peak power of the pulsed CO_2 laser with the additional sensitivity of the heterodyne receiver and is the most likely candidate for a long range (satellite) ranging system of high resolution. To date, systems have been built which produce approximately 100 mJoules in a 40 usec pulse producing range resolution of 5 metres over near horizontal range

up to 35km (6).

Although no systems have been reported which employ subnanosecond CO_2 lasers for ranging this is due in large measure to the absence of any real requirement to date for any increased range resolution in such systems. In fact subnanosecond pulses may be produced by modelocking techniques in pulsed CO_2 lasers operating at atmospheric or super-atmospheric pressure, and have been extensively studied in the content of target interaction and inertial confinement research.

The use of 10μm laser systems employing heterodyne receivers has become an important technique for velocity measurements, particularly in atmospheric studies, where the Doppler shift suffered by radiation scattered by aerosols in a natural or artificially induced air flow is used to monitor the air motion itself. Such systems, employing stabilised cw CO_2 lasers, have been used to monitor turbulent air flows associated with aircraft landing and take off, and mounted in the nose of an aircraft, to measure real air speed and as a means of detecting windshear (7). Resolution in the range 0.1-1 meters/sec is achieved.

Work is currently in progress on a proposed satellite born system which would be used to monitor the development of wind systems on a global basis. It is suggested that such a system would operate with a 10 Joule CO_2 laser producing pulses of a few microseconds duration at about 8 Hz with a velocity resolution of 1 metre per second (8). Doppler tracking of Lageos at 10.6μm has been achieved by the group at Lincoln Laboratory Firepond Facility (9) who have used a very stable master oscillator to drive a power amplifier to produce an output of several hundred watt chopped pulses of about 1 msec duration. Doppler tracking with a resolution of about 1 KHz was achieved, and the relatively complex Doppler spectrum could be interpreted in terms of the spin of the satellite, which is equipped with 4 germanium retroreflectors (intended for use at 10μm) located at the vertices of a tetrahedron.

PERFORMANCE OF POSSIBLE SYSTEM

As indicated above, any potential IR SLR system will require the use of a heterodyne receiver, where the dominant noise source is photon fluctuation in the local oscillator laser signal, as opposed to the

background noise dominated situation of direct detection receiver commonly used in the visible.

If we assume a pulsed CO_2 laser transmitting pulses of peak power P_T and duration $\tau \sim 1/B$ where B is the receiver bandwidth, from a telescope of effective transmitting and receiving aperture A_T, then the received signal power P_s after reflection from a retro at range R is given by

$$P_s = \frac{P_T A_T^2 A_R^2}{\lambda^4 R^4} \quad (1)$$

where L represents total system losses including atmospheric transmission, retroreflector losses and receiver losses, and A_R is the retroreflector area.

The receiver noise power P_N is $h\nu B/\eta$ where η is the detector quantum efficiency, h is Planck's constant and ν is the optical frequency (2.8×10^{13} Hz), so that the IF receiver signal-to-noise ratio is given by

$$(S/N) = P_s/P_N \sim \frac{E_p A_T A_R L\eta}{\lambda^4 R^4 h\nu} \quad (2)$$

where E_p is the pulse energy, assuming a perfect match between pulse duration and receiver bandwidth.

If we assume a value of 50cm for the diameter of both the transmitting and receiving telescope, a retroreflector diameter of 4 cm and system losses of 10^{-2} then the required laser characteristics are approximately as indicated in Table 1.

SATELLITE	P_T (peak)	E_p	τ_p	P(av) (10 Hz)
Lageos	12 GWatt	6 Joules	5×10^{-10} sec	60 watts
Geos	12 Mwatt	6 mJ	5×10^{-10} sec	60 Mwatts

Table 1 Required Laser Performance

To achieve the necessary pulse duration of $\lesssim$ 500 picoseconds, it would be necessary to use a multi atmosphere pulsed CO_2 laser, probably in the 2-5 atmosphere bracket, with the preferred modelocking technique

probably involving injection from a master oscillator. In this context achieving 6 mJ (for Geos) is a reasonable target but 6 Joules (for Lageos), even in a pulse train as opposed to a single pulse, represents a very difficult and expensive task, and one which would need very considerable development. Aside from achieving the necessary discharge performance one very significant problem could be the fundamental limitation of damage to optical components. A receiver for a potential IR SLR system would be required to operate with a cryogenically cooled detector element and to exhibit an IF bandwidth in excess of 1.5×10^9 Hz. This has been achieved but is difficult and expensive. The laser local oscillator could be required to frequency track over approximately ± 500 MHz to compensate for Doppler shift and would need to maintain frequency lock with the transmitter to a few MHz. The alignment of the receiver optics is critical to obtain efficient heterodyning and although there is a tolerance benefit of about factor of 20 in going to 10μm, considerable investment would be necessary like in new telescopes or in modification to existing hardware.

CONCLUSION

It is apparent from the above discussion that there is at present no overwhelming case in favour of developing 10μm wavelength SLR systems. There is a definite advantage at 10μm in terms of eye safety, a marginal benefit in terms of atmospheric transmission, no real advantage accruing from range rate data and in fact, although 10μm technology can be said to be in a relatively advanced state, there are very significant problems associated with producing a system which could range to Lageos with the requisite range resolution.

References

1. B. Greene. Third International Satellite Laser Ranging Workshop. Lagonissi 1978.

2. British Standard BS 4803.

3. D. Smith. Private Communication.

4. M.J. Taylor, P.H. Davies, D.W. Brown, W.F. Woods, I.A. Bell, C.J. Kennedy. Appl. Opt. 17, 885 (1978).

5. K.F. Hulme, B.S. Collins, G.D. Constant, J.T. Pinson. Opt. Quant. Elect. 13, 35 (1981).

6. J.M. Cruickshank, Appl. Opt. 18, 290 (1979).

7. R. Callan, J. Cannell, R. Foord, R. Jones, J.M. Vaughan, D.V. Willetts, A. Woodfield, Fifth UK Quantum Electronics Conf. Hull, September, 1981.

8. M. Huffaker, Paper presented at Coherent Laser Radar Conference, Aspen, July, 1980.

9. Leo J. Sullivan, SPIE Vol. 227 (1980).

THE LASER RANGING SYSTEM GRAZ - LUSTBÜHEL, AUSTRIA

G. KIRCHNER

Institute for Space Research
Austrian Academy of Sciences
Department: Satellite Geodesy

1. INTRODUCTION

In October 1978 the project "Construction of a Laser Ranging Facility" was approved by the Austrian Science Research Council. Until December 1979 the main components of the sytem had been specified using partly the advantage of a common planning together with the RGO, UK.

In December 1980 the two Laser emitters have been installed; in August 1981 the Mount and Telescope System has been delivered and placed in the dome at the Observatory Lustbühel in Graz. The computer and most of the instruments are already installed and operational.

2. SYSTEM CONSIDERATIONS

Originally it was planned to use a Nd:YAG short pulse laser system with estimated accuracy level of 10 cm or better; in December 1979 the decision was made to add a second laseremitter - a ruby laser with more energy output, but with longer pulses than the Nd:YAG laser to the ranging system to have more flexibility.

The philosophy throughout the system is:
- to use commercially available units for most instruments to simplify and accelerate the integration of the whole system;
- to use one standard interface for connecting all instruments, the two lasers and the mount electronics to the computer; this ist the IEEE -488 (HPIB, GPIB, IEC-Bus) interface. This enables simple and fast changing of instruments, adding new devices and reduces programming problems;
- and to make extensive use of computer power to control the whole laser ranging station. This allows great flexibility for the whole system.

3. THE LASER EMITTER SYSTEM (Figure 1)

a) The Nd:YAG-Laser

The oscillator is passively mode locked by KODAK 9740 dye; the oscillator mode is TEMoo. The pulse Selector extracts one single pulse out of the pulse train; this pulse is then amplified in

the double pass configuration amplifier (POLAREX method) and an additional amplifier. After frequency doubling - with a $KD^{x}P$ crystal - the remaining infrared light is removed and the YAG beam brought up to the Ruby beam diameter.

Pulse Width .....100 Picoseconds
Energy per Pulse .....100 Millijoules at 530 nm
Energy Stability .....$\pm$ 10 % for 90 % of the shots
Repetition Rate .....10 Hz, 5 Hz, 2.5 Hz
Beam Divergence .....0.1 milliard

b) The Ruby - Laser

The oscillator is passively Q-switched, the mode is TEMoo. This pulse is then amplified in the double pass amplifier.

Pulse Width .....3 ns, 6 ns; selectable
Energy per Pulse ..... 2.5 J; 4 J; according to pulse width
Repetition Rate .....up to 0.25 Hz
Beam Divergence .....0.1 milliard

c) General Remarks to both lasers

Both lasers are mounted on a common granite bench (320 x 100 cm) and placed in an air conditioned clean room in the main building of the observatory. Both laser beams are brought up to 40 mm diameter by means of the same beam expander telescope and directed with four mirrors within a closed, airtight path to the mount. Optical switching between YAG and Ruby laser is done by two mirrors, mounted on a high precision, computer controlled (IEEE-interface) translater on the granite bench.

Safety shutters in both oscillators prohibit unwanted laser pulses and enable - in the Nd:YAG oscillator - repetition rate selection without changing the flash lamp repetition rate.

Firing and charging of both lasers is computer controlled (IEEE - 488); repetition rates can be varied continously up to the specified maximum; epoch of firing can be predetermined with an accuracy of better than 50 Microseconds.

4. THE MOUNT AND TELESCOPE SYSTEM

Angular Coverage .....$\pm$ 290° Azimuth
$-$ 5° to 185° Elevation
Axis Wobble .....2 arc secs, both axis
Encoding System and Control:
Resolution .....0.0001°
Accuracy .....$\pm$ 1 arcsec,
Rate Commands .....0.0001 to 20 Degrees/s Azimuth
0.0001 to 5 Degrees/s Elevation

Receive Optics
Clear Aperture .....20 inches
Field of View .....23 arc secs to 3.9 arc min, selectable
Equipped with ISIT - TV Camera.

Transmit Optics
Clear Aperture.....2 inches; 4 inches beam diameter after beam expander output
Divergence .....5 to 200 arc secs variable
Mount Control .....Manual Mode; Computer Mode via IEEE-488 interface; Joystick Mode.

5. COMPUTER AND ELECTRONICS

The HP - 1000, Model 40, minicomputer with 128 kB memory and 19.6 MB cartridge disc is installed since 1980; it controls all instruments, the two lasers, the mount and the complete data flow. Standard I/O is the HP-IB (IEEE-488) interface. Via modem a connection to the UNIVAC 1100/81 computer is possible.

For time interval measurements the HP 5370A counter is used; the HP 5359A Time Synthesizer enables range gate control. Epoch time is determined with the HP 5328 Universal Counter.

For the echo detection originally it was planned to use Varian Crossed Field and Varian All-Electrostatic High Speed Photomultipliers; since these are not available in the moment, two RCA 8852 photomultipliers will be installed for the initial phase. This detection package with 3-A-filters, variable neutral-density filters and leading-edge, fixed-level discrimination is now unter construction.

A second HP 5370A counter can be used for high precision epoch time determination.

6. TIME KEEPING

The primary time standard is provided by the Lustbühel time keeping station which generates the time scale UTC(TUG) and contributes to TAI by two Cesium Beam Frequency Standards and four LORAN-C receivers. Further comparisons are performed, on a regular basis, via TV (terrestrial and satellite) and portable clock visits.

Time connection between this time standard and the laser station has been accomplished by fibre optics (1 Hz pulse and 10 MHz reference frequency).

7. SAFETY

Due to the location of the observatory Graz-Lustbühel - about 9.5 km distance to Graz Airport, within the controlled area - the authorities put heavy restrictions on the operation of the laser ranging system:

- Installation of a passive aircraft detection system with automatic stop of the laser activity (similar to the Kootwijk system); this system is already operational; the function will be tested by the authorities during the next weeks;
- Operation of the laser station only when Graz-Airport is closed (at present this is from 23^{oo} to 6^{oo}). This restricted operation time will probably be extended after the first, experimental period.
- Operation only after contacting the Air Traffic Control Center in Vienna and getting "clearance";
- In addition, a human observer is mandatory

8. CONCLUSION

If detection package construction and software integration continue without major problems, the beginning of the testphase can be expected early 1982.

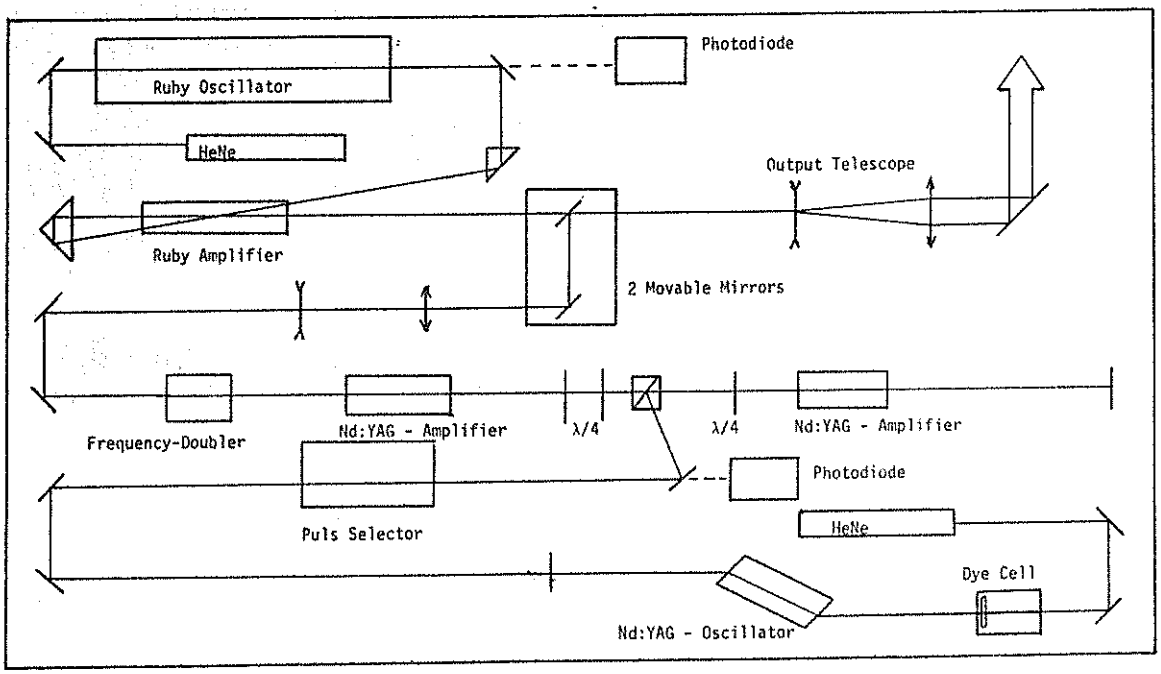

Figure 1: Block Diagram Of The Optical Lay - Out Of The QUANTEL Nd:YAG / Ruby - Lasersystem

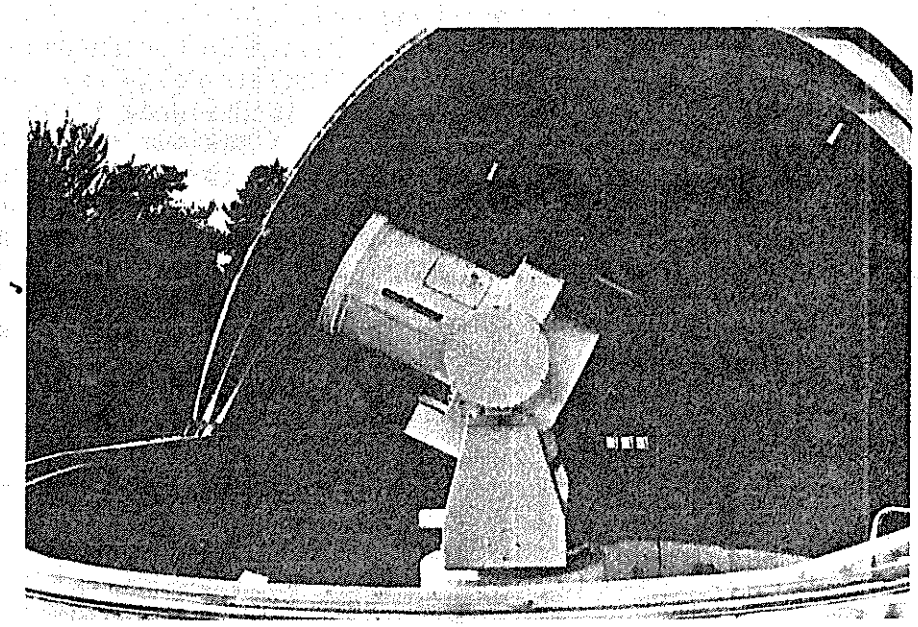

Figure 2: Mount And Telescope System

THE GERMAN/DUTCH MOBILE LASER RANGING SYSTEMS

PETER WILSON

INSTITUT FÜR ANGEWANDTE GEODÄSIE, FRANKFURT/MAIN
SONDERFORSCHUNGSBEREICH 78 (SATELLITENGEODÄSIE) DER TU MÜNCHEN

1. Introduction

In December 1980 the Institut für Angewandte Geodäsie, acting on behalf of the Sonderforschungsbereich 78 (Satellitengeodäsie) der TU München , entered into a contract with a Dutch group - Technisch Physikalische Dienst, TNO-TH, Delft - for the construction of a mobile laser ranging system. Financing for the contract was provided by the Bundesministerium für Forschung und Technologie (BMFT) through the Bereich Projektträgerschaften der Deutschen Forschungs- und Versuchsanstalt für Luft- und Raumfahrt (DFVLR) in Köln-Porz. With delivery to follow in early 1983 the system is designed to be capable of observing at the 1-2 cm noise level to a maximum range of approximately 12 000 km. As the result of efforts to co-ordinate the design, a second, identical system was ordered for the Satellite Observatory at Kootwijk in the Netherlands, with delivery to follow the first system by approximately 6 months. It is anticipated that the use of the two systems will also be co-ordinated in projects of common interest, particularly in the field of Crustal Dynamics and Earthquake Research such as that inaugurated by the NASA.

2. System configuration

The overall concept of the observing system is outlined in fig. 1, which illustrates the connecting links between major components. As can be seen from this block diagram, the system breaks down into

- the optical transmitter including telescope and laser;

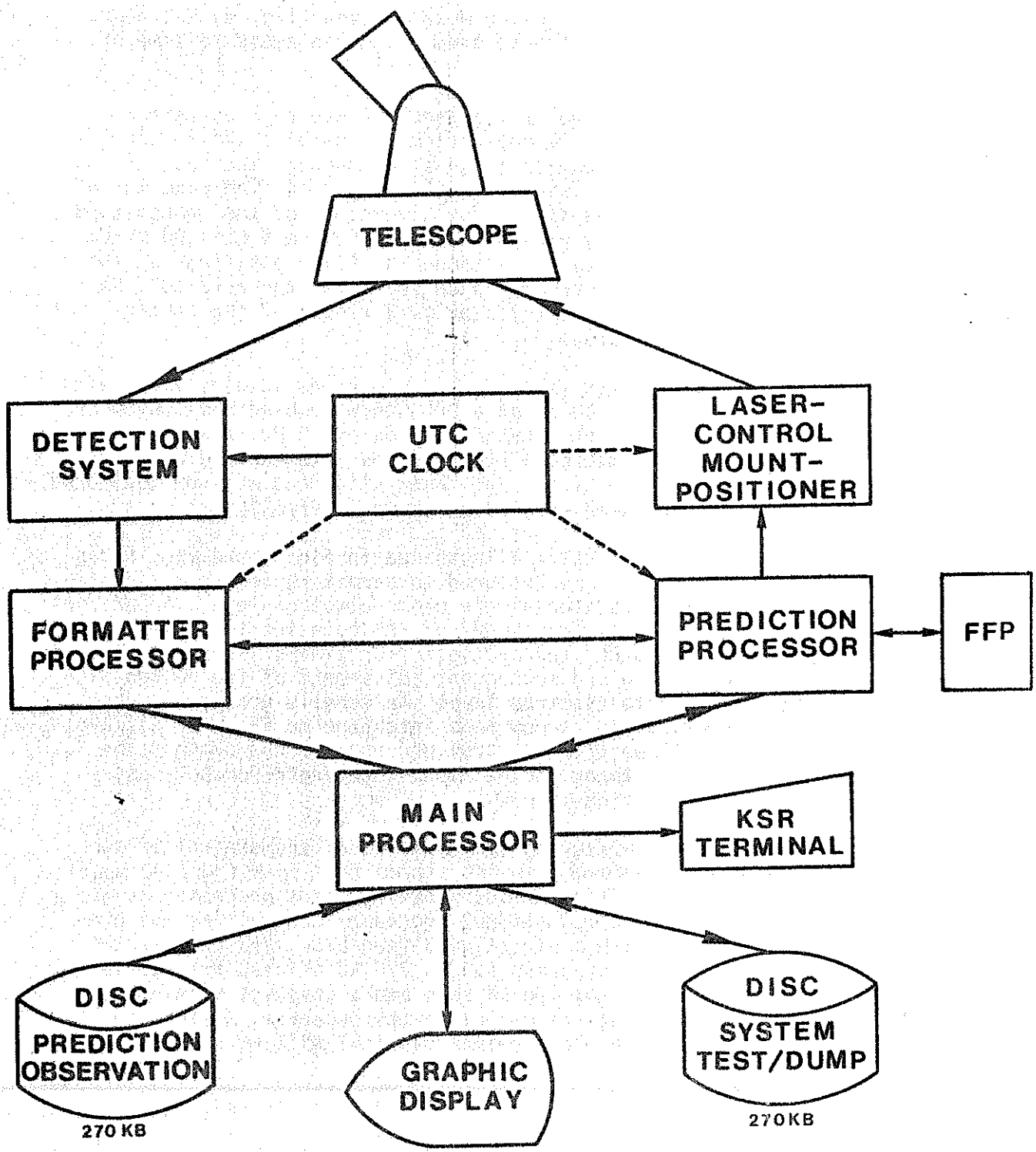

Fig. 1: The overall system concept

- the mount positioner and laser control unit;
- the detector package including UTC clock;
- the processors and their peripherals.

Although a discussion of the Coudé mount design (fig. 2) has been given in [1] it is useful here to draw attention again to some of the main features.

A single telescope is designed for use both as optical transmitter and receiver, the separation of outgoing and return pulses occurring at the beam splitter situated near the base of the mount, shortly before the laser and detector units. The diameter of the telescope objective is 40 cm. The divergence of the transmitted laser beam is continuously variable over the range 0,05-1,00 mrad. Laser and detector packages are attached in fixed positions at the base of the mount and are readily accessible for the operator. No loss of energy occurs at transmission as a result of the central obscuration of the telescope.

The Nd:YAP laser (fig. 3) [2] comprises an oscillator with one amplifier, producing 10 mJ at a frequency doubled wavelength of 539 nm (green) with a pulse repetition rate of 10 Hz. Alignment of the overall optical system will be performed with the aid of an externally mounted CW laser (fig. 2); laser alignment will be monitored via a separate He-Ne laser mounted as shown in fig. 3.

The detection system illustrated in fig. 4 and fig. 5 has been described in [3]. It is designed to permit rapid signal identification for observing at the single photo-electron level. A quadrant detector serves to enable adjustment of the pointing to maximise signal return at the main PMT and multiple-stop timing is used to facilitate signal recognition and subsequent adjustment of the return signal to the single photo-electron level. An echelle grating is used in place of the customary narrow band interference filter. This avoids the necessity for temperature control and permits use of the same optical configuration tuned to the laser wavelength for both day- and night-time observations.

The overall measuring system is under the control of two 8-bit Motorola 6809 micro-processors slaved to a 16-bit HP1000 model 5 micro-computer (fig. 1) [4]. A fast floating point processor is included to speed up the computational procedure controlling the prediction and pointing with a direct data feed-back link between the formater and prediction processors. 2 x 270 KB of disc storage is available to supplement the 128 KB core and a graphics terminal is included to provide visual feed-back to the observer. A TI-Silent 765 KSR (keyboard - send and receive) terminal will be used as an

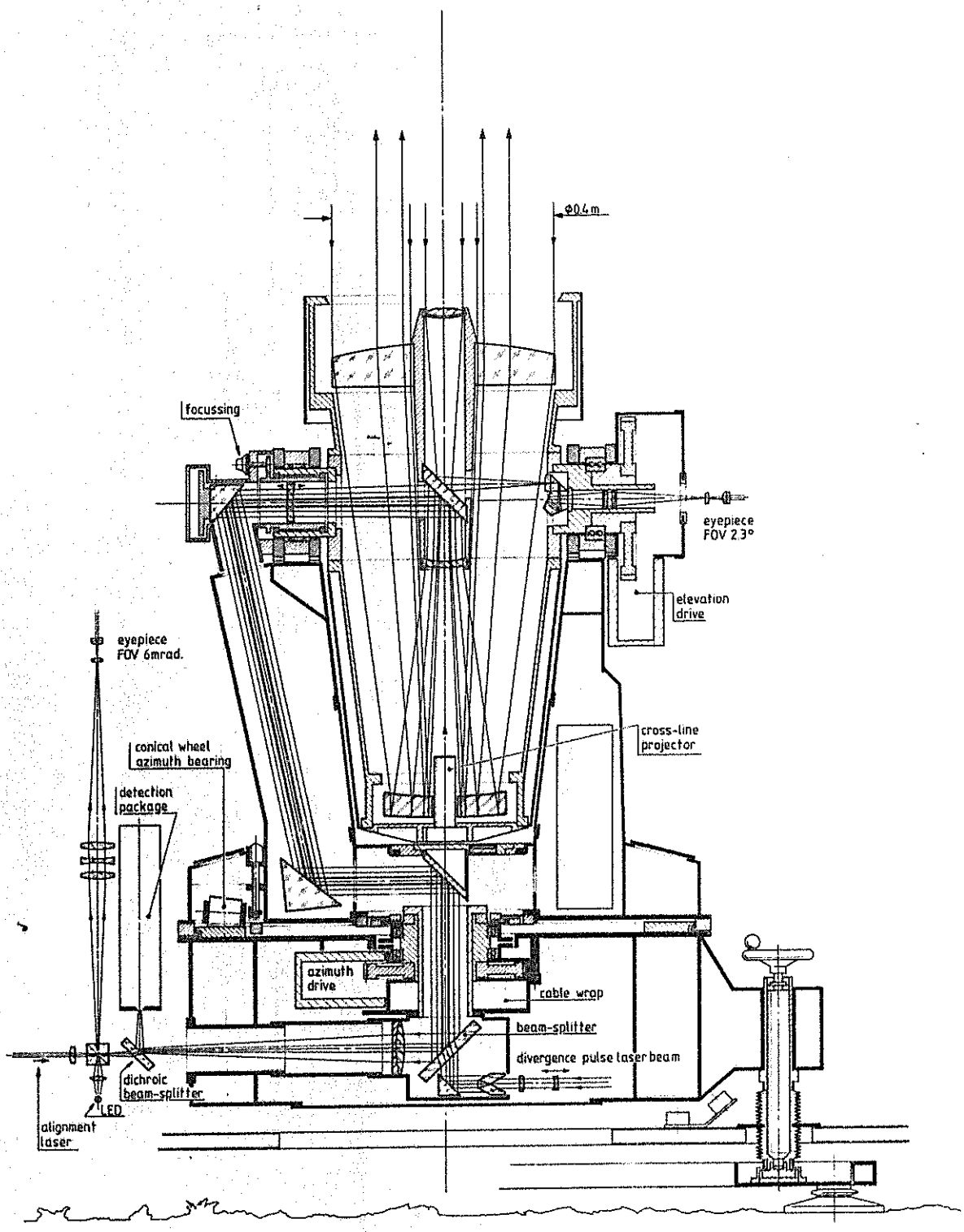

Fig. 2: Schematic of the mount and telescope

KLB - Nd:YAP-Lasersystem YL 143 S

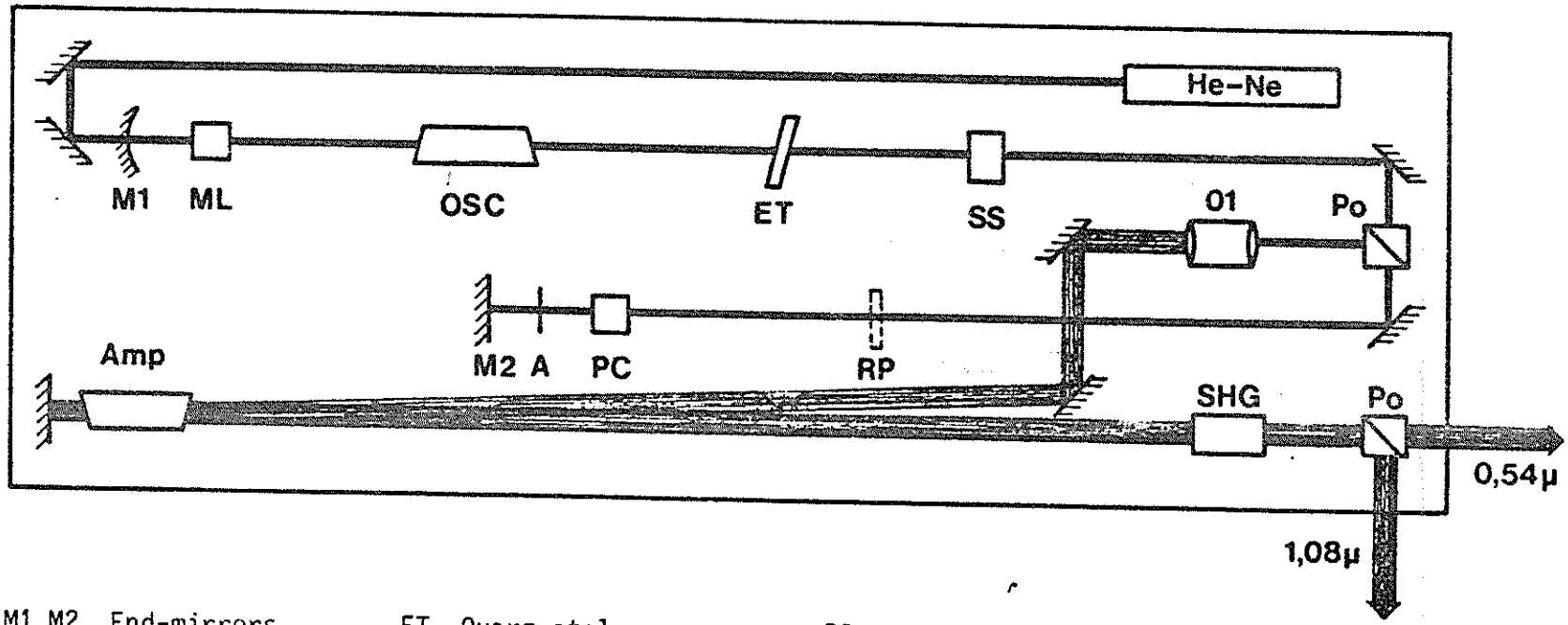

M1,M2	End-mirrors	ET	Quarz etalon	PC	Pockels cell
ML	KD*P mode-locker	SS	Safety shutter	A	Aperture
Po	Polarizer	01	Beam expander	Amp	Amplifier head
OSC	Oscillator head	RP	λ/2 Retardation plate	SHG	KD*P Frequency doubler

Fig. 3: Lay-out of the laser

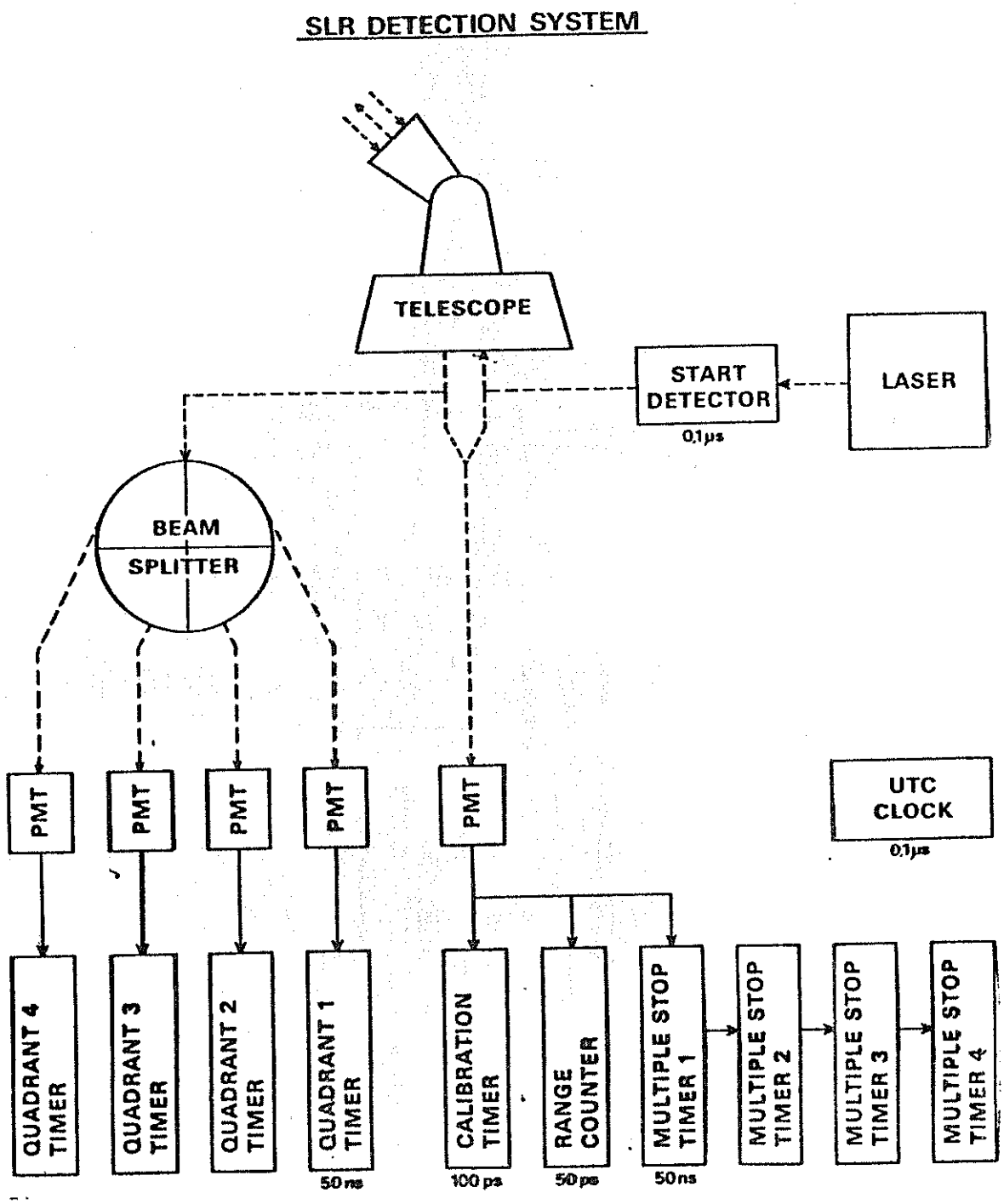

Fig. 4: Block diagram showing the detector concept

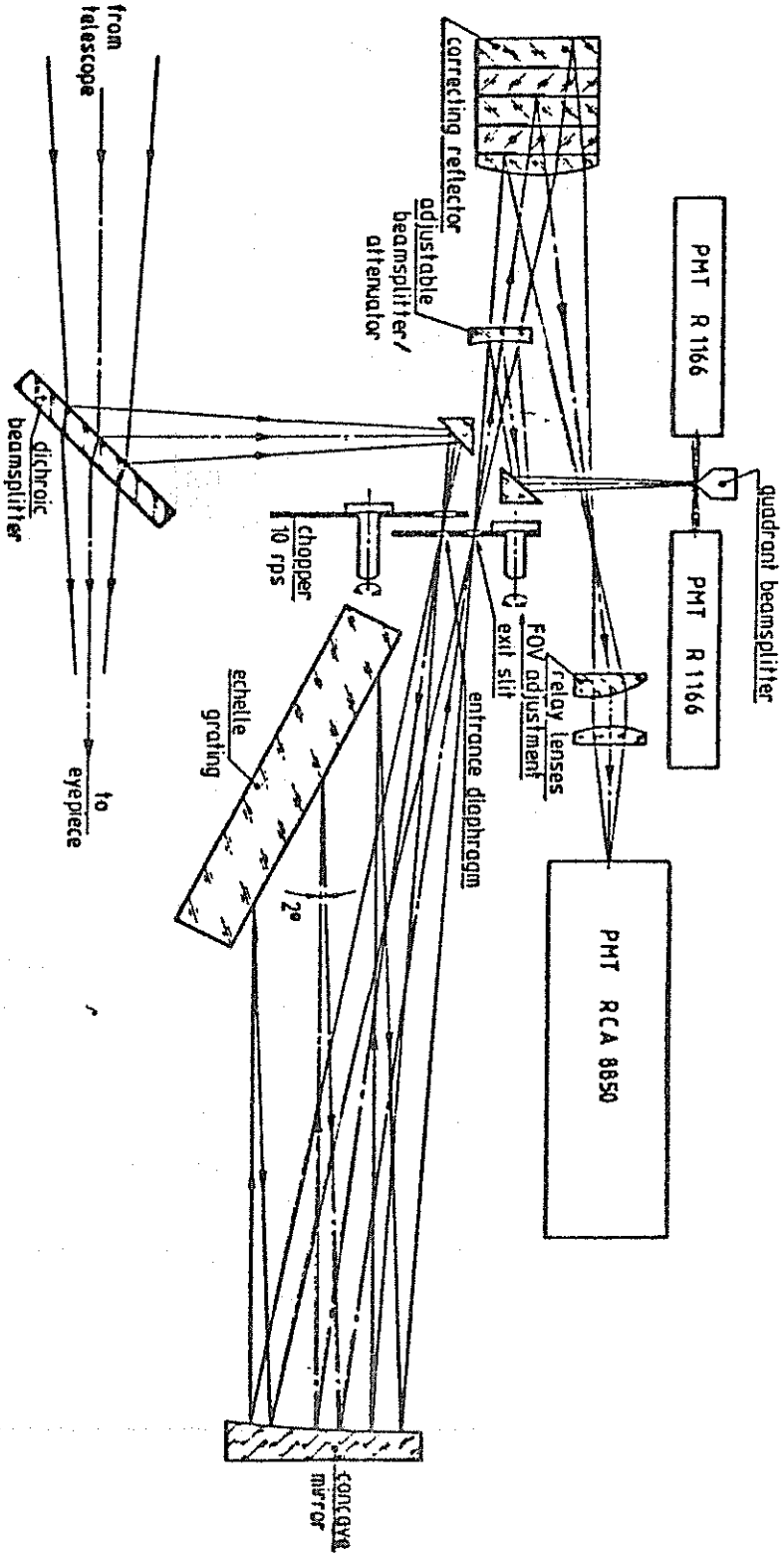

Fig. 5: Optical configuration of the detector package

input - output channel for communicating orbital updates and quick-look results between the system and the outside world.

The telescope, mount, laser (including power supply and cooling) and detector are configured together on a separate cart (fig. 6), which will be loaded into the vehicle for road transportation (fig. 7) and run out to a position adjacent to the ground marker for ranging operations (fig. 8). The system will be operated from its own independent power supply (fig. 7). In an air-freight configuration the total measuring system will fit onto a single standard freight pallet (fig. 9). Conversion from the air- to the road-transport or from road-transport to operational configuration will be possible within 24 hours, given suitable amenities and acceptable weather conditions.

3. The operational routine

The overall operational sequence is explained in fig. 10, whereby the most usual routine will be restricted to road travel, with only occasional air transfers necessary.

3.1 Setting up the system for observation

After arrival at the new site the system will first undergo routine checking and maintenance, during which time the time scale will be checked or reinstalled. The station position will usually be taken from a previously determined marker using a supplementary positioning device (fig. 11 and fig. 12). However, software is available which will enable the operators to determine station positions astronomically if required at the same time as the system orientation is made.

With the derived station position and the initiating vector provided via a data link such as GE-Mark III, telephone or telex, ephemerides will be calculated using an on-site prediction routine [5].

3.2 Range calibration

Much attention has been given to the design for range calibration. As it will be possible to range to terrestrial targets at arbitrary distances, the commonly practised technique of ranging to an external target board can also be used here. However, with the objective of eliminating any systematics identifiable at the 1 cm level, it is immediately apparent that

- an internally defined range undisturbed by atmospheric variations along the path,

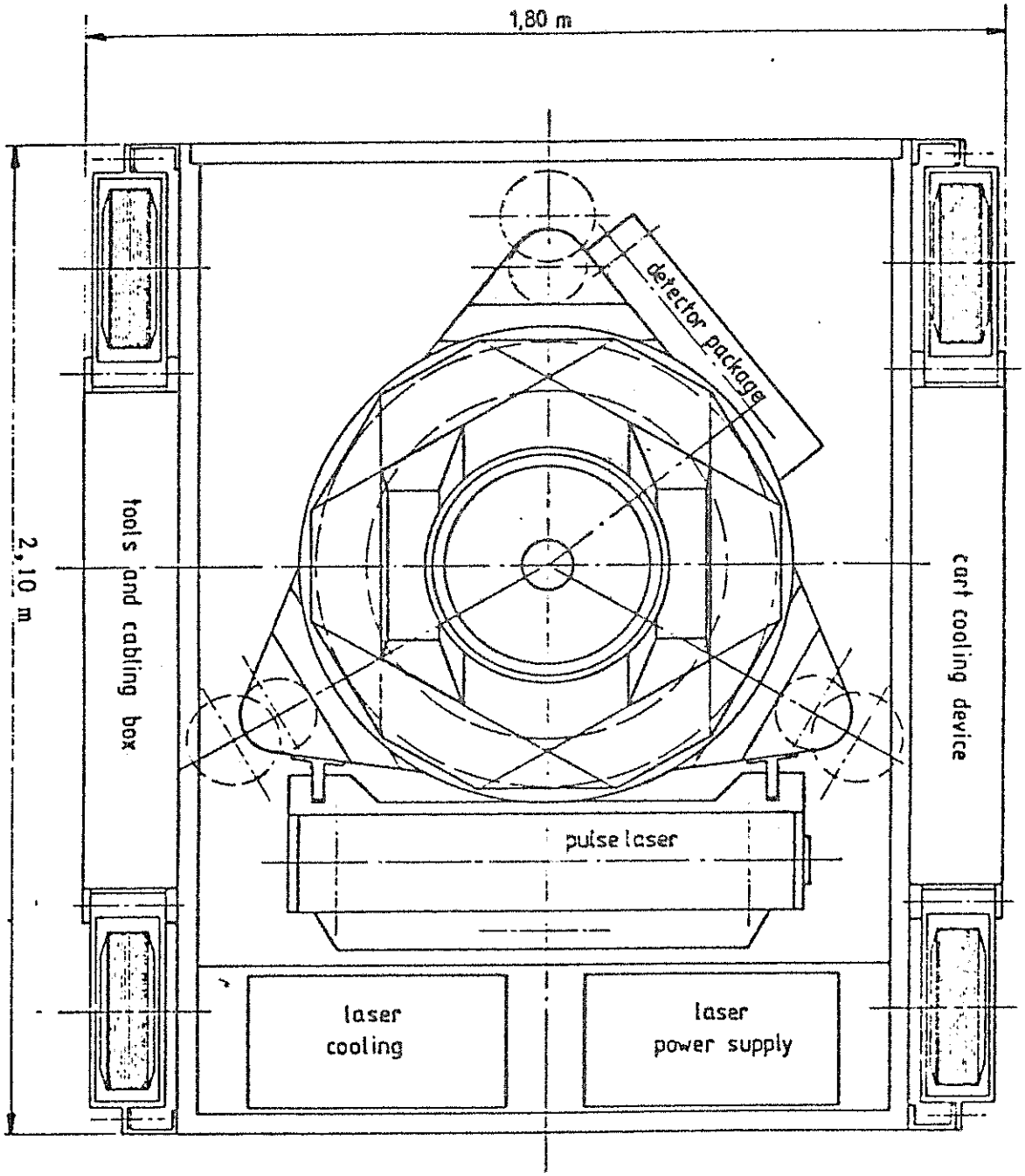

Fig. 6: Plan view of the observing cart

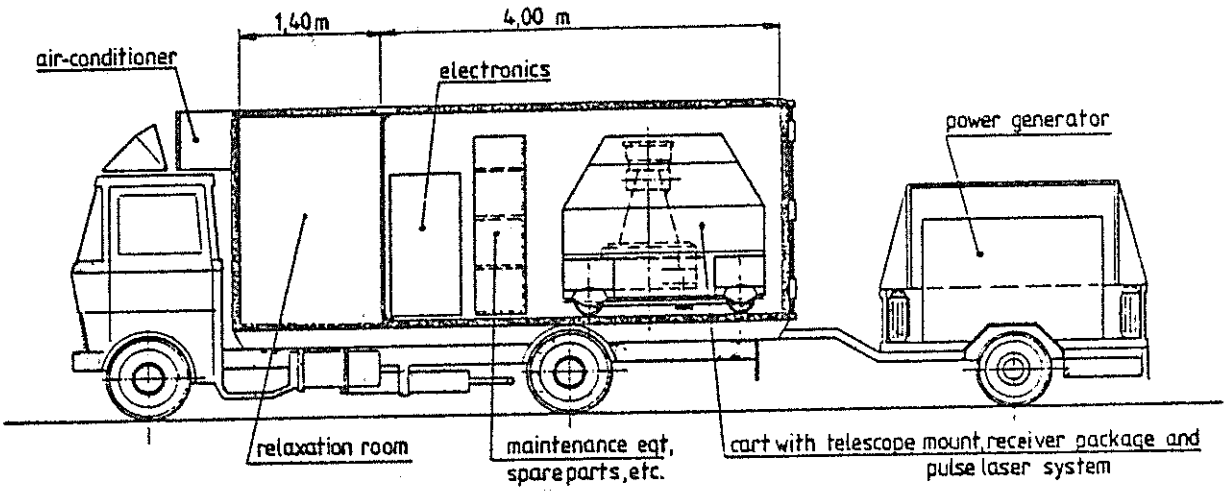

Fig. 7: The system assembled for road transportation

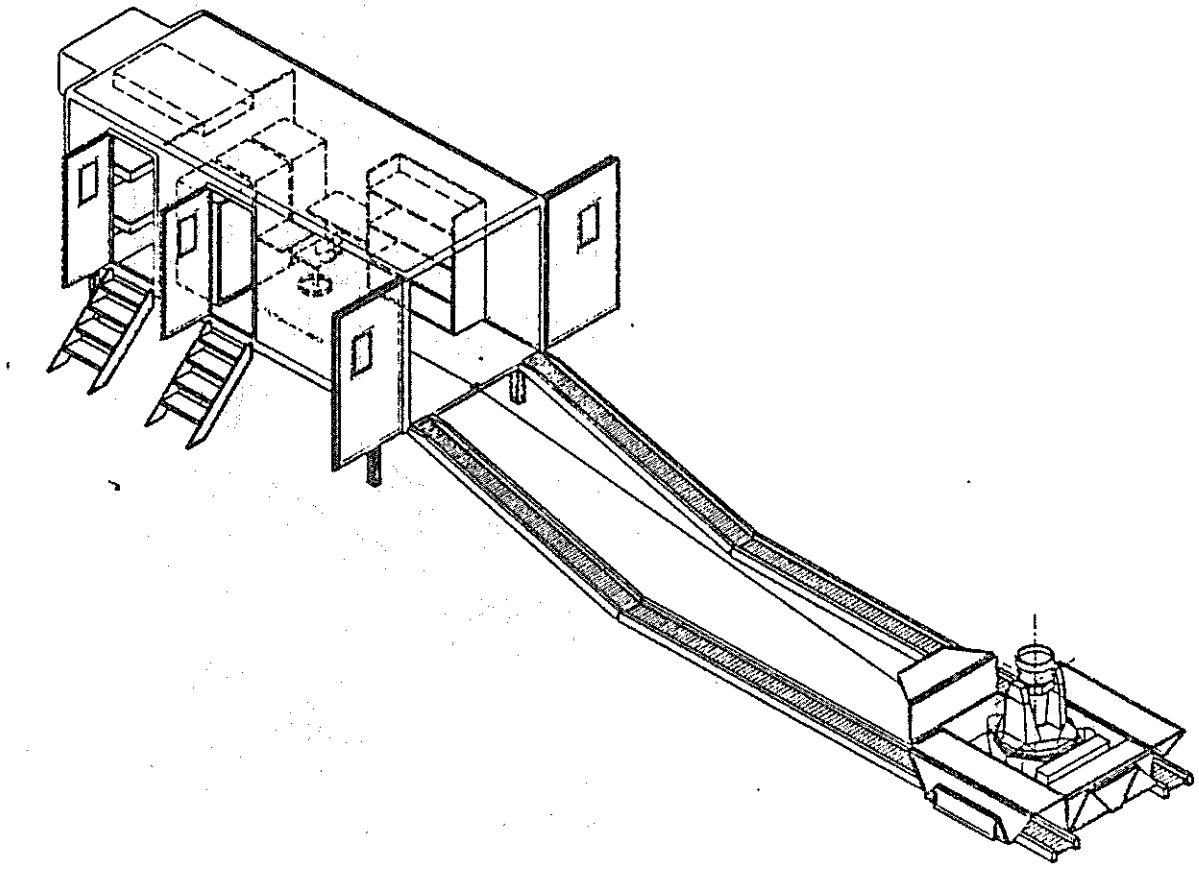

Fig. 8: The observing configuration

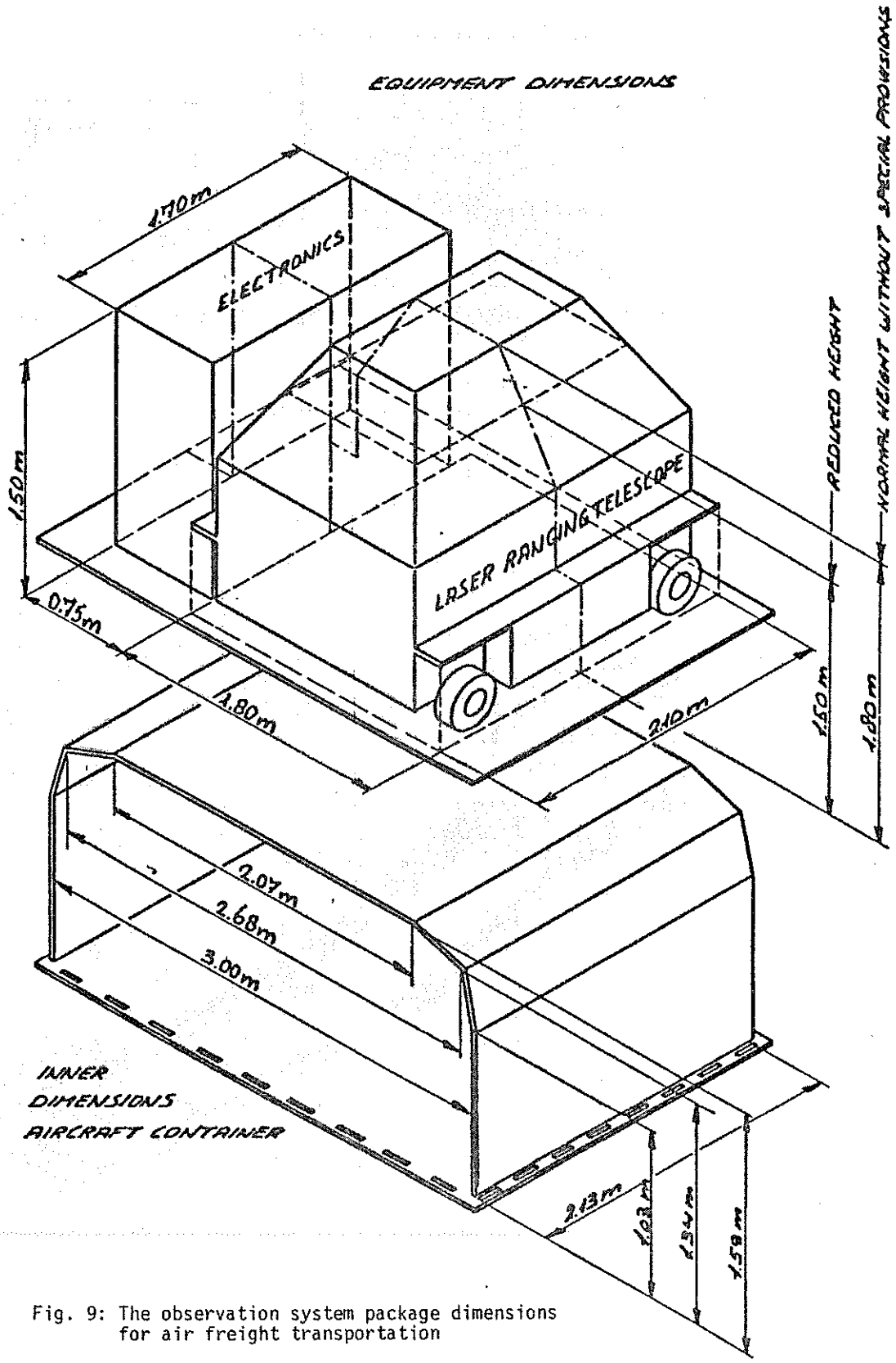

Fig. 9: The observation system package dimensions for air freight transportation

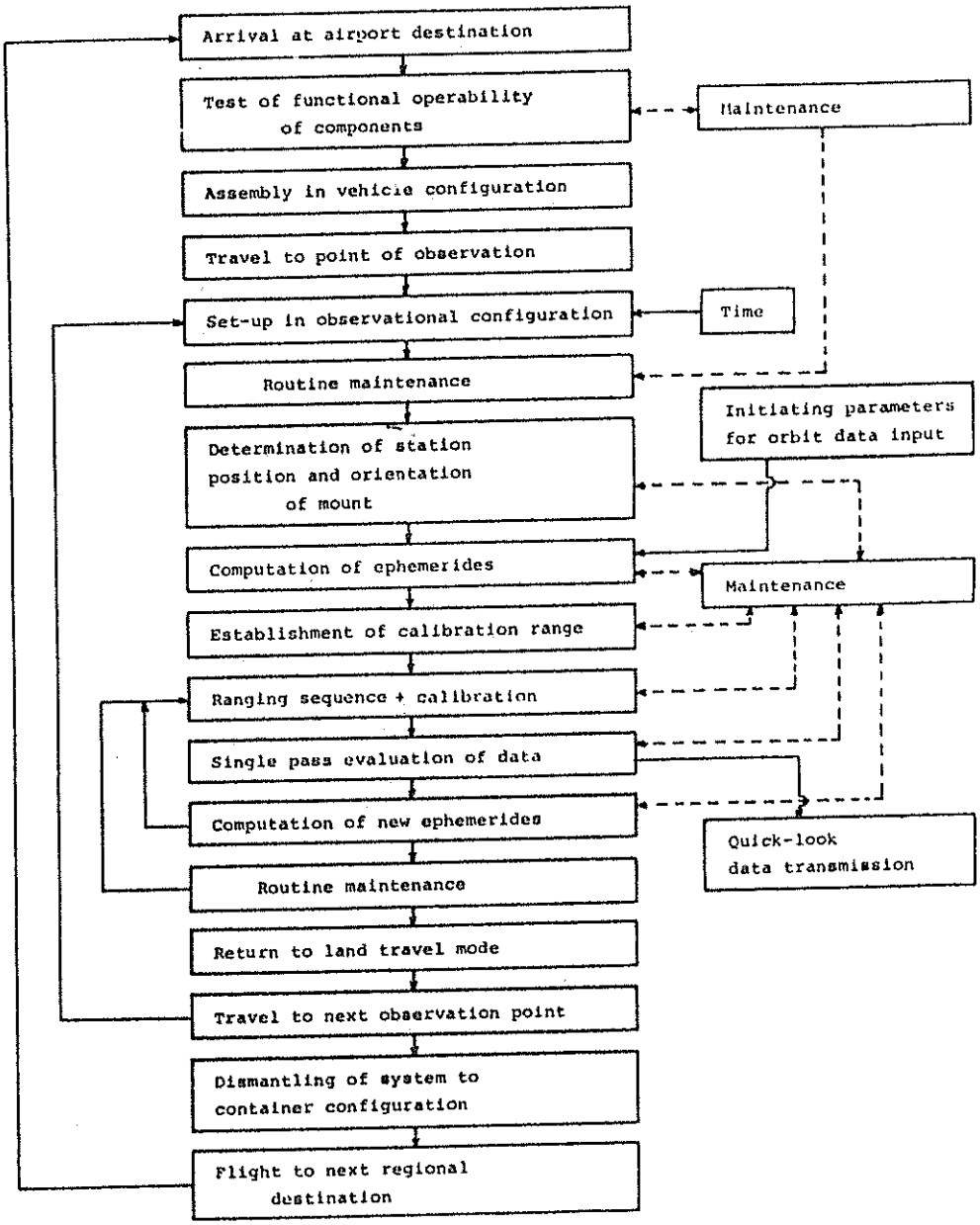

Fig. 10: The operational routine

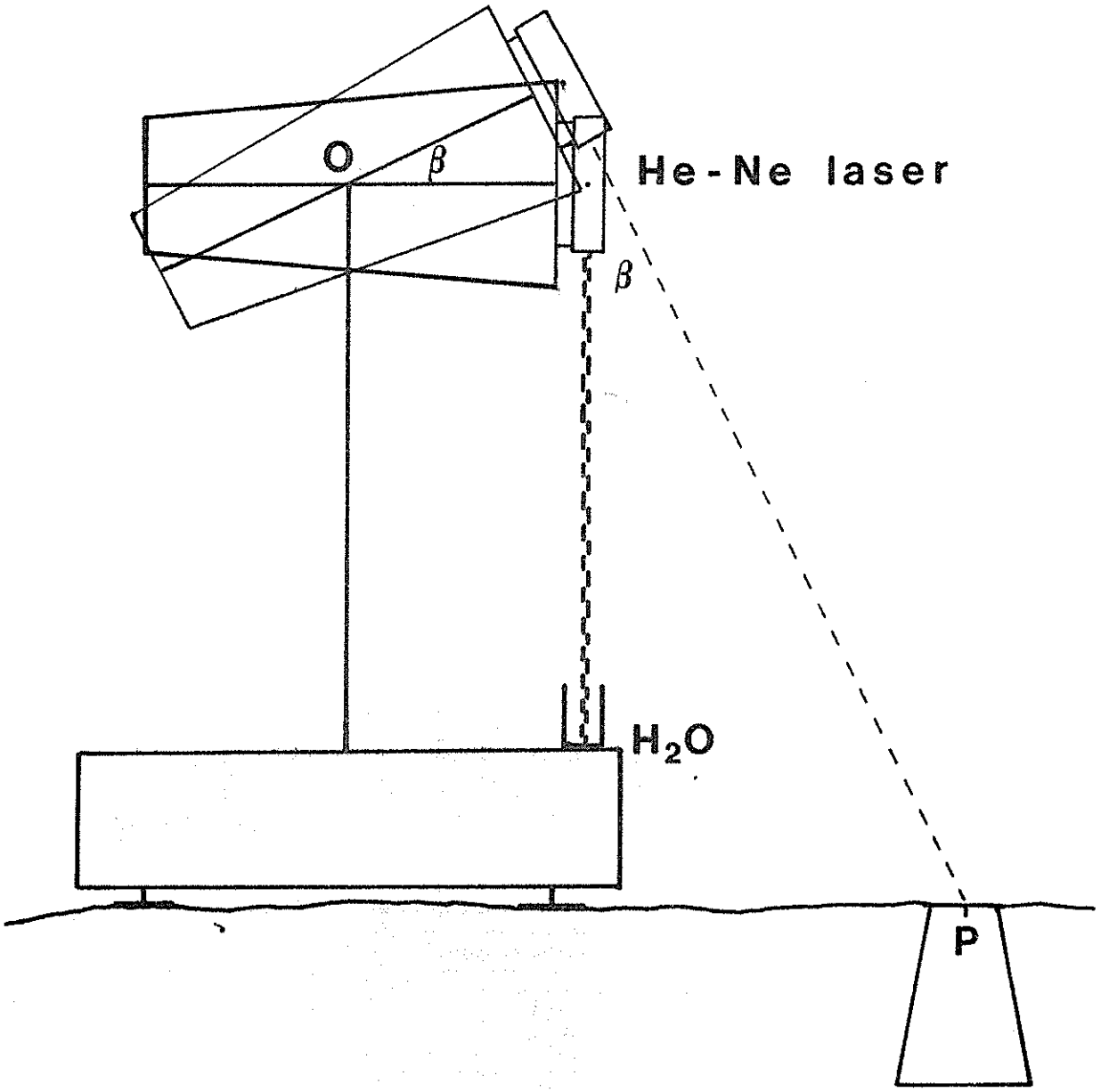

Fig. 11: Principle of transferring ground co-ordinates to the intersection of the axes of the mount

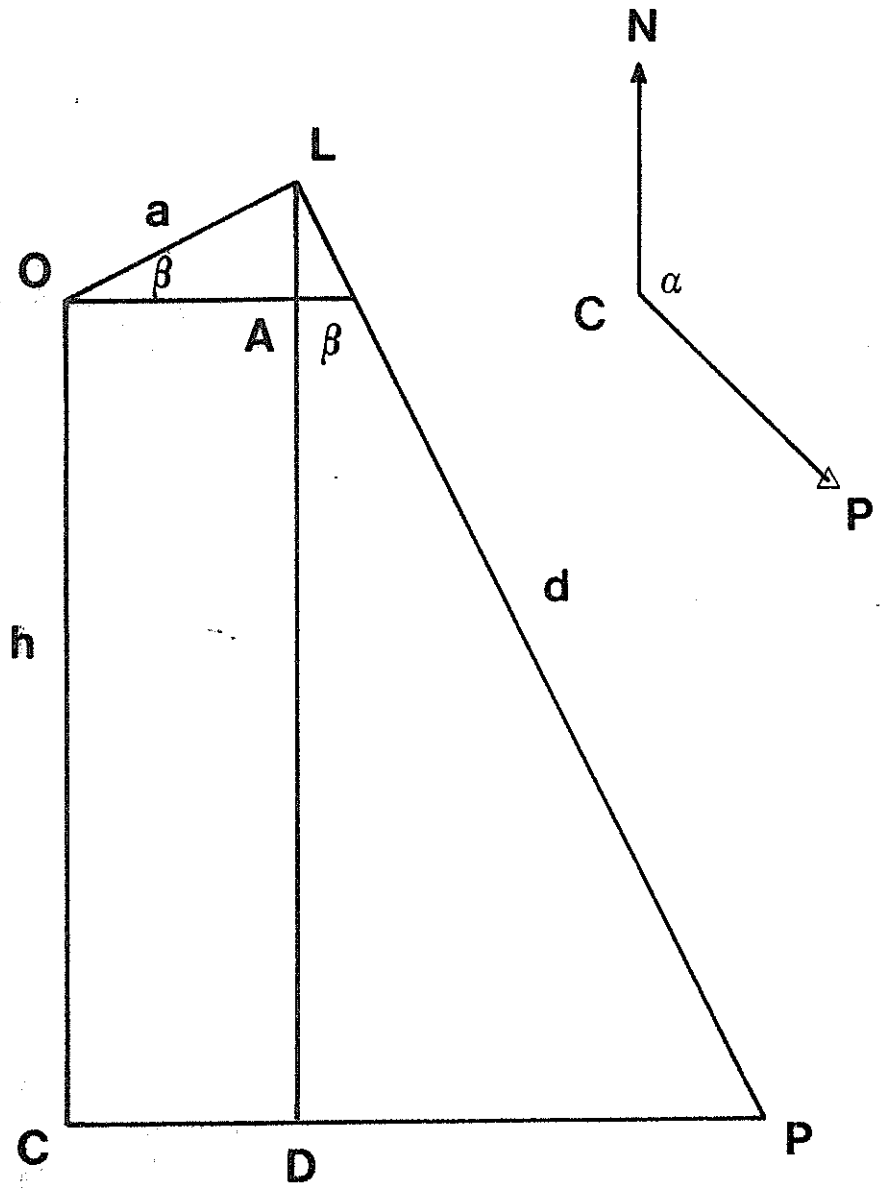

CP is the ex-centric distance, CO the ex-centric height. α is the azimuth of P from C.

$$CP = CD + DP = d \cdot \sin\beta + a \cdot \cos\beta$$

$$CO = DL - AL = d \cdot \cos\beta - a \cdot \sin\beta$$

Fig. 12: To transfer ground co-ordinates to O only d and ß must be measured. a is an instrumental constant

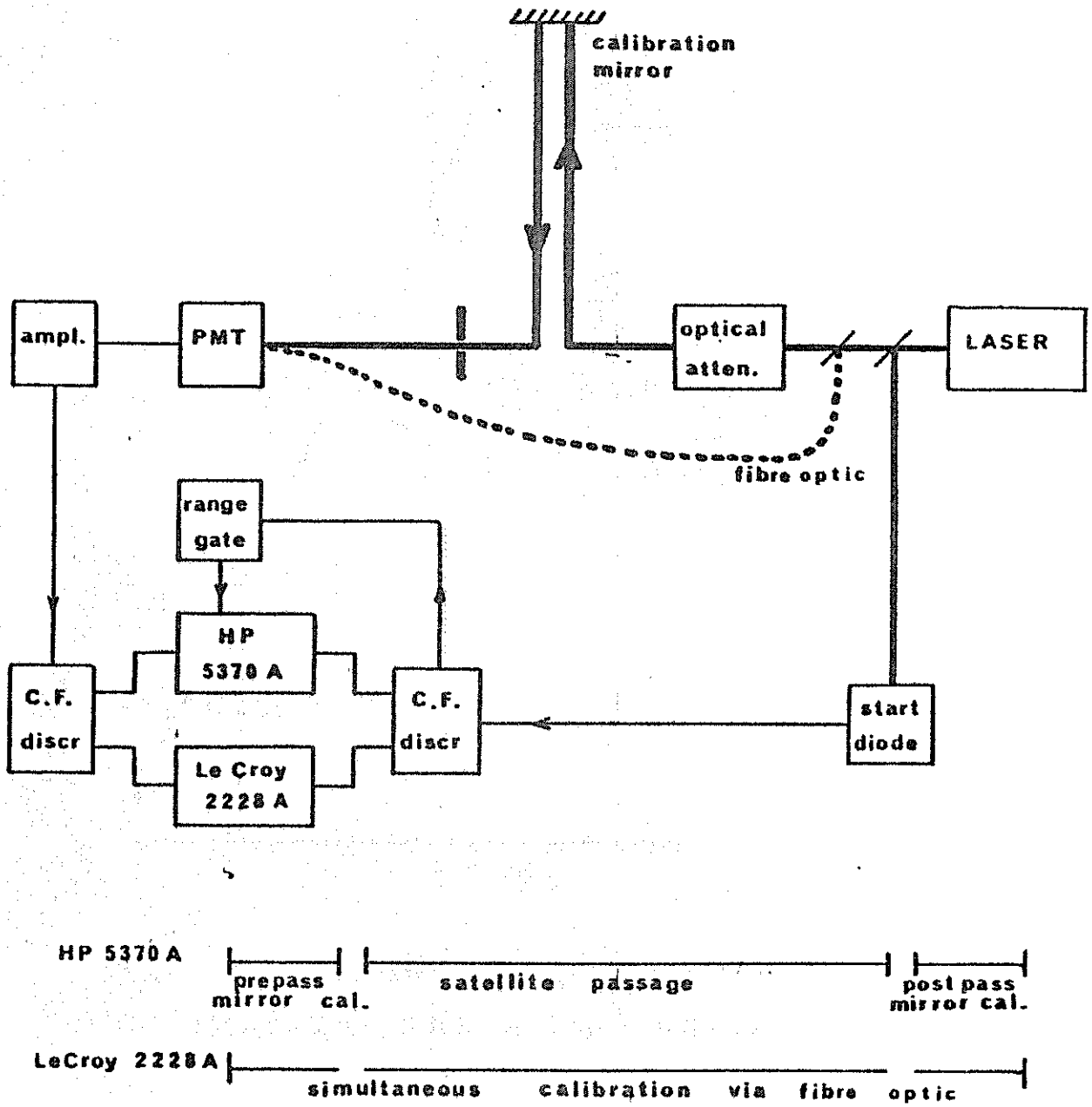

Fig. 13: The range calibration procedures

- and a pulse-by-pulse control of the ranged distance

are both desirable.

To achieve the first of these, pre- and post-pass calibrations are visualised using the defined range to a calibration mirror attached at the front of the telescope (fig. 13). For this, ranging is performed with the same HP 5370 A computing counter as that used to range to the satellite. At the same time, and throughout the satellite pass, parallel ranging will be performed over a second fixed range defined by a fibre-optic fed to the PMT (see also fig. 13). Constant fraction discriminators are used to furnish the start and stop signals to both the HP 5370 A and to a Le Croy 2228 A counter, whose task it will be to monitor the consistency of the fibre-optic calibration range throughout the pass.

4. Concluding comments

The systems described here have been designed with the objective of achieving high quality results with a mobile system, characterised by minimal systematic and a high level of alignment stability and operational reliability. To this end there has been some compromise of the requirement for diminishing volume and weight in the interest of accessibility and flexibility. The resulting systems will provide interesting alternatives in the growing family of relatively highly mobile laser ranging instrumentation.

5. Bibliography

[1] H. Visser and F.W. Zeeman - Mount and telescope for the German/Dutch mobile system - Fourth International Workshop on Laser Ranging Instrumentation, Austin, Texas, 1981.

[2] H. Puell - Subnanosecond laser systems for satellite ranging - Fourth International Workshop on Laser Ranging Instrumentation, Austin, Texas, 1981.

[3] H. Visser and F.W. Zeeman - Detection package for the German/Dutch mobile system - Fourth International Workshop on Laser Ranging Instrumentation, Austin, Texas, 1981.

[4] K.H. Otten - Software design for a multi-processor based mobile ranging system - Fourth International Workshop on Laser Ranging Instrumentation, Austin, Texas, 1981.

[5] E. Vermaat - Practical aspects of on-site prediction - Fourth International Workshop on Laser Ranging Instrumentation, Austin, Texas, 1981.